LUND UNIVERSITY

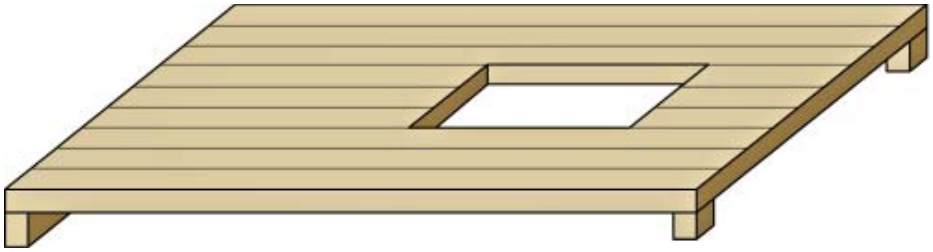

BEHAVIOUR OF CROSS LAMINATED TIMBER ELEMENTS WITH OPENINGS AT OUT-OF-PLANE LOADING CONDITIONS

CHRISTOPHER HAST and DANIEL FATEMI

Structural Mechanics

Master's Dissertation

DEPARTMENT OF CONSTRUCTION SCIENCES
DIVISION OF STRUCTURAL MECHANICS

ISRN LUTVDG/TVSM--20/5245--SE (1-134) | ISSN 0281-6679
MASTER'S DISSERTATION

BEHAVIOUR OF CROSS LAMINATED TIMBER ELEMENTS WITH OPENINGS AT OUT-OF-PLANE LOADING CONDITIONS

CHRISTOPHER HAST and DANIEL FATEMI

Supervisor: Dr **HENRIK DANIELSSON**, Division of Structural Mechanics, LTH.
Examiner: Professor **ERIK SERRANO**, Division of Structural Mechanics, LTH.

Printed by V-husets tryckeri LTH, Lund, Sweden, July 2020 *(Pl)*.

For information, address:
Division of Structural Mechanics,
Faculty of Engineering LTH, Lund University, Box 118, SE-221 00 Lund, Sweden.
Homepage: www.byggmek.lth.se

Abstract

The use of cross laminated timber (CLT) is expanding, its use is relatively new and universal design standards are lacking. One situation for which no universal design standard exists is that of a CLT plate element with an opening. A grillage method has been proposed as a convenient method to design such plate elements. The grillage method consists of analyzing a beam grillage model in terms of bending moment, shear force and deflection. This thesis examines the grillage method and compares it to corresponding finite element (FE) models. The FE models are modelled in Abaqus with three-dimensional shell elements using a composite layup tool in order to model the individual layers of CLT. Throughout the investigations three CLT compositions with differing layer thicknesses are used. Hence, cross section composition is included as a parameter in the study. Different methods to evaluate CLT beams are examined and applied to the grillage model; Gamma method and Timoshenko beam theory. For various opening geometries results from grillage models are compared to results from FE models. In the FE models results are extracted from paths coinciding with the geometry of the beams in the grillage models. The results show that the choice of beam theory does not impact the results from the grillage model significantly. When compared to FE models the grillage models give generally higher values for bending moment, shear force and deflection. Certain combinations of opening geometry and cross section composition causes a large discrepancy between the grillage model and the FE model.

Sammanfattning

Användningen av korslimmat trä (KL-trä) befinner sig i en expanderande fas. Tillämpningen av KL-trä som byggnadsmaterial är relativt nytt och övergripande dimensioneringsstandarder har ännu inte utvecklats fullt ut. Ett fall där inga allmänna dimensioneringsstandarder existerar är fallet plattelement av KL-trä med hål. En dimensioneringsmetod som utgår ifrån en balkrostmodell har föreslagits för att analysera sådana plattelement. Balkrostmodellen består av ett antal balkar vilandes på varandra för vilka man utvärderar böjmoment, tvärkraft och nedböjning. Arbetet syftar på att granska balkrostmodellen och jämföra resultaten från modellen med en motsvarande finita elementmodell (FE-modell). FE-modellen modelleras i Abaqus med tredimensionella skalelement där ett inbyggt kompositupplägningsverktyg används för att modellera de invidiuella lagren som bygger upp KL-träelementet. Utvärderingen utförs för tre olika KL-träuppbyggnader där de ingående lagrens tjocklekar varieras. Därmed inkluderas även KL-träuppbyggnaden som en parameter i studien. Olika teorier för att utvärdera KL-träbalkarna redovisas; Gammametoden och Timoshenkos balkteori. Resultaten från de olika modellerna jämförs för olika hålgeometrier. I FE-modellen hämtas resultaten från så kallade "paths" vilka sammanfaller geometriskt med balkarna i balkrostmodellen och fungerar som stigar i modellen varifrån man hämtar resultat. Utvärderingen visar att valet av balkteori inte påverkar jämförelsen i en betydande utsträckning. Jämförelsen mellan FE-modellen och balkrostmodellen visar att balkrostmodellen generellt ger högre värden för böjmoment, tvärkraft och nedböjning. Vissa kombinationer av hålgeometrier och KL-träuppbyggnad påvisade stora avvikelser i jämförelsen mellan FE-modell och balkrostmodell.

Acknowledgements

This Master's dissertation was written during the spring of 2020 at Lund University, Department of Construction Sciences: Division of Structural Mechanics.

The authors of this thesis would like to thank their supervisor Henrik Danielsson for his support throughout the work. Henrik has provided unlimited guidance, undivided attention and thorough oversight without which the writing of this dissertation would have been impossible. The authors also acknowledge their examiner Erik Serrano who has been the source of abundant input, great ideas and an overall jolly mood. It is truly a joyous endeavour to work beside Erik.

The authors thank Lund University for the superb education that they have had the privilege of receiving, which the writing of this thesis has been a part of. A special thanks is also dedicated the authors partners Lovisa Hast and Klara Broman who have supported the authors for years prior to, and during, the writing of this dissertation.

Lund, June 2020
Christopher Hast and Daniel Fatemi

Notations and Symbols

General notations

( )' - Derivative of ( )
$\int$ ( ) - Integral of ( )
( )$^{-1}$ - Inverse of ( )
max - Maximum of
( )" - Second derivative of ( )
$\sum$( ) - Sum of ( )
( )^{T} - Transpose of ( )

Latin letters

a - Length of part of beam before point load
a_i - Distance between the centre of layer i and the neutral axis of the CLT element
A - Area of cross section
$\mathbf{a}$ - Nodal displacement vector
$\mathbf{a}^e$ - Element nodal displacement vector
$\mathbf{A}$ - Transformation matrix
$\mathbf{A}_1$, $\mathbf{A}_2$, $\mathbf{A}_3$ - Transformation matrices for different alternate coordinate systems
b - Length of part of beam after point load
b_{beam} - Width of CLT beam
$b_{beam,y}$ - Width of beam at distance y along beam height
b_{board} - Width of a constituent board of CLT element
b_{eff} - Contributing width of the plate
b_x - Width of the cross section perpendicular to the x-axis
b_y - Width of the cross section perpendicular to the y-axis
c_1 - Factor for calculating torsional moment of inertia
C_{xx} - Component of compliance matrix
$\mathbf{C}$ - Compliance matrix
$\bar{\mathbf{C}}$ - C-matrix
D_{xx} - Component of constitutive matrix
$\mathbf{D}$ - Constitutive matrix
E - Elastic modulus
E_0 - Elastic modulus parallel to fibre direction
E_{90} - Elastic modulus perpendicular to fibre direction
E_{xx} - Elastic modulus valid in the principle direction
$E(y)$ - Elastic modulus at distance y along beam height
$f_{vk,090}$ - Characteristic longitudinal shear strength
$f_{vk,9090}$ - Characteristic rolling shear strength
$\mathbf{f}$ - Global force vector

$\mathbf{f}_l$ - Global load vector
$\mathbf{f}_l^e$ - Element load vector
$\bar{\mathbf{f}}_l^e$ - Element load vector in local coordinate system
G - Shear modulus for cross section
G_{090} - Longitudinal shear modulus
G_{9090} - Rolling shear modulus
G_{eff} - Effective shear modulus
G_i - Shear modulus of layer i in CLT element
G_{xx} - Shear modulus valid in between principle directions
$G(y)$ - Shear modulus at distance y along beam height
$\mathbf{G}$ - Transformation matrix
h - Height of beam cross section
$h_{element}$ - Total height of CLT element
i - Label for layer in CLT element
I - Moment of inertia
I_{eff} - Effective moment of inertia
I_{net} - Net moment of inertia
I_{tor} - Torsional moment of inertia
$I_{x,net}$ - Net moment of inertia around the global y-axis
$I_{y,net}$ - Net moment of inertia around the global x-axis
$I_{\bar{y}}$ - Moment of inertia around the local y-axis
$I_{\bar{z}}$ - Moment of inertia around the local z-axis
k_1 - Axial stiffness
k_2 - Torsional stiffness
k_L - Denotes the longitudinal layer closest to the center of gravity of the CLT plate.
k_{sys} - System effects factor
k_{tor} - Factor for calculating torsional moment of inertia
$\mathbf{K}$ - Global stiffness matrix
$\mathbf{K}^e$ - Element stiffness matrix
$\bar{\mathbf{K}}^{\mathbf{e}}$ - Stiffness matrix expressed in local coordinate system
$l_{element}$ - Total length of CLT element
l_{ref} - Reference length used when calculating the effective moment of inertia
L - Length of beam or CLT element
m - Distributed bending moment per meter beam width
M_r - Bending moment capacity
M_{xy} - Bending moment around the global y-axis, valid for the transversal beams.
M_{yx} - Bending moment around the global x-axis, valid for the longitudinal beams.
$M_{\bar{y}}$ - Bending moment around local y-axis
$M_{\bar{z}}$ - Bending moment around local z-axis
$M(x)$ - Bending moment at distance x along beam
$M^{0-1}(x)$ - Bending moment at distance x along beam valid between points 0 and 1 along the beam
$M^{1-2}(x)$ - Bending moment at distance x along beam valid between points 1 and 2 along the beam
N - Normal force
$N(x)$ - Normal force at distance x along beam
$\bar{\mathbf{N}}$ - Local shape function matrix
o_i - Centre of gravity for layer i as a distance from the lower edge of the cross section

P - Point load
q - Line load acting on beam
q_x - Load working in the longitudinal direction of the beam
$q_{\bar{x}}$ - Local axial load
q_y - Load working in the transversal direction of the beam
$q_{\bar{y}}$ - Transversal load acting in the local y-direction
$q_{\bar{z}}$ - Transversal load acting in the local z-direction
$q_{\bar{\omega}}$ - Local torsional load
R_A - Reaction force at support A
R_B - Reaction force at support B
S_{CLT} - Shear stiffness of CLT cross section
$S_{x,net}$ - Net static moment around the x-axis
$S_{y,net}$ - Net static moment around the y-axis
$S(y)$ - Static moment at distance y along beam height
SF4 - Shear force acting on the section of the CLT plate facing in the direction of coordinate axis 1
SF5 - Shear force acting on the section of the CLT plate facing in the direction of coordinate axis 2
SM1 - Moment that generates normal stress parallel to coordinate axis 1
SM2 - Moment that generates normal stress parallel to coordinate axis 2
t_{board} - Thickness of constituent board of CLT element
t_i - Thickness of layer i in CLT element
T - Torsion
u - Displacement in the longitudinal direction of beam
u_1 - Prescribed displacement in direction 1
u_2 - Prescribed displacement in direction 2
u_3 - Prescribed displacement in direction 3
ur_1 - Prescribed rotation around axis 1
ur_3 - Prescribed rotation around axis 3
$\bar{u}$ - Displacement in local x-direction
$\bar{u}_p$ - Particular solution for displacement in local x-direction
$\mathbf{u}$ - Local displacement vector
$\mathbf{u}_h$ - Homogeneous displacement solution
$\mathbf{u}_p$ - Particular displacement solution
v - Displacement in the transversal direction of beam
$v(x)$ - Deflection at distance x along beam
$V_{r,long}$ - Capacity with respect to longitudinal shear stress
$V_{r,roll}$ - Capacity with respect to rolling shear stress
V_{xz} - Shear force acting vertically in the cross section coinciding with the xz-plane
$V_{\bar{x}\bar{z},r}$ - Capacity with respect to longitudinal shear stress in local xz-direction
V_{yz} - Shear force acting vertically in the cross section coinciding with the yz-plane
$V_{\bar{y}}$ - Shear force acting in local y-direction
$V_{\bar{y}\bar{z},r}$ - Capacity with respect to rolling shear stress in local yz-direction
$V_{\bar{z}}$ - Shear force acting in local z-direction
$V(x)$ - Shear force at distance x along beam
$V^{0-1}(x)$ - Shear force at distance x along beam valid between points 0 and 1 along the beam

$V^{1-2}(x)$ - Shear force at distance x along beam valid between points 1 and 2 along the beam
$w_{element}$ - Total width of CLT element
$\bar{w}$ - Displacement in local z-direction
$\bar{w}_p$ - Particular solution for displacement in local z-direction
W_{net} - Net bending resistance
x - Distance along beam
x_1, x_2, x_3 - Coordinate axis in the primary coordinate system
x_1', x_2', x_3' - Coordinate axis in the alternate coordinate system
$\bar{x}$ - Local x-axis
y - Vertical distance from the center of mass of cross section
$\bar{y}$ - Local y-axis
z_b - Bottom lever arm for determining the net bending resistance
z_t - Top lever arm for determining the net bending resistance
$\bar{z}$ - Local z-axis

Greek letters

γ_1, γ_3, γ_5 - Reduction factors used in the Gamma method describing the contribution to the total stiffness from the current layer
γ_{xx} - Shear strain component of strain vector
ε - Normal strain
ε_{xx} - Component of strain vector
ε_{xx}' - Component of strain vector in alternate coordinate system
$\boldsymbol{\varepsilon}$ - Strain vector
$\boldsymbol{\varepsilon'}$ - Strain vector in alternate coordinate system
Θ - Angle of rotation in reference to the horizontal plane
κ - Shear correction factor
γ - Shear strain
ν - Poisson's ratio
ν_{090} - Poisson's ration for the longitudinal radial plane
ν_{900} - Poisson's ration for the longitudinal tangential plane
ν_{9090} - Poisson's ration for the transversal radial plane
ν_{xx} - Poisson's ratio in the three dimensional case
σ - Normal stress
σ_{xx} - Component of stress vector
σ_{xx}' - Component of stress vector in alternate coordinate system
$\boldsymbol{\sigma}$ - Stress vector
$\boldsymbol{\sigma'}$ - Stress vector expressed in alternate coordinate system
τ - Shear stress
$\bar{v}$ - Displacement in local y-direction
$\bar{v}_p$ - Particular solution for displacement in local y-direction
$\bar{\varphi}$ - Rotation around local x-axis
$\bar{\varphi}_p$ - Particular solution for rotation around local x-axis

Contents

1 Introduction

1.1 Background

The use of cross laminated timber (CLT) elements in building construction is an expanding practice in both Sweden as well as internationally. A CLT element is a plate shaped element that consists of several layers of wooden boards. Each layer is stacked in such a way that the boards are orientated perpendicularly in relation to the boards in the neighboring layers, as seen in Figure 1.1. The strength and stiffness of wood varies with the direction of the loading relative to the orientation of the fibre direction. The layered structure serves to combine different directional capacities. Hence the product possesses load bearing capacity in several directions both for in-plane and out-of-plane loading, meaning it can be used as both floor and wall elements. CLT elements are prefabricated in a factory setting which allows extensive customization. The mode of production coupled with the physical properties allows for great architectural freedom in shaping CLT elements (Jeleč et al., 2018).

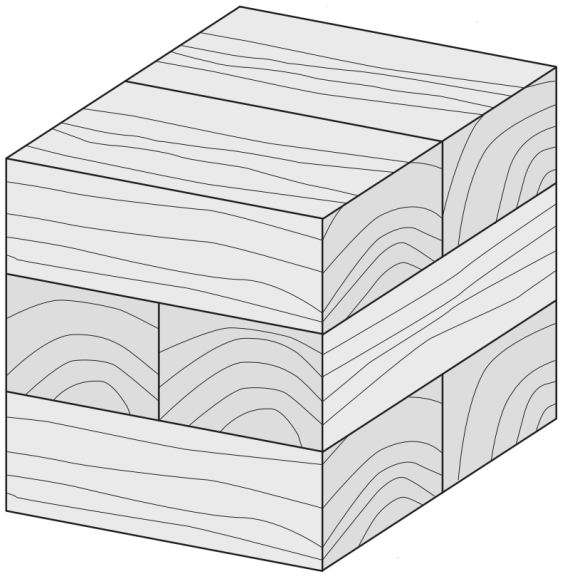

Figure 1.1: Orientation of boards in CLT element (Borgström and Fröbel, 2019)

CLT elements are used in the construction of diverse structures. It is used in the construction of small houses, multi-story buildings, hall buildings, sport facilities as well as bridges. CLT elements are versatile as they can be assembled into a wide range of shapes. The positive aspects of CLT elements do not only concern logistical or mechanical properties. The use of wood also carries environmental benefits. It is a renewable material and the production process has a low energy consumption. Bi-products that arise during the construction of CLT elements, such as wood chips or sawdust, can be recycled or burned for energy. At the end of the service life of an element, the material can be recycled into other products and later be burned for energy as a final stage. These properties positions wood as a sustainable construction material as the material can be used with minimal waste during its entire life cycle (Borgström and Fröbel, 2017). In a study comparing the life cycle, environmental impact and carbon emission of a building constructed using either reinforced concrete or CLT elements it was shown that the timber alternative had a lower environmental impact and lower carbon emissions (Robertson et al., 2012). The benefits of using wood in general and CLT elements specifically are many and varied as described. The use of CLT elements is on the rise and extensive research about its properties has been carried out and is carried out continuously. However, the history of CLT is relatively short.

CLT elements are relatively new in comparison to the more commonly used construction materials such as concrete and steel. The idea was originally developed in Austria during the early 1990s. Since its development the use of CLT has increased exponentially. This is reflected in the production of CLT in Europe which has increased from zero up to 600 000 cubic meters per year in the time period from its inception to 2015, see Figure 1.2 (Borgström and Fröbel, 2017). It can also be mentioned that the trend of rapidly increasing production of CLT seem to continue over the coming years as the production of CLT in Europe is estimated to exceed 1 000 000 cubic meters in 2020 (GWMI, 2019).

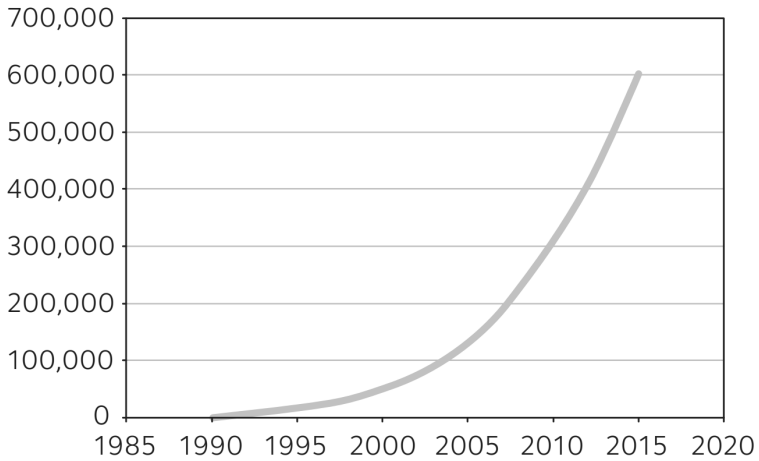

Figure 1.2: Graph showing the production of CLT elements in cubic meters in Europe between year 1990 and 2015 (Borgström and Fröbel, 2019)

The current relevant Eurocode, *Eurocode 5: Design of timber structures - Part 1-1: General - Common rules and rules for buildings*, from 2004 does not include specific design rules for CLT elements. The European standard specifically dealing with CLT, European standard for CLT EN16351 defines requirements and sets out provisions regarding the performance characteristics but does not provide design procedures. The lack of common design guidelines means that designers use handbooks and specifications from manufactures when designing structures using CLT elements (Jeleč et al., 2018). The technical committee responsible for developing Eurocodes, CEN/TC250, has set up a working group tasked with creating a new section in Eurocode concerning CLT. The section is meant to include common design rules. A standardized product declaration is also to be developed (Falk et al., 2016).

Openings in CLT elements

In the design of structures sometimes irregular geometries need to be considered. A common irregular geometry that is present in most house construction is openings. Openings are for example needed in order to allow for installations and perhaps most important stairs and staircases to pass through floors and walls. Also, architectural shapes and expressions may also involve challenging openings in floors and walls. The lack of a unified code regarding design means that there is no standard procedure for designing CLT elements with openings. Because of the complex structure of CLT the material is more suited for certain geometries and loading situations than other wood based building materials. An example of this phenomenon is the in-plane loading of a beam with irregular geometry due to an opening in the beam. In this case, the CLT element's capacity regarding stresses perpendicular to the axial direction of the beam exceeds the capacity of a glue laminated timber beam thanks to the orientation of the layers. This specific topic has been researched in order to examine the shear flow across the cross section. The research has been conducted using finite element models in order to conduct a parameter study and evaluate proposed simplifications (Jeleč et al., 2016).

Another relevant combination of loading situation and geometry is that of an opening in a CLT floor element loaded in the out-of-plane direction. It is common for both installations such as pipes and cables as well as stairs and staircases to pass between storeys in such way that openings in the floor is required. Instructions regarding fire safety exist for these situations as seen in Figure 1.3 but for the design of the floor element itself in regards to strength information is scarce.

In order to design floor elements with openings, finite element models are primarily used. In addition to this analysis method there is a proposed simplified analytical method of analysing plates with openings. The method consists of setting up a grillage of beams (Wallner-Novak et al., 2017). In order to find out the accuracy and limitations of this method it could be evaluated through a parameter study and a comparison between the results from the model with results from advanced finite element models. The general grillage method is only applicable to a plate element where the opening is placed at a certain distance from the edges of the plate. It is not applicable to an opening along the edge of a plate.

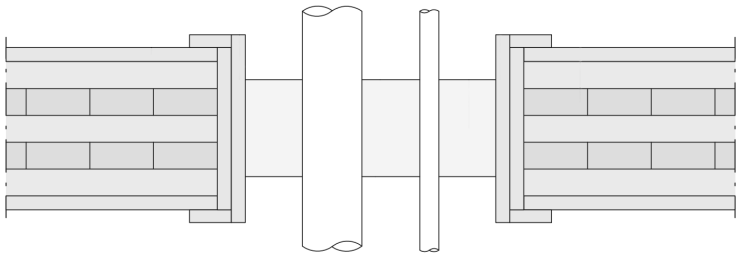

Figure 1.3: Detail showing opening in CLT floor element (Borgström and Fröbel, 2019)

There exists different ways to calculate the stiffness of a CLT cross section. In Bernoulli-Euler beam theory shear deformations are neglected. When dealing with CLT these shear deformations are not insignificant. Approximate methods to account for the shear flexibility of CLT elements have been developed. One example of such methods is the so called Gamma method. It reduces the bending stiffness based on the lay-up and the length of the beam. Alternatively, Timoshenko beam theory can be used. Timoshenko beam theory accounts for shear deformations without the need for additional methods. However, depending on which theory or method is used calculated deflections may differ (Borgström and Fröbel, 2017).

1.2 Aim and objective

The aim of this master's dissertation is to evaluate the general grillage method proposed by Wallner-Novak et al. (2017) regarding the accuracy of the method in describing section forces and deflections in CLT element plates with openings loaded in the out-of-plane direction. Parameters are investigated in order to determine how they affect the accuracy of the method compared to finite element analysis using three-dimensional shell elements. The parameters studied within the work presented here include:

- Size, location and shape of opening
- Method used to calculate section properties
- How the beams are connected in the grillage model
- Composition of layers in the CLT cross section

It is also of interest to evaluate whether the general grillage method can accurately predict the utilization of the shear force and bending moment capacity of a CLT plate element in the mentioned loading situation. In order to fulfill the aim of this dissertation, the following objectives are identified:

- Investigate the distribution of bending moment and shear forces according to the general grillage model.
- Investigate the effect of using different theories when calculating deflections of the beams according to the general grillage method.
- Compare the results from the general grillage method with results from finite element models using three-dimensional shell elements.
- Identify parameters that affect the comparison between the grillage model and finite element models.
- Investigate how different CLT cross section compositions affect the comparison between grillage model and finite element model,

1.3 Method

The general grillage method was implemented in a parametric MATLAB-script. The program, MATLAB, was used to calculate bending moment and shear force distributions as well as deflection along the beams. Different beam theories and different connections between the beams are implemented in the MATLAB-script. Additionally, finite element models are analysed in the finite element software Abaqus CAE. The results from the general grillage models are compared to those from the finite element models. This comparison constitutes the basis of a parameter study where the effects of different parameters are investigated.

1.4 Limitations

The geometry of the CLT plate investigated in this work is predetermined in several ways. The width and length of the CLT plate are predetermined to five meters and seven meters, respectively. The composition is restricted in such a way that only five layer CLT plates are investigated. The total thickness of the five layers together is also predetermined to 200 mm. However, the thickness of each individual layer constituting the CLT plate is varied. This to create different distributions between longitudinal and transversal thicknesses and thereby also different stiffness and strengths in the two orthogonal directions of the CLT plate cross section compositions.

Three different compositions are evaluated in this work, these three compositions are chosen based on adaptions of the CLT cross section composition with the aim of increased strength and stiffness (longitudinal and transversal). Also, the material parameters of the constituent boards in the different CLT plates are equal for every board. This is done to further limit the number of different possibilities of the CLT cross section composition.

Throughout the work, only centrally placed openings are studied to limit the extent of the parameter study. Only rectangular openings are investigated. This means that the parameters concerning the size, location and shape of the openings are limited to the length, width and size of the openings in the parameter study.

The load case is predetermined to consist of a simply supported CLT board resting on two supports and loaded with a constant surface load. The plate is supported along both its short sides. No additional load cases are evaluated in this work for the CLT plate.

1.5 Disposition

Chapter 2

Properties of wood and CLT, details the material science of wood and common properties of CLT.

Chapter 3

Structural modelling analysis, describes the Bernoulli Euler and Timoshenko beam theories. The gamma method and grillage model are explained. The implementation of three-dimensional beams is also explained. Lastly the calculation of bending moment and shear capacity of a CLT cross section is described.

Chapter 4

Finite element model, describes how the implemented finite element models are modelled.

Chapter 5

Comparison between grillage models and finite element model, investigates the difference between implementing different beam theories in the grillage model. The stiffness of a CLT cross section is analysed by comparing results from different beam theories to results from a finite element model. A general comparison between results from the grillage model and finite element model is carried out.

Chapter 6

Parameter study, compares maximum bending moment, shear force and deflection results from the grillage model to those from a finite element model.

Chapter 7

Discussion, the results and conclusions are discussed further.

Chapter 8

Summary of results and conclusions, the results are summarized and conclusions are made based on the results. Thoughts about further studies in this subject are brought up.

2 Properties of wood and CLT

Wherever wood has been available it has been used as a building material throughout history. The widespread use is of course a result from its availability but also the advantageous properties of wood. For the purpose of using wood as a building material it is relevant to explore the properties of wood. This chapter aims to explain in detail what these properties are and how they relate to CLT elements.

2.1 Anatomy and growth

The source of wood, trees

Every aspect of the anatomy of wood is a direct result of a function present in its origin, the tree. The adaptation of trees to their environment is seen on every structural level, from the shape of the tree to the microscopic structure. Trees have a cylindrical shape because it is the most aerodynamically optimal shape to resists wind loads. Branches reach out in order for the leaves they carry to be exposed to sunlight, facilitating photosynthesis. The material structure consists of fibres oriented in the axial direction, an efficient composition for resisting lateral wind loads and vertical self-weight. Growth prestresses the wood reducing the risk of crushing under compressive stresses (Johansson, 2016).

Because wood is a natural material there is a huge variability in its physical properties. This variability has many sources. The genetic stock leads to different properties between species as well as within species. Furthermore, environmental growing conditions such as climate, water supply and availability of nutrients, just to name a few, have a large impact on the physical properties. The physical properties of wood also result from the internal structure. This structure can be analysed on different scales resulting in different properties depending on the size of the specimen examined. However, the material displays anisotropy and natural variation on all levels of structural organization (Bodig and Jayne, 1982).

The molecular basis

It is customary to divide wood into four different anatomical levels. From smaller to larger scale the levels are; micro, meso, macro and massive. The properties and structures in the different levels are naturally connected and thus interdependent. The subject of this thesis deals with the properties of wood on the massive scale but in order to fully understand these properties, the other anatomical levels must be touched upon (Dahl, 2009).

At the molecular level wood consists mainly of cellulose, hemicellulose and lignin. Cellulose is a natural polymer with the form of a long chain made up of glucose monomers. Cellulose can be arranged in crystalline or amorphous form where the crystalline form is impermeable to water whilst water can bond to the amorphous form. A cellulose molecule in wood contains both crystalline and amorphous parts. Hemicelluloses are a group of molecules. Like cellulose they are polymers but include a mixture of saccharide monomers. In contrast to cellulose hemicelluloses are low in cryistallinity and are made up of short chains of monomers. Lignin is a large and irregular molecule. The three types of molecules are assembled into a structure known as microfibril. It consists of a core of highly crystallized cellulose surrounded by a mix of non-crystalline cellulose and hemicelluloses which is in turn sheathed in a layer of lignin. The microfibril can be described as a fibre-composite where crystallized cellulose make up the fibre part, this is illustrated in Figure 2.1. The remaining non-crystallized cellulose, hemicellulose and lignin is analogous to a matrix. The fibre part provides tensile strength while the matrix provides stiffness (Dinwoodie, 1989).

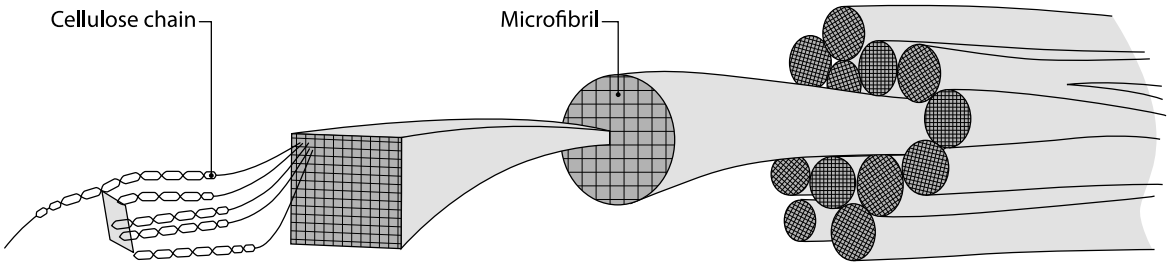

Figure 2.1: Structure and bundling of microfibril (SwedishWood, 2017a)(edited)

The cell

The microfibril is the building block of the microstructure of wood. On this anatomical level wood consists of cells mostly orientated in the axial direction of the stem. These cells can be described as fibres with a length of 2–6 mm (Burström, 2007). The axially oriented cells are called tracheids and make up 90%–95% of the volume. The tracheids are hollow tubes with a cross section shape that is roughly rectangular. The cell walls can be divided into two sections, the outer primary wall and the secondary wall that is further divided into three sublayers. The layers are defined by their chemical makeups and the orientation of the microfibril (Dahl, 2009). The primary wall consists of loosely packed randomly oriented microfibrils. The secondary wall consists of three layers, as seen in Figure 2.2, where the middle layer contributes the most to the mechanical properties of wood. It makes up to 85% of the wall thickness and its constituent microfibrils are orientated in a helical manner with an angle of approximately 10 degrees in relation to the axial direction of the cell. The middle layer of the secondary cell wall has a large influence on the mechanical properties of wood due to its thickness and structure. There are also other kinds of cells than the tracheids. Some are orientated radially with the function of transporting fluids and nutrients but these cells contribute negligibly to the mechanical properties of wood (Dinwoodie, 1989).

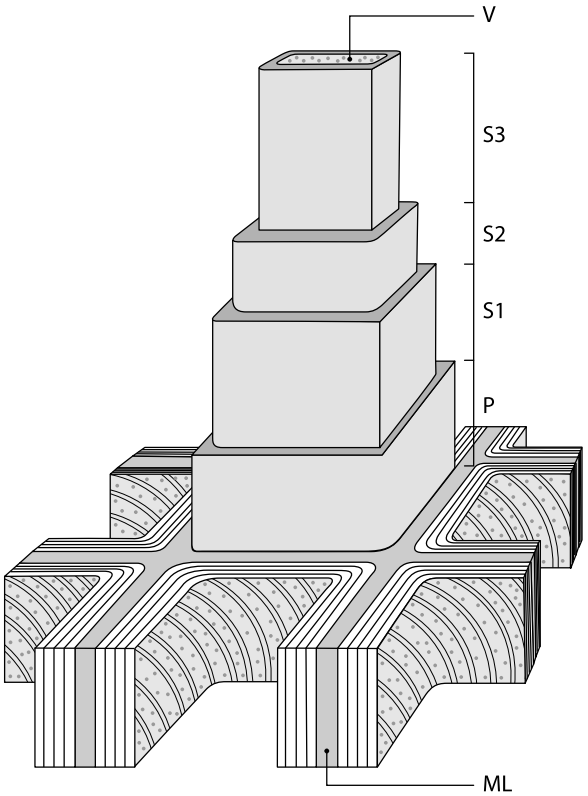

Figure 2.2: Cross section of wood fibre showing the different walls (SwedishWood, 2017a)(edited)

Meso, macro and massive scale

The structure of wood at the meso scale refers to the division of wood into bands known as earlywood and latewood. New wood cells are grown in the region just behind the bark known as the cambium. The growth is dormant during the winter, occurs at a fast rate during spring and slows down during the summer eventually stopping completely during autumn. The wood formed during the rapid growth period is known as earlywood. The cells of earlywood have thinner cell walls than the cells of the latewood. The density of earlywood is also lower than that of latewood. The growth cycle during one year creates the characteristic growth rings of dark and light regions. This structure can be seen in the cross section of a tree trunk as exemplified in Figure 2.3.

The macro scale refers to the scale at which the structure can be observed without a microscope. At this scale the different parts of the bark can be observed. The bark consists of an outer bark layer followed by the phloem and cambium. It is the cambium where the cell division occurs. Sap containing sugar is transported downwards through the phloem. The rest of the stem is called the xylem and contains the wood. The outer part of the xylem is referred to as sapwood, it transports water and nutrients upwards. The inner part is known as heartwood. The heartwood is technically dead meaning that it does not carry out metabolic processes. It is denser, has a lower water content and is darker in color. On the macro scale the annual rings can clearly be seen.

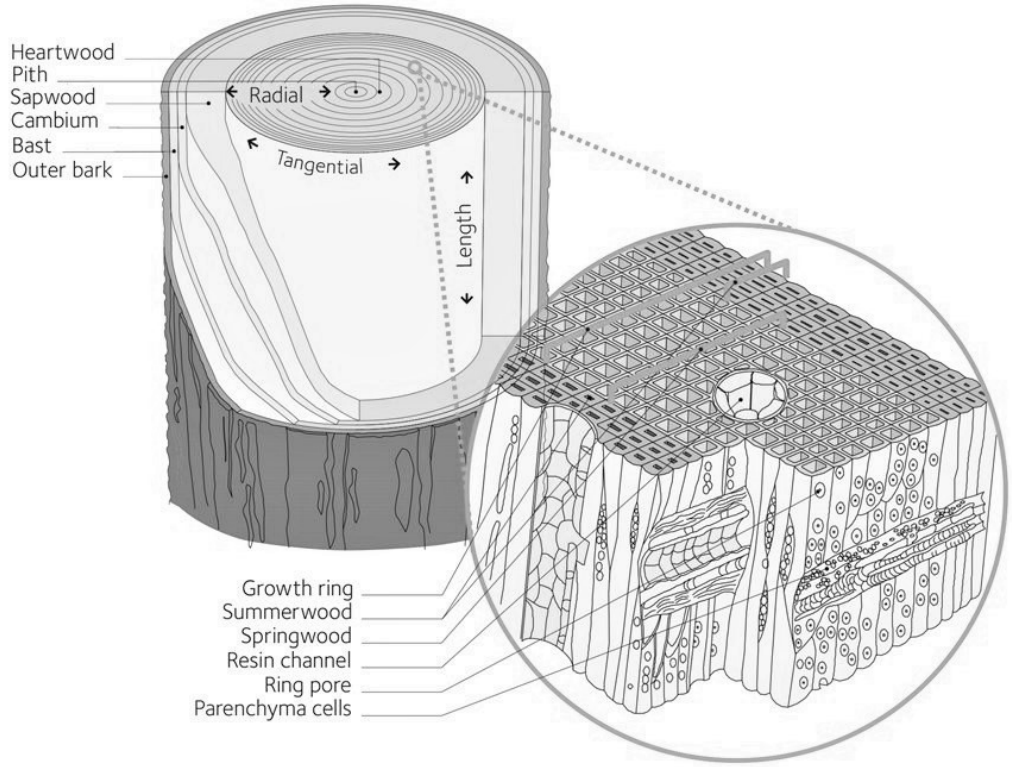

Figure 2.3: Composition of tree trunk detailing the annual rings (SwedishWood, 2017b)

It is the annual rings that determine the principle directions of wood. The directions are longitudinal, radial and tangential. Wood from coniferous trees exhibit vastly different strength and stiffness in the different directions. The stiffness in the longitudinal direction is 15–20 times higher than in the radial direction, and 20–30 times higher than in the tangential direction. An effect of the thin cell walls of the earlywood is a comparatively low shear stiffness in the radial-tangential plane, just 5% compared to the longitudinal stiffness in most softwood species. Another aspect of the macro scale is the direction of the wood fibre, also called the grain direction of the wood. It is normal for the grain to be aligned at angle within 4% to the axial direction of the tree. The phenomena known as spiral graining reduces the stiffness of lumber because lumber is sawed in relation to the direction of the stem, not the direction of the grain (Dahl, 2009).

There are many irregularities present in wood, the most serious one being knots. They are a result of the growth of branches that are then embedded into the growing stem. Knots decrease the strength and stiffness considerably. However the presence of knots can increase the shear capacity by preventing potential shear planes from forming and sliding relative to each other. A wood specimen that is completely free from irregularities is describes as clear wood. The properties of clear wood can be quantified precisely in absolute terms. For larger pieces of wood such as whole boards, the characteristic properties are often described in terms of a certain percentile from a large group of tested samples. The characteristic orhtotropic behaviour of wood is clearly a result of the highly directional structure at the macro level which is in turn a consequence of the submacro structures (Dahl, 2009).

The massive scale refers to wood specimens that are products of sawing or gluing with cross sectional dimensions typically larger than 100 mm. At this level the irregularities and heterogeneous nature of wood makes it impossible to describe the mechanical properties precisely because of the high amount of variation between specimens (Dahl, 2009). The material properties are therefore described using statistical definitions. Large amounts of specimens are tested and the properties are categorized according to percentiles. For design purposes, the characteristic values of strengths is decided from the fifth percentile. Hence, 95% of tested samples have a higher strength than the characteristic value (Isaksson et al., 2016).

In conclusion, it can be stated that wood has a complicated structure with different features depending on at which scale it is examined. The structure results in an orthotropic material with huge differences in strength and stiffness depending on the material orientation. It is a natural material with irregularities and a large range in material properties. In order to classify wood for structural purposes, wood needs to be graded and described by the use of statistical measures.

2.2 Orthotropy

Hooke's law describes the relationship between the stress σ and the strain ε. In the one-dimensional case Hooke's law is written as follows.

$$\sigma = E\varepsilon \tag{2.1}$$

The constant denoted as E, known as the elastic modulus or Young's modulus, describes the stiffness of the material. It describes how much stress is generated from strain. The corresponding equation for the three-dimensional state consists of a relationship between vectors with several stress and strain components, $\boldsymbol{\sigma}$ and $\boldsymbol{\varepsilon}$. A matrix known as the constitutive matrix, $\mathbf{D}$, is analogous to the elastic modulus and the relationship between stress and strain is given by the following expression.

$$\boldsymbol{\sigma} = \mathbf{D}\boldsymbol{\varepsilon} \tag{2.2}$$

The vectors and matrix have the following definitions.

$$\boldsymbol{\sigma} = \begin{bmatrix} \sigma_{11} \\ \sigma_{22} \\ \sigma_{33} \\ \sigma_{12} \\ \sigma_{13} \\ \sigma_{23} \end{bmatrix}; \quad \mathbf{D} = \begin{bmatrix} D_{11} & D_{12} & D_{13} & D_{14} & D_{15} & D_{16} \\ D_{21} & D_{22} & D_{23} & D_{24} & D_{25} & D_{26} \\ D_{31} & D_{32} & D_{33} & D_{34} & D_{35} & D_{36} \\ D_{41} & D_{42} & D_{43} & D_{44} & D_{45} & D_{46} \\ D_{51} & D_{52} & D_{53} & D_{54} & D_{55} & D_{56} \\ D_{61} & D_{62} & D_{63} & D_{64} & D_{65} & D_{66} \end{bmatrix}; \quad \boldsymbol{\varepsilon} = \begin{bmatrix} \varepsilon_{11} \\ \varepsilon_{22} \\ \varepsilon_{33} \\ \gamma_{12} \\ \gamma_{13} \\ \gamma_{23} \end{bmatrix} = \begin{bmatrix} \varepsilon_{11} \\ \varepsilon_{22} \\ \varepsilon_{33} \\ \varepsilon_{12} + \varepsilon_{21} \\ \varepsilon_{13} + \varepsilon_{31} \\ \varepsilon_{23} + \varepsilon_{32} \end{bmatrix} \tag{2.3}$$

The constitutive matrix is presented in the most general form where it contains 36 unique material parameters. In this form it is cumbersome to handle. It can be proved that if the strain energy of a given state only depends on the strain state, not the conditions that led to the strain state, the constitutive matrix is symmetric.

$$\mathbf{D} = \mathbf{D}^T \tag{2.4}$$

This reduces the number of unique material parameters to 21. This is called hyperelasticity. Through the use of symmetry, the constitutive matrix can be condensed in order to reduce the number of material parameters. They can be categorized depending on symmetry properties of the material. If there are no planes of symmetry, the material is said to be anisotropic and the constitutive matrix can not be reduced. The simplest form of symmetry consists of one symmetry plane. Next is two symmetry planes which inherently implies that there is a third symmetry plane. Three planes of symmetry is called orthotropy and is the relevant case for wood. There is also transverse isotropy meaning that the material has physical properties that are symmetrical around an axis that is the normal to a transverse plane. Within these planes the material is then isotropic. An isotropic material has an infinite number of symmetry planes meaning that it has the same physical properties in all directions (Ottosen and Petersson, 1992).

The constitutive matrix can be simplified through the use of symmetry planes through a relatively simple procedure. Matrices are expressed in an alternative coordinate system through transformation, which is done with transformation matrices.

$$\boldsymbol{\sigma}' = \mathbf{A}\boldsymbol{\sigma}\mathbf{A}^T \tag{2.5}$$

The transformation matrix, $\mathbf{A}$, is defined by the base vectors of the alternative coordinate system expressed in the old coordinate system. From the orthotropic case with three symmetry planes three transformation matrices can be set up.

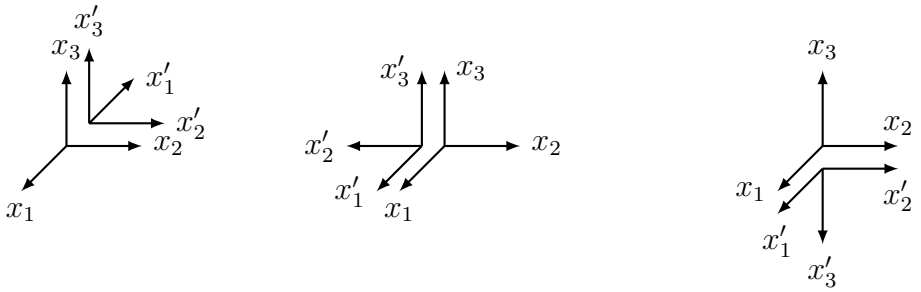

Figure 2.4: Figure showing the alternate coordinate systems in comparison to the original coordinate system

$$\mathbf{A}_1 = \begin{bmatrix} -1 & 0 & 0 \\ 0 & 1 & 0 \\ 0 & 0 & 1 \end{bmatrix} \qquad \mathbf{A}_2 = \begin{bmatrix} 1 & 0 & 0 \\ 0 & -1 & 0 \\ 0 & 0 & 1 \end{bmatrix} \qquad \mathbf{A}_3 = \begin{bmatrix} 1 & 0 & 0 \\ 0 & 1 & 0 \\ 0 & 0 & -1 \end{bmatrix} \tag{2.6}$$

The stress matrix is expressed in the alternative coordinate system using the transformation matrix A_3. Here the stress matrix is presented in matrix form as opposed to the condensed vector form.

$$\boldsymbol{\sigma}' = \begin{bmatrix} 1 & 0 & 0 \\ 0 & 1 & 0 \\ 0 & 0 & -1 \end{bmatrix} \begin{bmatrix} \sigma_{11} & \sigma_{12} & \sigma_{13} \\ \sigma_{21} & \sigma_{22} & \sigma_{23} \\ \sigma_{31} & \sigma_{32} & \sigma_{33} \end{bmatrix} \begin{bmatrix} 1 & 0 & 0 \\ 0 & 1 & 0 \\ 0 & 0 & -1 \end{bmatrix} = \begin{bmatrix} \sigma_{11} & \sigma_{12} & -\sigma_{13} \\ \sigma_{21} & \sigma_{22} & -\sigma_{23} \\ -\sigma_{31} & -\sigma_{32} & \sigma_{33} \end{bmatrix} \tag{2.7}$$

Comparing the two stress matrices the following identities are determined.

$$\sigma_{13}' = -\sigma_{13} \qquad \sigma_{23}' = -\sigma_{23} \tag{2.8}$$

$$\varepsilon_{13}' = -\varepsilon_{13} \qquad \varepsilon_{23}' = -\varepsilon_{23} \tag{2.9}$$

Equation (2.2) is applicable in the alternative coordinate system.

$$\boldsymbol{\sigma}' = \mathbf{D}\boldsymbol{\varepsilon}' \tag{2.10}$$

From equations (2.2) and (2.10) the following expressions are found.

$$\sigma_{11} = D_{11}\varepsilon_{11} + D_{12}\varepsilon_{22} + D_{13}\varepsilon_{33} + 2D_{14}\varepsilon_{12} + 2D_{15}\varepsilon_{13} + 2D_{16}\varepsilon_{23} \tag{2.11}$$

$$\sigma'_{11} = D_{11}\varepsilon'_{11} + D_{12}\varepsilon'_{22} + D_{13}\varepsilon'_{33} + 2D_{14}\varepsilon'_{12} + 2D_{15}\varepsilon'_{13} + 2D_{16}\varepsilon'_{23} \tag{2.12}$$

From the transformation, equation (2.7), it is known that $\sigma_{11} = \sigma'_{11}$. Combining equations (2.11), (2.12) and (2.9) the following expression holds true.

$$\begin{aligned} &D_{11}\varepsilon_{11} + D_{12}\varepsilon_{22} + D_{13}\varepsilon_{33} + 2D_{14}\varepsilon_{12} + 2D_{15}\varepsilon_{13} + 2D_{16}\varepsilon_{23} = \\ &D_{11}\varepsilon_{11} + D_{12}\varepsilon_{22} + D_{13}\varepsilon_{33} + 2D_{14}\varepsilon_{12} - 2D_{15}\varepsilon_{13} - 2D_{16}\varepsilon_{23} \end{aligned} \tag{2.13}$$

It is deduced from this expression that $D_{15} = 0$ and $D_{16} = 0$. When examining other components of the stress matrix in the same manner as above it is also found that $D_{25} = D_{26} = D_{35} = D_{45} = D_{46} = 0$. When this operation is done using one of the other transformation matrices additional elements of the constitutive matrix are found to be zero. This results in the constitutive matrix as shown below.

$$\mathbf{D} = \begin{bmatrix} D_{11} & D_{12} & D_{13} & 0 & 0 & 0 \\ D_{21} & D_{22} & D_{23} & 0 & 0 & 0 \\ D_{31} & D_{32} & D_{33} & 0 & 0 & 0 \\ 0 & 0 & 0 & D_{44} & 0 & 0 \\ 0 & 0 & 0 & 0 & D_{55} & 0 \\ 0 & 0 & 0 & 0 & 0 & D_{66} \end{bmatrix} \tag{2.14}$$

The above form of the constitutive matrix is characteristic of orthotropic materials.

2.3 Constitutive properties

An orthotropic material has six elastic moduli. Three describe the relationship between normal strain and stress in the principal directions. The other three describe the relationship between shear strain and stress in the orthotropic planes. The latter three are called shear moduli.

$$E_{11} \qquad E_{22} \qquad E_{33} \qquad G_{12} \qquad G_{13} \qquad G_{23} \tag{2.15}$$

These parameters enter the constitutive matrix and their exact position can be determined through some brief identification. For this purpose it is suitable to handle the inverted constitutive matrix known as the material compliance matrix, $\mathbf{C}$.

$$\mathbf{C} = \mathbf{D}^{-1} \tag{2.16}$$

Hooke's law can now be rewritten using the material compliance matrix.

$$\boldsymbol{\varepsilon} = \mathbf{C}\boldsymbol{\sigma} \tag{2.17}$$

Which in the expanded form is stated as:

$$\begin{bmatrix} \varepsilon_{11} \\ \varepsilon_{22} \\ \varepsilon_{33} \\ \gamma_{12} \\ \gamma_{13} \\ \gamma_{23} \end{bmatrix} = \begin{bmatrix} C_{11} & C_{12} & C_{13} & 0 & 0 & 0 \\ C_{21} & C_{22} & C_{23} & 0 & 0 & 0 \\ C_{31} & C_{32} & C_{33} & 0 & 0 & 0 \\ 0 & 0 & 0 & C_{44} & 0 & 0 \\ 0 & 0 & 0 & 0 & C_{55} & 0 \\ 0 & 0 & 0 & 0 & 0 & C_{66} \end{bmatrix} \begin{bmatrix} \sigma_{11} \\ \sigma_{22} \\ \sigma_{33} \\ \sigma_{12} \\ \sigma_{13} \\ \sigma_{23} \end{bmatrix} \tag{2.18}$$

The elements in the compliance matrix can be determined through experimental testing. However, it is not possible to apply strains individually. Due to the Poisson effect application of normal stress in one direction causes normal strains in the other principal directions. The strain parallel to the applied stress is called the active strain and the others the passive strains. The ratio of passive strain to active strain is defined as Poisson's ratio.

$$-\nu_{ij} = \varepsilon_{jj}/\varepsilon_{ii} \tag{2.19}$$

The indices denote between which principal directions the ratio is defined. Consequently six Poisson's ratios can be defined in the three-dimensional case.

$$\nu_{12} \qquad \nu_{13} \qquad \nu_{23} \qquad \nu_{21} \qquad \nu_{31} \qquad \nu_{32} \tag{2.20}$$

In a uniaxial loading test where stress is applied in one principal direction the strains that arise can be described with the use of equation (2.18). First for stress applied in the x_1 direction.

$$\varepsilon_{11} = C_{11}\sigma_{11} \qquad \varepsilon_{22} = C_{21}\sigma_{11} \qquad \varepsilon_{33} = C_{31}\sigma_{11} \tag{2.21}$$

The same applies in the other principal directions.

$$\varepsilon_{11} = C_{12}\sigma_{22} \qquad \varepsilon_{22} = C_{22}\sigma_{22} \qquad \varepsilon_{33} = C_{32}\sigma_{22} \tag{2.22}$$

$$\varepsilon_{11} = C_{13}\sigma_{33} \qquad \varepsilon_{22} = C_{23}\sigma_{33} \qquad \varepsilon_{33} = C_{33}\sigma_{33} \tag{2.23}$$

A similar test can be done to apply shear stress in each principal shear plane. The ratio between the shear strain and stress can be measured directly because only shear strain is produced when applying a shear stress.

$$\gamma_{12} = C_{44}\sigma_{12} \qquad \gamma_{13} = C_{55}\sigma_{13} \qquad \gamma_{23} = C_{66}\sigma_{23} \tag{2.24}$$

From measuring the slope of the stress-strain curve during testing the different elastic modulus are determined.

$$\begin{aligned} \frac{\sigma_{11}}{\varepsilon_{11}} &= E_{11} \qquad \frac{\sigma_{22}}{\varepsilon_{22}} = E_{22} \qquad \frac{\sigma_{33}}{\varepsilon_{33}} = E_{33} \\ \frac{\sigma_{12}}{\gamma_{12}} &= G_{12} \qquad \frac{\sigma_{13}}{\gamma_{13}} = G_{13} \qquad \frac{\sigma_{23}}{\gamma_{23}} = G_{23} \end{aligned} \tag{2.25}$$

A comparison between equations (2.25) and (2.21), (2.22), (2.23) and (2.24) yield the following identities.

$$\begin{aligned} E_{11} &= \frac{1}{C_{11}} \qquad E_{22} = \frac{1}{C_{22}} \qquad E_{33} = \frac{1}{C_{33}} \\ G_{12} &= \frac{1}{C_{44}} \qquad G_{13} = \frac{1}{C_{55}} \qquad G_{23} = \frac{1}{C_{66}} \end{aligned} \tag{2.26}$$

From this it can be concluded that the diagonal of the compliance matrix is made up of the elastic moduli. In order to identify the elements not on the diagonal the expression for Poisson's ratio is used. First equation (2.21) is substituted into (2.19) which yields the following results.

$$-\nu_{12} = C_{21}/C_{11} \qquad -\nu_{13} = C_{31}/C_{11} \tag{2.27}$$

The same is done with equations (2.22) and (2.23).

$$-\nu_{21} = C_{12}/C_{22} \qquad -\nu_{23} = C_{32}/C_{22} \tag{2.28}$$

$$-\nu_{31} = C_{13}/C_{33} \qquad -\nu_{32} = C_{23}/C_{33} \tag{2.29}$$

The diagonal elements of the compliance matrix are identified in equation (2.26) and can be substituted into the above equations in order to establish the following relationships.

$$\begin{aligned} C_{12} &= \frac{-\nu_{21}}{E_{22}} \qquad C_{13} = \frac{-\nu_{31}}{E_{33}} \qquad C_{23} = \frac{-\nu_{32}}{E_{33}} \\ C_{21} &= \frac{-\nu_{12}}{E_{11}} \qquad C_{31} = \frac{-\nu_{13}}{E_{11}} \qquad C_{32} = \frac{-\nu_{23}}{E_{22}} \end{aligned} \tag{2.30}$$

All elements in the compliance matrix have now been identified.

$$\begin{bmatrix} \frac{1}{E_{11}} & \frac{-\nu_{21}}{E_{22}} & \frac{-\nu_{31}}{E_{33}} & 0 & 0 & 0 \\ \frac{-\nu_{12}}{E_{11}} & \frac{1}{E_{22}} & \frac{-\nu_{32}}{E_{33}} & 0 & 0 & 0 \\ \frac{-\nu_{13}}{E_{11}} & \frac{-\nu_{23}}{E_{22}} & \frac{1}{E_{33}} & 0 & 0 & 0 \\ 0 & 0 & 0 & \frac{1}{G_{12}} & 0 & 0 \\ 0 & 0 & 0 & 0 & \frac{1}{G_{13}} & 0 \\ 0 & 0 & 0 & 0 & 0 & \frac{1}{G_{23}} \end{bmatrix} \tag{2.31}$$

As stated before, the compliance matrix is symmetric. This implies the following identities.

$$C_{21} = C_{12} \qquad C_{31} = C_{13} \qquad C_{32} = C_{23} \tag{2.32}$$

From the above identities it can be shown that only three Poisson's ratios are independent.

$$\frac{\nu_{12}}{E_{11}} = \frac{\nu_{21}}{E_{22}} \qquad \nu_{21} = \nu_{12}\frac{E_{22}}{E_{11}} \tag{2.33}$$

$$\frac{\nu_{13}}{E_{11}} = \frac{\nu_{31}}{E_{33}} \qquad \nu_{31} = \nu_{13}\frac{E_{33}}{E_{11}} \tag{2.34}$$

$$\frac{\nu_{32}}{E_{33}} = \frac{\nu_{23}}{E_{22}} \qquad \nu_{32} = \nu_{23}\frac{E_{33}}{E_{22}} \tag{2.35}$$

Should the above assumptions be accepted the symmetric compliance matrix that is expected for an orthotropic material is obtained.

$$\begin{bmatrix} \frac{1}{E_{11}} & \frac{-\nu_{12}}{E_{11}} & \frac{-\nu_{13}}{E_{11}} & 0 & 0 & 0 \\ \frac{-\nu_{12}}{E_{11}} & \frac{1}{E_{22}} & \frac{-\nu_{23}}{E_{22}} & 0 & 0 & 0 \\ \frac{-\nu_{13}}{E_{11}} & \frac{-\nu_{23}}{E_{22}} & \frac{1}{E_{33}} & 0 & 0 & 0 \\ 0 & 0 & 0 & \frac{1}{G_{12}} & 0 & 0 \\ 0 & 0 & 0 & 0 & \frac{1}{G_{13}} & 0 \\ 0 & 0 & 0 & 0 & 0 & \frac{1}{G_{23}} \end{bmatrix} \tag{2.36}$$

Matrix (2.31) is inverted in order to find the constitutive matrix.

$$\begin{bmatrix} \frac{1-\nu_{23}\nu_{32}}{E_{22}E_{33}\lambda} & \frac{\nu_{21}-\nu_{23}\nu_{31}}{E_{22}E_{33}\lambda} & \frac{\nu_{31}-\nu_{23}\nu_{32}}{E_{22}E_{33}\lambda} & 0 & 0 & 0 \\ \frac{\nu_{21}-\nu_{23}\nu_{31}}{E_{22}E_{33}\lambda} & \frac{1-\nu_{31}\nu_{13}}{E_{11}E_{33}\lambda} & \frac{\nu_{23}-\nu_{21}\nu_{13}}{E_{11}E_{33}\lambda} & 0 & 0 & 0 \\ \frac{\nu_{31}-\nu_{21}\nu_{32}}{E_{22}E_{33}\lambda} & \frac{\nu_{23}-\nu_{21}\nu_{13}}{E_{11}E_{22}\lambda} & \frac{1-\nu_{21}\nu_{12}}{E_{11}E_{22}\lambda} & 0 & 0 & 0 \\ 0 & 0 & 0 & G_{12} & 0 & 0 \\ 0 & 0 & 0 & 0 & G_{13} & 0 \\ 0 & 0 & 0 & 0 & 0 & G_{23} \end{bmatrix} \tag{2.37}$$

$$\lambda = \frac{1}{E_{11}E_{22}E_{33}}(1 - 2\nu_{21}\nu_{32}\nu_{13} - \nu_{13}\nu_{31} - \nu_{23}\nu_{32} - \nu_{12}\nu_{21}) \tag{2.38}$$

The principal directions can be translated to the principal directions for wood which, as stated before, is longitudinal, tangential and radial direction.

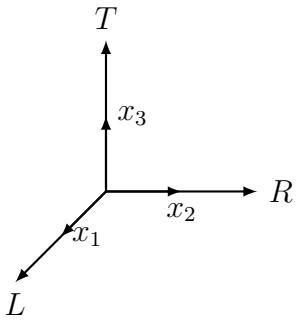

Figure 2.5: Description of the principal directions of wood relative to the coordinate sytem

$$1 = L \qquad 2 = R \qquad 3 = T \tag{2.39}$$

Whether the above identities can be directly applied to wood specimens depends on the orientation of the principal directions in the examined specimen. This in turn can depend on the location in the stem from which the piece of wood is taken, see further in Figure 2.6. Depending on this condition, the principal directions of different pieces of wood align to a rectangular orthotropic material coordinate system to varying degrees.

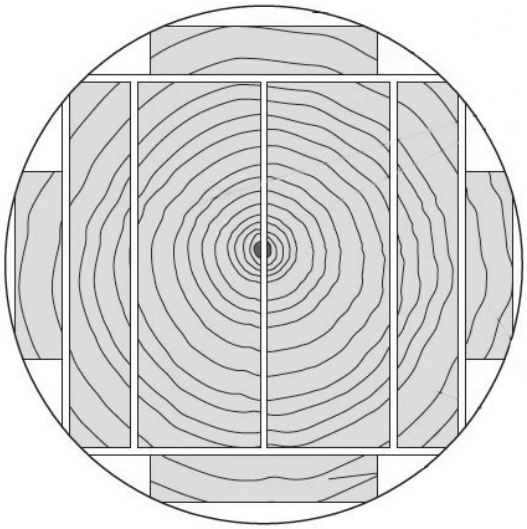

Figure 2.6: Figure showing how sawn pieces align with the principal directions of wood (SwedishWood, 2017c)

2.4 Strength of wood and engineering elastic parameters

As stated previously the strength of wood depends on the orientation of the stress in relation to the principal directions. It also depends on whether the stresses are tension or compression stresses. The purpose of this report is to analyse bending moment distributions, shear force distributions and deflections. In this regard it is interesting to deal with ultimate strength limits. The important factor is stiffness. The stiffness as expressed by the constitutive matrix is based on the elastic engineering parameters. For this report the following values have been chosen as they represent the mean values for C24 structural timber (Berg et al., 2019).

Table 2.1: Used values, Elastic and shear moduli

Elastic engineering parameters [MPa]					
E_{11}	E_{22}	E_{33}	G_{12}	G_{13}	G_{23}
11000	370	370	690	690	69

2.5 Cross laminated timber

Cross laminated timber is a composite building material consisting of at least three layers glued boards or planks. The layers are oriented perpendicular in relation to each other. The constituent timber is graded depending on quality and sorted into strength classes according to the European standard SS-EN 14081-1. At the present moment, there exists no industry wide standard for dimensions or strength classes for CLT elements. Each manufacturer has their own combinations of dimensions for the constituent boards and strength classes. Despite there being no official standard there are common dimensions and strength classes used. There are also common dimensions for the elements and common configurations of boards within them. In Tables 2.2 and 2.3 common values are given for dimensions and properties. In Table 2.3 the length refers to the length of an element during manufacture, in effect the maximum length.

Table 2.2: Common values for constituent boards

Parameter	Common	Available
Thickness, t_{board}	20 – 45 mm	20 – 60 mm
Width, b_{board}	40 – 200 mm	40 – 300 mm
Strength class	C14 – C30	–
Width to thickness ratio	4 : 1	–

Table 2.3: Common values for single elements during manufacture

Parameter	Common	Available
Height, $h_{element}$	80 – 300 mm	60 – 500 mm
Width, $w_{element}$	1.2 – 3.0 m	up to 4.8 m
Length $l_{element}$	16 m	up to 30 m
Number of layers	$3, 5, 7, 9$	up to 25

CLT elements are produced by gluing together boards lengthwise into longer boards through finger-jointing. The long boards are then placed together to form sheets, in some cases they are glued to each other. The sheets are finally pressed together into into the multilayered product. The composition of the layers can be customized. Thicker boards or boards with a higher strength grade can be used for the surface layers in which the stresses during common types of loading are the highest. In this way the strength and quality of the material can be utilized efficiently.

When evaluating the strength of wood, the natural variability of wood is taken into account. For CLT elements, the effect of this variation is lessened by what is called the system effect. Because the element consists of several individual boards the effect of the natural variation between boards is lessened. The result is that the characteristic strength in CLT elements is somewhat higher than in individual boards. The system effect is expressed in calculations through the use of the variable k_{sys} which is used when calculating the design strength (Borgström and Fröbel, 2017).

If a comparison is made between a component made out of CLT and an identical component made out of common structural timber, the variability in capacity between different specimens is less for the components made of CLT than for the components made out of solid structural timber. This is because CLT components include several boards combined together with different capacities and the risk that the weakest cross sections would coincide in the same direction and layer in the plate is small (Borgström and Fröbel, 2017).

No specific strength grades are defined for CLT elements and therefore the bending moment resistance can be increased in regards to the system effect by adopting a system effects factor k_{sys} into the capacity calculation. The value of k_{sys} differs between text books, but in this work the factor is determined according to the following conditions (Borgström and Fröbel, 2017):

$$k_{sys} = min\begin{cases} 1.15 \\ 1 + 0.1 b_{eff} \end{cases} \tag{2.40}$$

Where b_{eff} is the contributing element width in meters. In the future, specific strength classes for CLT elements may be developed in the same way as they exist for glued laminated timber products. This would replace the use of the factor k_{sys} (Borgström and Fröbel, 2017).

3 Structural modelling and analysis

In order to investigate the section forces and displacements in a CLT element, a model of some kind needs to be set up. To model a CLT plate, different methods can be applied with varying degrees of complexity and accuracy in the results. One simple modelling method is to use a beam grillage model which represents a simplification of the CLT element, and calculate the section forces and displacements in the constituent beams. This methodology is uncomplicated as only commonly used formulas are needed to calculate the section forces and displacements in the beams. The results may be difficult to translate in a suitable way to represent the section forces and displacements in the investigated CLT element. Another option when creating a model corresponding to the investigated CLT element is to create a finite element model. This option requires more complex calculations and is exclusively done using computer programs.

Also, the level of complexity in a finite element model can be adjusted based on how the model is created. To fully simulate the reality, a three-dimensional solid model can be created where all connections and contacts within the CLT element are modelled individually. This is a complex and demanding modelling methodology and requires not only a lot of time to create the model but also requires large computational power. To reduce the complexity but still doing a three-dimensional model, a three-dimensional shell model can be created instead. This reduces the complexity in the model, and thereby also the time consumption for creating and analysing the model but still getting accurate results in relation to reality. Creating a shell model instead of a full three-dimensional solid model means that the CLT element is only modelled as a plane model, implementing a composite layup feature to the model instead of creating a full three-dimensional solid model.

In this work, several calculations with different compositions and geometries have been evaluated. Therefore, the time consumption creating and analyzing the model is crucial and the critical factor when choosing methodologies for this project. Regarding this, a beam model representing a CLT plate originally described by Wallner-Novak et al. (2017) was initially set up and analyzed. A three-dimensional shell model with a composite layup was also implemented to be able to do a comparison between the results obtained using the different methods.

Different beam theories can be adopted to determine the section forces and displacements in a beam model. Each theory takes different properties into account which means that the different theories may end up with different results. Also, the different theories include various grades of complexity which means that the required time and knowledge may also differ between them. With these parameters in mind it is obvious that it is important to adopt a suitable method for the specific task. Here, three different approaches were adopted for the constituent beams; two-dimensional Bernoulli-Euler beam theory, two-dimensional Timoshenko beam theory as well as a three-dimensional Bernoulli-Euler beam model. In the three-dimensional model the connections between the different beams are modelled with the option of making the connections fully rigid.

The basis for the three different approaches chosen in this project to evaluate the beam grillage model involves different levels of consideration. In the first-mentioned approach, adopting Bernoulli-Euler beam theory, no consideration is taken to deformations due to shear strains in the beams. That because of the assumption made in this theory that plane sections remain plane and perpendicular to the beam axis during bending (Heyden et al., 2017). However, there is a way to estimate and thereby in a way consider the shear strains also in the Bernoulli-Euler beam theory. This is done by implementing a method called the Gamma method which adjusts the bending stiffness of a CLT element to take into account the shear deformations of transverse layers in an approximate manner, see Section 3.3.

In the second-mentioned approach where the Timoshenko beam theory is adopted, deformations due to shear strains are included in the model initially and no additional methods are required in this approach to consider shear strains (Borgström and Fröbel, 2017). In the third-mentioned approach the Bernoulli-Euler beam theory is adopted once again which implies the same reasoning about the shear strains as for the first approach is valid here. This means that the Gamma method is also adopted in this approach. However in this case the beam grillage is modelled as a structure composed of interconnected tree-dimensional beams and not as individual simply supported beams as done in the two first approaches presented. This entails that also the connections between the beams are modelled and enables the possibility of modelling a rigid connection between the beams.

3.1 Bernoulli-Euler beam theory

The primary assumptions made within the Bernoulli-Euler beam theory comprise that plane sections initially plane and perpendicular to the beam axis remain plane and perpendicular to the beam axis, meaning no shear deformation, during bending as well as the assumption that the beam deformation is small (Heyden et al., 2017).

The assumption that plane sections remain plane and perpendicular to the center line of the beam along the whole length of the beam is described in Figure 3.1 below. In the box below the beam in the figure, two examples are shown that do not conform to Bernoulli-Euler beam theory; the left figure shows a plane cross section but that is not perpendicular to the center line of the beam along the whole beam length. The cross section in the figure acts according to Timoshenko beam theory which is further described in Section 3.2. The right figure in the box illustrates a cross section that is neither plane nor perpendicular to the center line of the beam, this is permissible in neither Bernoulli-Euler nor Timoshenko beam theory (Heyden et al., 2017).

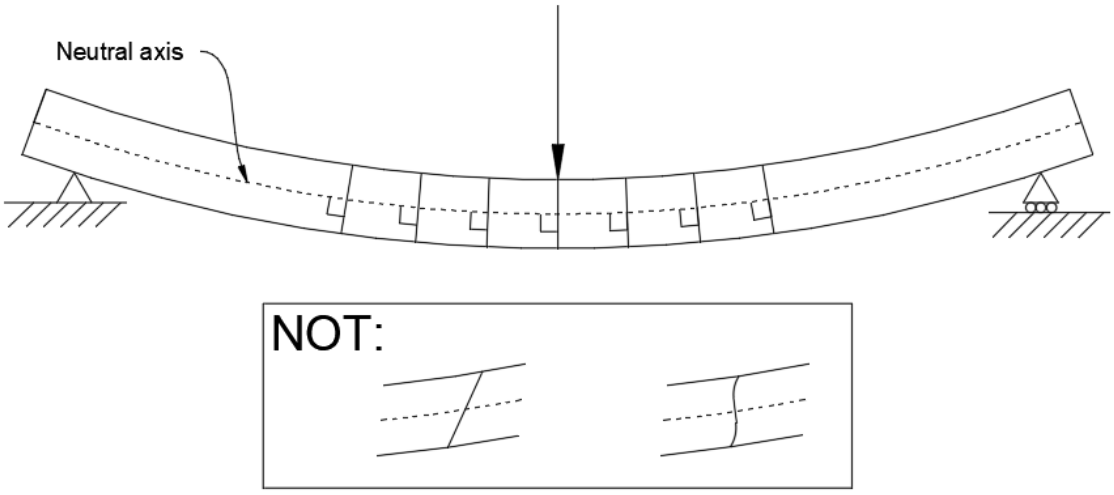

Figure 3.1: Illustration of the primary assumptions made in the Bernoulli-Euler beam theory

To calculate the section forces and displacements for a simply supported beam using Bernoulli-Euler beam theory commonly available equations may be used. For a simply supported beam loaded with a uniformly distributed load, referring to Figure 3.2, the following equations are adopted (Isaksson et al., 2016):

$$\begin{cases} M(x) = \dfrac{qLx}{2} - \dfrac{qx^2}{2} \\ V(x) = q\left(\dfrac{L}{2} - x\right) \\ v(x) = \dfrac{qL^3x}{24EI_{net}}\left(1 - 2\dfrac{x^2}{L^2} + \dfrac{x^3}{L^3}\right) \end{cases} \tag{3.1}$$

In the previous equations q denotes uniformly distributed load acting on a simply supported beam. L represents the length of the beam and x the position along the beam length where the bending moment $M(x)$, the shear force $V(x)$ and the deflection $v(x)$ are evaluated, see Figure 3.2. Beyond this, when determining the deflection the net moment of inertia I_{net} as well as the elastic modulus E are required for the cross section. Assuming a symmetrical cross section EI_{net} is calculated as follows:

$$EI_{net} = b \int_{-h/2}^{h/2} E(y) y^2 dy \tag{3.2}$$

and if E is constant throughout the cross section the relation can be rewritten to:

$$EI_{net} = E \frac{bh^3}{12} \tag{3.3}$$

where E is the constant elastic modulus in the cross section, b the width of the cross section and h its height.

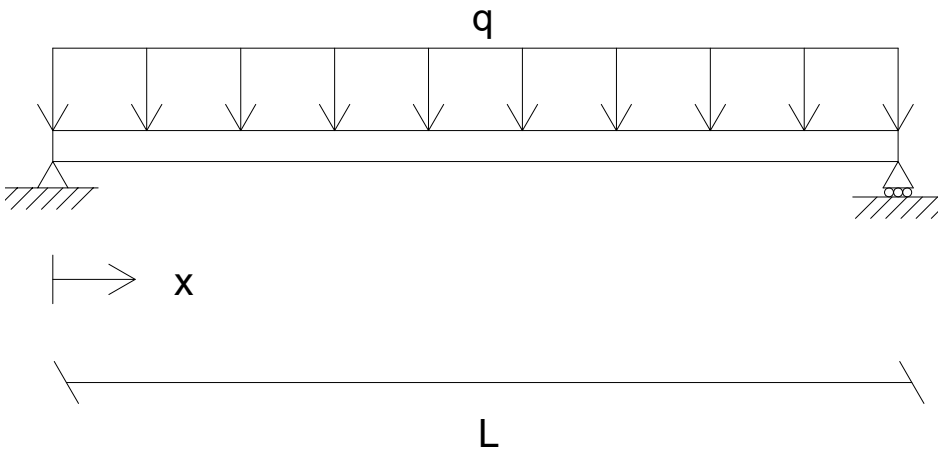

Figure 3.2: Load case for a simply supported beam loaded by a uniformly distributed load.

For a point load, arbitrarily positioned, acting on a simply supported beam the following equations are used to determine the section forces and deflection along the beam. Note that for the section forces different equations are used depending on which side of the point load the investigated section is located (Isaksson et al., 2016):

$$\begin{cases} M^{0-1}(x) = \dfrac{Pbx}{L} \\ M^{1-2}(x) = \dfrac{Pa(L-x)}{L} \\ V^{0-1}(x) = R_A = \dfrac{Pb}{L} \\ V^{1-2}(x) = -R_B = -\dfrac{Pa}{L} \\ v^{0-1}(x) = \dfrac{PLbx}{6EI_{net}}\left(1 - \dfrac{b^2}{L^2} - \dfrac{x^2}{L^2}\right) \\ v^{1-2}(x) = \dfrac{PLa(L-x)}{6EI_{net}}\left(\dfrac{2x}{L} - \dfrac{a^2}{L^2} - \dfrac{x^2}{L^2}\right) \end{cases} \tag{3.4}$$

In the previous equations P denotes the point load acting on the simply supported beam. The notation for L and x are the same as for the case with a uniformly distributed load. The lengths a and b denote the distance between the left, and right, support to the point load, see Figure 3.3. The indices $0-1$ and $1-2$ represent the part of the beam between the left support and the point load, and between the right support and the point load, respectively. The bending moment is denoted by M, the shear force by V and the deflection by v as in previous equations. Additionally, the net moment of inertia I_{net} as well as the elastic modulus E are needed to determine the deflection.

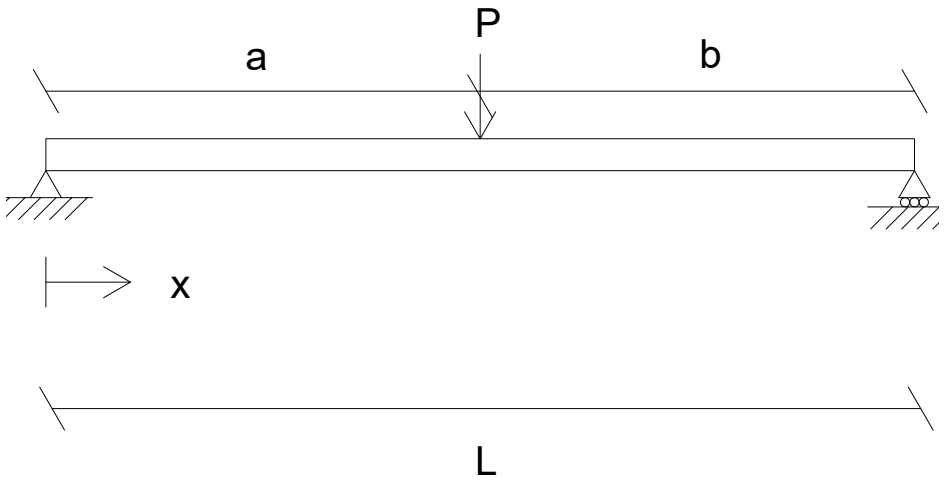

Figure 3.3: Load case for a simply supported beam loaded by an arbitrary placed point load.

The net moment of inertia, I_{net}, for the above equations is calculated using the parallel axis theorem, presented below. Note that the net moment of inertia is calculated per meter width of the plate, to easier relate results from the beam model with results from models of entire CLT plates.

$$I_{net} = \sum \frac{t_i^3}{12} + \sum t_i a_i^2 \tag{3.5}$$

Where t_i is the thickness of the respective layer and a_i is the distance between the center of each layer and the neutral axis of the CLT plate, see illustration in Figure 3.4. As seen in the figure each layer is rotated 90 degrees in-plane, in relation to the adjacent layers.

Depending on which axis the bending moment acts around, matching moment of inertia must be used in calculations regarding deflection. The stiffness of the layers in the transversal direction in relation to the examined face, is neglected. Only the stiffness of the layers in the longitudinal direction are accounted for in the calculations of the net moment of inertia. This means that for bending moment around the y-axis layers 1, 3 and 5 are accounted for in the net moment of inertia calculation. Likewise, for bending moment around the x-axis layers 2 and 4 are accounted for, see Figure 3.4.

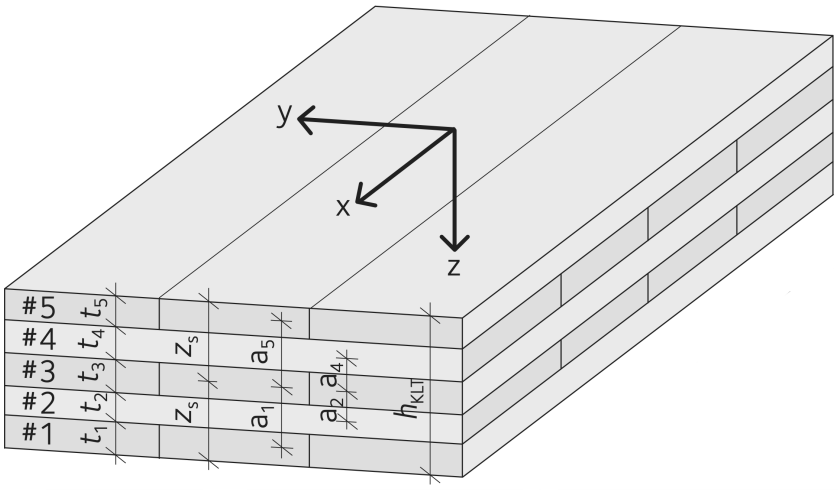

Figure 3.4: Illustration of the current directions and dimensions used to determine the net moment of inertia (Borgström and Fröbel, 2019)

3.2 Timoshenko beam theory

Timoshenko beam theory describes bending of a beam accounting for shear strains. Hence, Timoshenko beam theory accounts for deflections in a beam in a more realistic way compared to Bernoulli-Euler beam theory. This is especially true in the case of high and/or composite beams where shear deformation can constitute a considerable part of the total deformation.

Although, better precision comes with the price of more complex calculations. Complexity is added by the fact that Timoshenko beam theory is based on two independent variables, the deflection, v, and the rotation, Θ. This fact entails more complicated boundary conditions which increases the complexity of the calculations.

For beams that are tall in relation to their length, or composite beams, it is reasonable to implement Timoshenko beam theory because neglecting the shear deformation can lead to inaccurate results in these cases. CLT elements are composite elements where the layers exhibit varying shear flexibility depending on the material direction. Therefore, the shear strains present in the elements are significant and should not be neglected.

The derivation of the expressions to determine the deflections using Timoshenko beam theory begin at the constitutive relations which are derived from the equilibrium state together with the section forces. The section forces derived from the displacement, are in turn used to derive the relations presented below.

$$\begin{cases} N(x) = \int_A \sigma dA \\ M(x) = \int_A -y\sigma dA \\ V(x) = \int_A \tau dA \end{cases} \tag{3.6}$$

Where $N(x)$, $M(x)$ and $V(x)$ are the normal force, bending moment and shear force respectively. As no residual stresses are present in the current case, the integrated stresses are given by solely the material properties according to:

$$\begin{cases} \sigma = E\varepsilon = E(u' - y\Theta') \\ \tau = G\kappa\gamma = G\kappa(v' - \Theta) \end{cases} \tag{3.7}$$

which inserted into equation (3.6) gives the following relations:

$$\begin{cases} N(x) = \int_A \sigma dA = EAu' \\ M(x) = \int_A -y\sigma dA = EI\Theta' \\ V(x) = \int_A \tau dA = GA\kappa(v' - \Theta) \end{cases} \tag{3.8}$$

In the previous equations G denotes the shear stiffness and κ the shear correction factor. Calculations of the shear stiffness and shear correction factor are presented later in this chapter. ε denotes the normal strain and γ denotes the shear strain. A represents the cross section area and y denotes the vertical distance from the center of mass of the cross section. The variables u, v as well as Θ represent two displacements, vertical and normal directions, as well as rotation. E denotes the elastic modulus and I denotes the moment of inertia. σ denotes the normal stress and τ the shear stress.

Insertion of the expressions for the section quantities into the equilibrium equations, give the following expressions presented below. There, q_x and q_y represent the external load working in the longitudinal and transversal direction of the beam, respectively, and m the bending moment per meter beam width.

$$\begin{cases} EAu'' = -q_x \\ GA\kappa(\nu'' - \Theta') = -q_y \\ EI\Theta'' + GA\kappa(v' - \Theta) = -m \end{cases} \tag{3.9}$$

Six boundary conditions are required to solve for the displacements in the system of equations. Defining these six boundary conditions results in the following relations for the displacement of a beam according to Timoshenko beam theory. The displacements u, Θ and v are prescribed directly upon solution. For known loads (static boundary conditions) the below stated relations can be used.

$$\begin{cases} u' = N/EA \\ \Theta' = M/EI \\ (v' - \Theta) = V/GA\kappa \end{cases} \tag{3.10}$$

As the complete detailed derivation of the Timoshenko beam theory is not within the scope of this project a reference to alternative literature is made for more in-depth derivations. It can also be mentioned that the Timoshenko beam theory converges towards the Bernoulli-Euler beam theory if the shear modulus is increasing towards infinity and the rotational inertia is negligible.

In order to implement Timoshenko beam theory when evaluating CLT beams, certain cross section parameters are needed. These include the shear correction factor, κ, and the effective shear stiffness for the cross section, G_{eff} (Borgström and Fröbel, 2017). For a CLT beam these cross section parameters are calculated for both the longitudinal direction and the transversal. S_{CLT} denotes the shear stiffness of the CLT cross section.

$$\kappa = \frac{\left(\sum \left(EI + EAa_i^2\right)\right)^2}{\sum G_i b_{beam} t_i \int_h \frac{S^2(y)E^2(y)}{G(y)b_{beam}(y)} dy} \tag{3.11}$$

$$S_{CLT} = \kappa \sum G_i b_{beam} t_i \tag{3.12}$$

$$G_{eff} = \kappa \sum G_i = \frac{S_{CLT}}{\left(\sum b_{beam} t_i\right)} \tag{3.13}$$

3.3 Gamma method

In Bernoulli-Euler beam theory the presence of shear strain is neglected. Thus, the calculated deflection of a beam using this beam theory is under-estimated. To improve results from the Bernoulli-Euler beam theory the so-called Gamma method can be used (Borgström and Fröbel, 2017).

The Gamma method is detailed in Eurocode 5. It is an approximate method for evaluating the deformation caused by shear flexibility in the transverse layers of the CLT element. Implementation of the method is simple for 3- and 5-layer elements but in the case of elements consisting of more than five layers a more in-depth calculation is required (Borgström and Fröbel, 2017).

The Gamma method introduces an effective moment of inertia, I_{eff}, that can be used when calculating deflections. The effective moment of inertia constitutes a simplified way to take the contribution of shear deformations into account. The method is applicable without modifications for elements with three or five layers. It works by introducing a reduction factor, γ, in the parallel axiom theorem. The contribution from shear deflections depend on the length of the examined beam so a reference length, l_{ref} is used. The reference length differs depending on the support conditions of the beam. For a simply supported beam the reference length equals the actual length. For a continuous beam with at least two spans the reference length is achieved by reducing the actual length by 20 percent. For a cantilever beam the reference length equals twice the actual length (Borgström and Fröbel, 2017).

Three layered element

Layers are numbered from the bottom up. The gamma values for each layer in the longitudinal direction is calculated. The transverse layers are neglected.

$$\gamma_1 = 1 \tag{3.14}$$

$$\gamma_3 = \frac{1}{1 + \frac{\pi^2 t_3}{l_{ref}^2} \cdot \frac{t_2}{G_{9090}}} \tag{3.15}$$

Where l_{ref} is the reference length mentioned previously and t_2 and t_3 represent the thickness for layer 2 and 3, referring to Figure 3.5 below. Finally, G_{9090} denotes the rolling shear modulus. The shear that occurs in the R-T-plane of wood, see equation (2.39) and Table 2.1 in Chapter 2.

Using the above calculated gamma values, the distances from the center of the element to the center of each longitudinal layer is calculated. At first, the distance to layer 1 is calculated as shown below, note that the parameter $w_{element}$ denotes the plate width and is set to one meter, meaning that the effective stiffness is calculated per meter width of the CLT plate. As with t_2 and t_3, t_1 denotes the thickness of layer 1, referring to Figure 3.5.

$$a_1 = \frac{\gamma_3 w_{element} t_3 (\frac{t_1}{2} + t_2 + \frac{t_3}{2})}{\gamma_1 w_{element} t_1 + \gamma_3 w_{element} t_3} \tag{3.16}$$

Using the distance to layer 1 previously calculated, the distance to layer 3 is calculated in a simpler way shown below.

$$a_3 = \frac{t_1}{2} + t_2 + \frac{t_3}{2} - a_1 \tag{3.17}$$

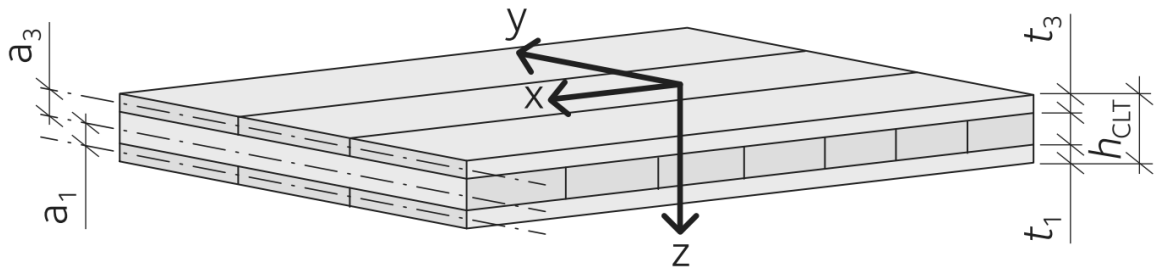

Figure 3.5: Figure showing the direction convention when using the gamma method (Borgström and Fröbel, 2019)

The effective moment of inertia is then calculated using the parameters calculated above together with the thickness of each individual layer.

$$I_{eff} = \frac{w_{element} t_1^3}{12} + \gamma_1 t_1 a_1^2 + \frac{w_{element} t_3^3}{12} + \gamma_3 t_3 a_3^2 \tag{3.18}$$

Five layered element

The calculation steps are similar for a five layered element as for a three layered element shown above. The same notation is used, t_1, t_2 and t_3 denotes the thickness of each individual layer, in this case a fourth and fifth layer is added and thereby also the parameters t_4 and t_5. The thickness of each individual layer is illustrated in Figure 3.6 below. The rest of the parameters used to calculate the gamma values are identical with the three layered case.

$$\gamma_1 = \frac{1}{1 + \frac{\pi^2 t_1}{l_{ref}^2} \cdot \frac{t_2}{G_{9090}}} \tag{3.19}$$

$$\gamma_3 = 1 \tag{3.20}$$

$$\gamma_5 = \frac{1}{1 + \frac{\pi^2 t_5}{l_{ref}^2} \cdot \frac{t_4}{G_{9090}}} \tag{3.21}$$

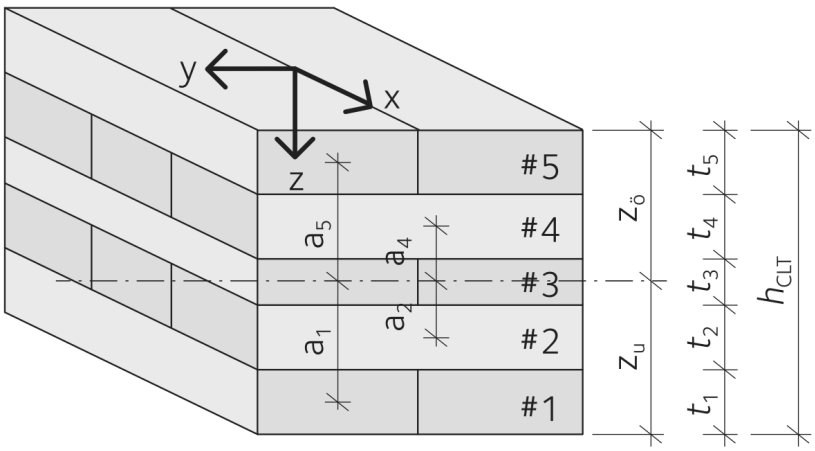

Figure 3.6: The different layers and distances for five layered CLT element (Borgström and Fröbel, 2017)

Using the three calculated gamma values the distances a_1, a_2 and a_3 can then be calculated.

$$a_3 = \frac{\gamma_1 w_{element} t_1 (\frac{t_1}{2} + t_2 + \frac{t_3}{2}) - \gamma_5 w_{element} t_5 (\frac{t_3}{2} + t_4 + \frac{t_5}{2})}{\gamma_1 w_{element} t_1 + \gamma_3 w_{element} t_3 + \gamma_5 w_{element} t_5} \tag{3.22}$$

$$a_1 = \frac{t_1}{2} + t_2 + \frac{t_3}{2} - a_3 \tag{3.23}$$

$$a_5 = \frac{t_3}{2} + t_4 + \frac{t_5}{2} + a_3 \tag{3.24}$$

Finally, the effective moment of inertia for a five layered element is calculated using the parameters calculated above.

$$I_{eff} = \frac{w_{element} t_1^3}{12} + \gamma_1 t_1 a_1^2 + \frac{w_{element} t_3^3}{12} + \gamma_3 t_3 a_3^2 + \frac{w_{element} t_5^3}{12} + \gamma_5 t_5 a_5^2 \tag{3.25}$$

Note that the above equations are valid for elements where all layers have the same material parameters.

3.4 Beam grillage method

The simplification proposed to evaluate CLT plates with openings consist of setting up a grillage of simply supported beams. The beam model used and evaluated in this project is developed by Wallner-Novak et al. (2017) and is described further in this chapter. The accuracy and correctness of the results obtained from this model compared to a real CLT plate is not documented in Wallner-Novak et al. (2017) more than that it is a conservative approach. The beam model includes six beams in total. The model in whole is presented in Figure 3.7.

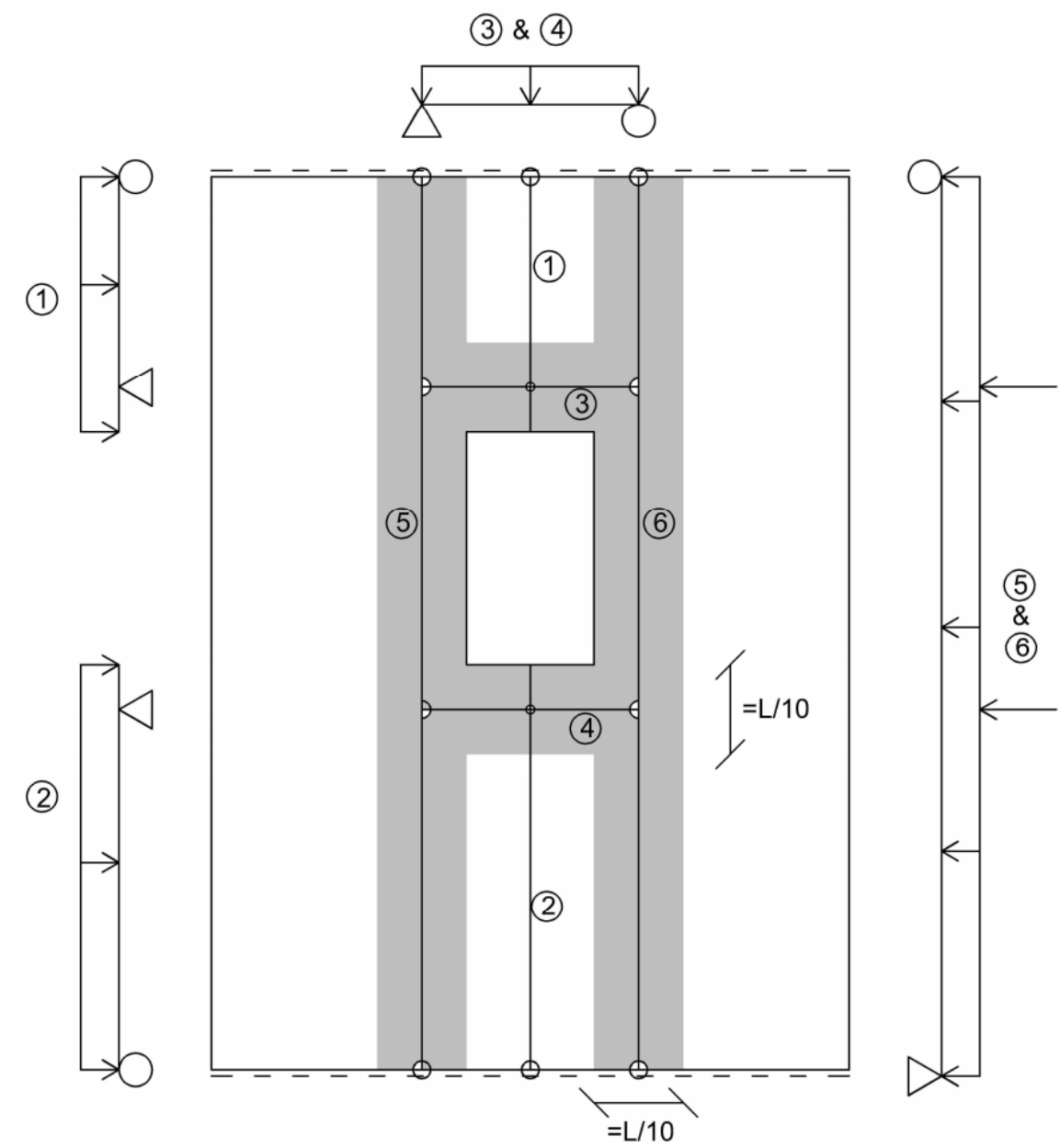

Figure 3.7: Illustration of the beam grillage model (Wallner-Novak et al., 2017).

In Figure 3.7, L denotes the span or length of the CLT plate while the gray shaded area illustrates the fictive beam widths of the beams included in the grillage model.

Beam 1 and 2 are used to calculate the load on beam 3 and 4. According to the model, beam 1 rests upon beam 3. The reaction force exerted by the supporting beam 3, on beam 1 resting on it, can be calculated using common static mechanics. This reaction force is applied to the supporting beam 3 as a uniformly distributed line load that acts per meter along the beam length. Beam 3 and 4 are in turn supported by beams 5 and 6. The reaction forces are applied as point loads on beams 5 and 6. Additionally, beam 5 and 6 are also loaded with the surface load acting on the plate element. The purpose of beam 1 and 2 is thereby solely to determine the load acting on beams 3 and 4. Section forces, capacity and deflection are therefore not calculated for beams 1 and 2. Beams 3 and 4 act as simply supported beams subjected to distributed load. Beams 5 and 6 also act as simply supported beams with distributed loads with the addition of two point loads generated from beam 3 and 4. According to the model, beam 5 and 6 will be loaded identically regardless of the position of the hole (assuming that the position of the hole fulfills certain criteria to enable the model to work) because the grillage model is inherently symmetrical.

The section forces are easily calculated with the assumption that the beams are simply supported. The moment of inertia for the beams can be calculated using the gamma method. It is then important to remember that beams 3 and 4 are oriented perpendicular to beams 5 and 6 resulting in a different moment of inertia. Generally the plate element will be placed so that the strong direction is aligned with the long side of the plate. This means that beams 5 and 6 will be stiffer and have larger bending moment capacity than beams 3 and 4.

Wallner-Novak et al. (2017) claims that an opening which surface area is smaller than 10% of the plate's total surface area does not need to be evaluated specifically in addition to the checks done on a plate with no opening. Obviously, the claim concerning solely the area of the opening does not hold true for all situations. An opening running across the entire width of a plate and nine percent of the length would meet the stated requirements but cut the plate into two pieces.

In order to be used, the grillage model implies certain requirements that comes with the model layout. The assembly of beams replacing the cross laminated timber element results in certain requirements to fulfill to even be able to set up this type of beam model. In the model, the beam width is set to the length of the strong direction of the plate divided by ten as an engineering approximation. As the layout of this beam model requires that there are beams on all sides of the hole this entails the requirement that the hole cannot be placed closer than one beam width from any of the plate edges. This is a weakness of this model as holes at the edges of floor elements, also called recesses or notches, cannot be analyzed properly using this model.

Recesses or notches are commonly used when designing connections between elements and the possibility to analyze these situations are crucial when designing buildings (Borgström and Fröbel, 2017).

The grillage model also assumes hinged connections between the different beams in the model which entails that phenomena such as torsion are ignored. This is an assumption that further pushes the model away from the real case, as a plate element with a larger hole is in fact experiencing torsional moments near the hole (Wallner-Novak et al., 2017).

3.5 Implementation of three-dimensional beams

A way to consider torsion in the model and possibly get a more accurate result similar to the real case, is to evaluate the grillage model as a three-dimensional beam system using three-dimensional beam elements. Doing this will enable the design of the connection between the beams in the grillage model. This implies that it becomes possible to make the connections between beams rigid and thereby enable transfer of bending moments and torsion between the beams in the model. Using three-dimensional beam elements means that more degrees of freedom are defined, for this case 6 degrees of freedom are defined for each node in the system. A reference is made to Figure 3.8 for an illustrative description of how the different degrees of freedom are defined in each node.

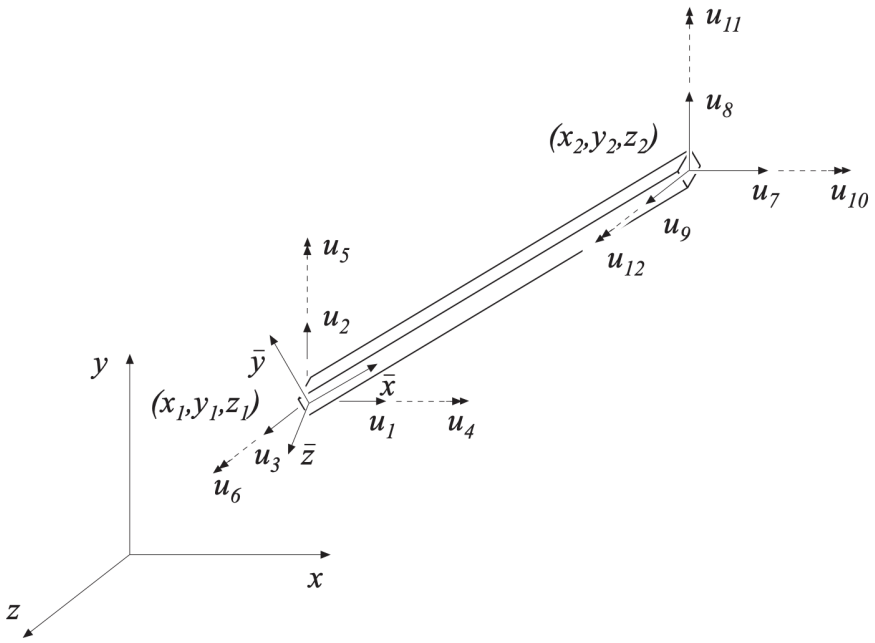

Figure 3.8: The degrees of freedom for a three-dimensional beam (Austrell et al., 2004)

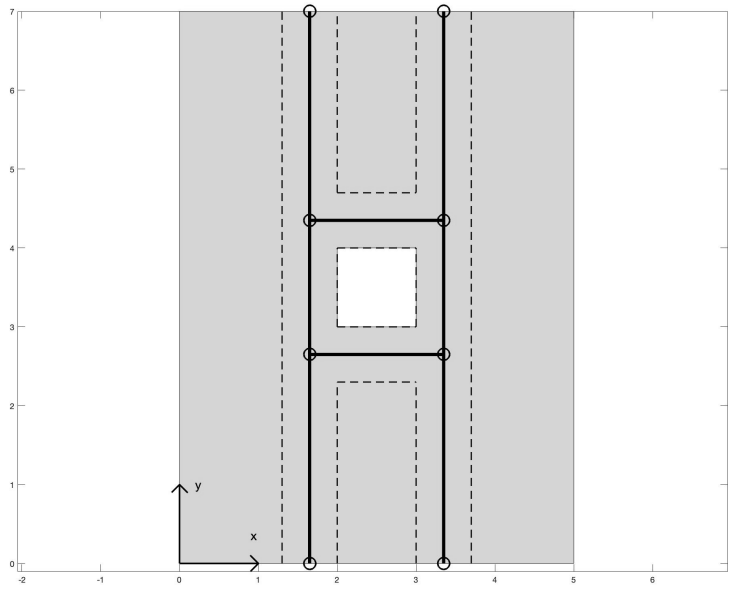

Figure 3.9: Illustration of the nodes defined for the 3D beam system

One node is placed in every point where a beam element begins or ends as well as in every point connecting the elements to each other. In Figure 3.9 the defined nodes in the grillage model are marked with a circle, a total of eight nodes are defined for this beam system. This results in a model consisting of eight individual elements, each of these going between two of the nodes, see Figure 3.9.

By setting up this beam system and defining two sets of topology matrices and boundary conditions, one for the free and one for the rigid connection between the beams, the system can be evaluated for both cases. The influence of torsion can thereby be considered and evaluated properly by changing the connection to rigid between the beams and investigate the change in results. For the case with rigid connections, moment is transferred between the beams. However, for the case with hinged connections duplicate degrees of freedom are required for the rotations about the global y-axis, see Figure 3.9. This results in a total of 48 degrees of freedom in the system with restrained connections and 52 degrees of freedom for the free connection.

In order to calculate the section forces and displacements for the three-dimensional model, the global stiffness matrix $\mathbf{K}$ and load vector $\mathbf{f_l}$ must be determined. The element stiffness matrix $\mathbf{K^e}$ and load vector $\mathbf{f_l^e}$ are determined for each individual element and then assembled into one global stiffness matrix and load vector. See Appendix A.1 for the complete standard formulation of the system and the solution for determining the global stiffness matrix and load vector (Austrell et al., 2004).

With the stiffness matrix and load vector determined for the system they can then be used for determining the global displacement vector for the system. This is done by solving the following system of equations (Austrell et al., 2004):

$$\mathbf{Ka} = \mathbf{f} \tag{3.26}$$

By extracting the element displacements from the global displacement vector for the system the section forces and displacements can be determined in local directions along the beam elements included in the model (Austrell et al., 2004).

The complete calculations are presented in Appendix A.2 and finally arrives in the following expressions for the different section forces (Austrell et al., 2004):

$$\begin{aligned}
N &= EA\frac{d\bar{u}}{d\bar{x}} & V_{\bar{y}} &= -EI_{\bar{z}}\frac{d^3\bar{v}}{d\bar{x}^3} & V_{\bar{z}} &= -EI_{\bar{y}}\frac{d^3\bar{w}}{d\bar{x}^3} \\
T &= GI_{tor}\frac{d\bar{\varphi}}{d\bar{x}} & M_{\bar{y}} &= -EI_{\bar{y}}\frac{d^2\bar{w}}{d\bar{x}^2} & M_{\bar{z}} &= EI_{\bar{z}}\frac{d^2\bar{v}}{d\bar{x}^2}
\end{aligned} \tag{3.27}$$

These section forces are determined for arbitrarily chosen positions on the respective beams in the model. Due to this fact, complete moment and shear force distribution diagrams can be plotted for all the included beams which are then compared with the results obtained from the two-dimensional beam analyses.

When implementing three-dimensional CLT beams into the model the torsional stiffness I_{tor} must be evaluated.

$$I_{tor} = k_{tor} c_1 \frac{h_{element}^3 w_{element}}{3} \tag{3.28}$$

Where the factor k_{tor} depends on whether gaps and cracks are present in the CLT plate according to:

$$k_{tor} = \begin{cases} 0.65 \text{ for CLT with gaps and cracks present} \\ 0.8 \text{ for CLT without gaps and cracks present} \end{cases} \tag{3.29}$$

The factor c_1 is calculated by using an estimated relation depending on the thickness of the CLT plate, $h_{element}$ and the width of the plate, $w_{element}$ (Borgström and Fröbel, 2017).

$$c_1 = 1 - 0.63 \frac{h_{element}}{w_{element}} + 0.052 \left(\frac{h_{element}}{w_{element}} \right)^5 \tag{3.30}$$

3.6 Capacity

The results obtained from the different methods and theories contain bending moment and shear force as well as deflection. To check if the absolute values of these results are acceptable, criteria are needed to verify the capacity. The limit value for the deflection in the plate is set to a chosen magnitude collected from for instance Eurocode where $L/250$ to $L/300$ are commonly used magnitudes for floors (Isaksson et al., 2016). However, for the bending moment and shear force, the capacity depends on the element lay-up and material strength values of the investigated CLT plate. Therefore, the evaluation of the limit values regarding bending moment and shear force in the plate requires particular calculations for each specific case.

3.6.1 Bending moment capacity

The characteristic bending moment capacity for the CLT plate is determined using the following formula (Borgström and Fröbel, 2017):

$$M_r = W_{net} k_{sys} f_{mk} \tag{3.31}$$

The net bending resistance W_{net} of the plate is calculated by (Borgström and Fröbel, 2017)

$$W_{net} = \frac{I_{net}}{z_s} \tag{3.32}$$

with I_{net} according to equation (3.5) and z_s denoting the distance between the bottom edge to the neutral axis of the CLT cross section.

As all the results obtained for the section forces are calculated as forces per meter width of the plate, the width b in these equation are set to one meter accordingly (Borgström and Fröbel, 2017).

The system effects factor k_{sys} is determined based on the conditions described in equation (2.40) where b_{eff} is the contributing width of the plate measured in metres. As the width of the beams included in the grillage model described previously is set to 0.7 m for this investigation it is assumed to also be a reasonable estimation of the contributing width of the beams in the grillage model. However, for the plate in whole, analyzed in the finite element model, the contributing width of the element is more complex to define without more ground to it. Regarding this uncertainty, the most reasonable and safe choice to make is to neglect the increase in strength due to the system effects in the plate. This entails that for this particular case the system effect factor k_{sys} is set to 1.0.

For the characteristic strength, f_{mk}, different values may be applied depending on the quality of the wood used to construct the CLT board. In this work an assumption is made that the wood quality is a structural timber of type C24 which yields a characteristic strength f_{mk} equal to 24 MPa, but other qualities may be adopted instead (Borgström and Fröbel, 2017).

3.6.2 Shear force capacity

To determine the characteristic shear force capacity for a CLT plate, two cases are considered, longitudinal and rolling shear. For longitudinal shear, referring to Figure 3.10, the characteristic capacity is determined using the following formula (Borgström and Fröbel, 2017):

$$V_{\bar{x}\bar{z},r} = \frac{f_{vk,090} I_{x,net} b_x}{S_{x,net}} \tag{3.33}$$

Where $I_{x,net}$ is the net moment of inertia of the plate and $S_{x,net}$ is the net static moment around the $\bar{y}$-axis, see Figure 3.10. The characteristic longitudinal shear strength $f_{vk,090}$ for the plate depends on the strength class of the boards. The width b_x denotes the width of the cross section perpendicular to the x-axis, referring to Figure 3.10.

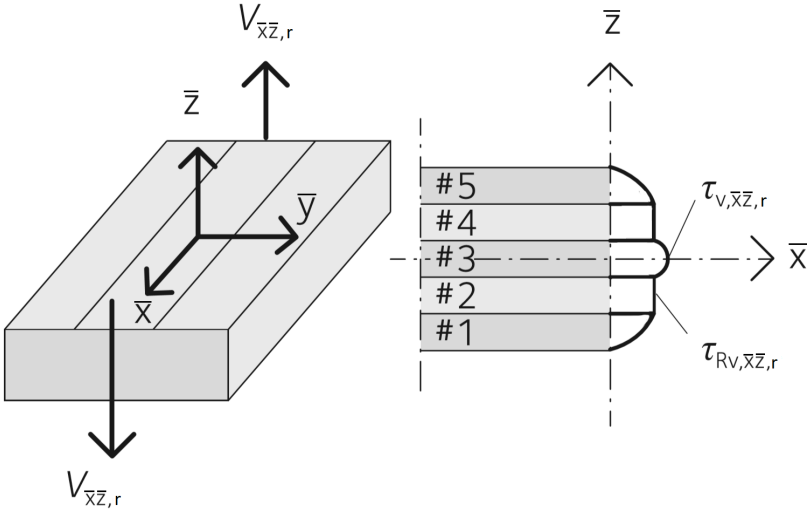

Figure 3.10: Illustration of longitudinal shear (Borgström and Fröbel, 2019)(edited)

For rolling shear, referring to Figure 3.11, the characteristic capacity is determined using the following formula (Borgström and Fröbel, 2017):

$$V_{\bar{y}\bar{z},r} = \frac{f_{vk,9090} I_{y,net} b_y}{S_{y,net}} \tag{3.34}$$

Where $I_{y,net}$ is the net moment of inertia of the cross section and $S_{y,net}$ is the net static moment around the x-axis, see Figure 3.11. The characteristic rolling shear strength $f_{vk,9090}$, for C24, is equal to 1.1 MPa. The width b_y denotes the width of the cross section perpendicular to the x-axis, referring to Figure 3.10, and is set to one meter.

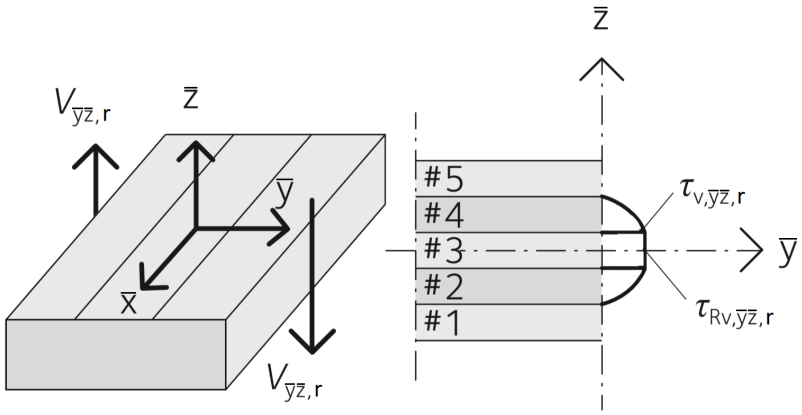

Figure 3.11: Illustration of rolling shear (Borgström and Fröbel, 2019)(edited)

The net moment of inertia is calculated using the parallel axis theorem. However, for the net static moment per meter plate width the following formulas are used to determine their magnitude (Borgström and Fröbel, 2017).

If the center of gravity for the CLT plate is placed within the currently considered layer:

$$S_{net} = \sum_{i=1}^{k_L} t_i a_i + \frac{\left(\frac{t_{k_L}}{2} - a_{k_L}\right)^2}{2} \tag{3.35}$$

If the center of gravity for the CLT plate is not placed within the currently considered layer:

$$S_{net} = \sum_{i=1}^{k_L} t_i a_i \tag{3.36}$$

Where k_L denotes the longitudinal layer closest to the center of gravity of the plate, a_{k_L} is the distance from the neutral axis of the CLT plate to the center of gravity of this layer and t_{k_L} its thickness. The parameter a_i is the distance between the center of the current layer and the neutral axis of the CLT plate. The parameter t_i denotes the thickness of the current layer.

For the beam model described in previous sections, different capacities are obtained in the different beams since they are directed either in the plate's longitudinal (strong) or transverse (weak) direction. For the beams directed in the longitudinal direction of the plate a larger capacity is obtained than for the beams directed in the transverse direction (Borgström and Fröbel, 2017).

4 Finite element model

A finite element (FE) model of a CLT plate with an opening was set up using the computer program Abaqus. The results from the finite element model contain values of section forces and displacements. Results from the FE-analyses were then compared with the results from the beam grillage, from which results were calculated according to the theories and methods described in Chapter 3. The project aims at investigating different geometries for openings in the CLT plate element. The variations in geometry such as placement and size of the opening required the use of a parametric Python script. Such a script was written and used to create and analyze the model in Abaqus. Using a python script, for creating and analysing the finite element model, provided a simple way of changing the geometry by the means of fast alterations in python code. It also enabled loops to be implemented, which is perfect for changing different parameters automatically in between iterations. The method provided the basis for conducting the parameter study that analyses the different parameters individually.

4.1 Generation of the model

The finite element model was generated by initially creating a part with a certain geometry and assigning properties corresponding to CLT. For this a three-dimensional shell element was used. At first the model is generated with an arbitrary geometry. In order to model the distinct layers of CLT that have different global fiber directions, the three-dimensional shell element was created using a composite layup consisting of 5 layers. This results in a three-dimensional shell element with a layup consisting of five different layers, assigned separate fiber directions, where each layer has orthotropic material properties. It is also possible to define the thickness of each layer individually which enables the use of different layer thicknesses in the CLT element.

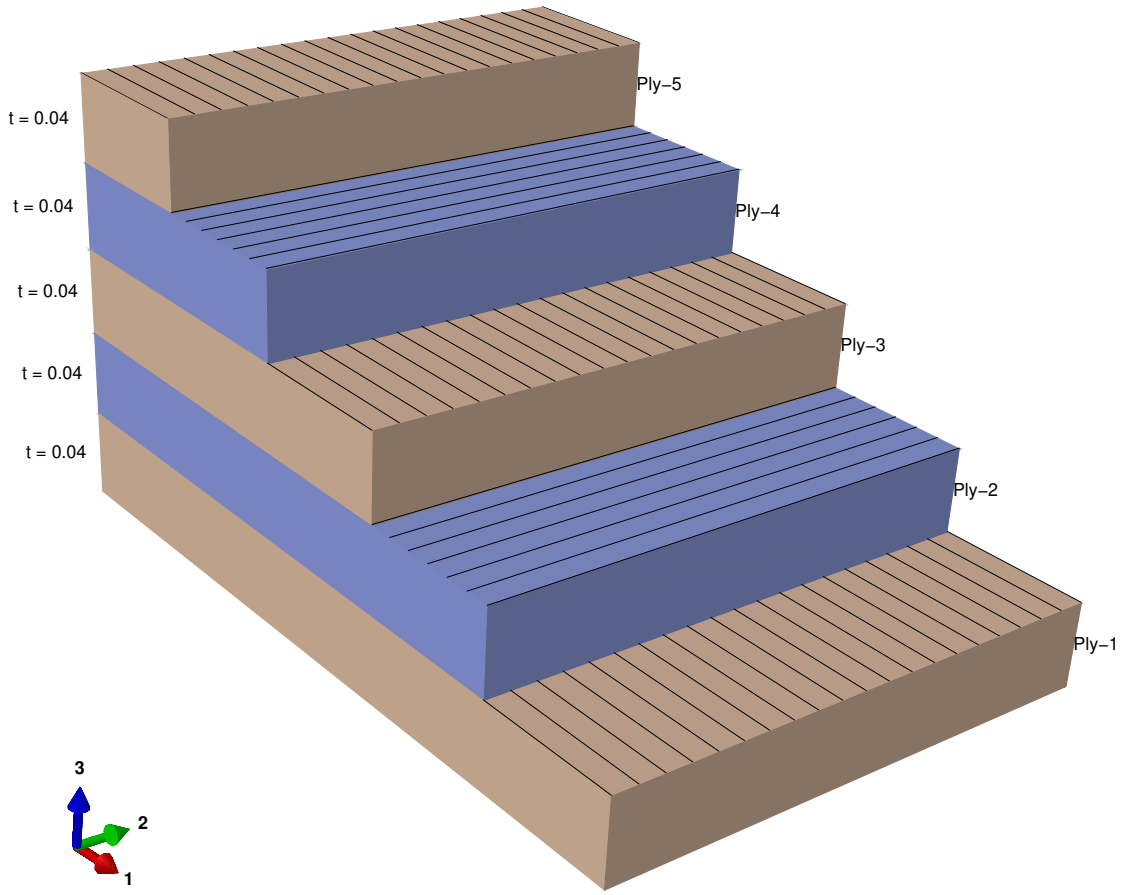

Figure 4.1: Composite layup of finite element model

The resulting composite layup created in Abaqus is presented in Figure 4.1. As can be read in the figure the outer layers as well as the middle layer were assigned fiber directions parallel to axis 1 in reference to the global directions in Figure 4.1. Layers 2 and 4 were assigned fiber directions parallel to axis 2 in reference to the global directions.

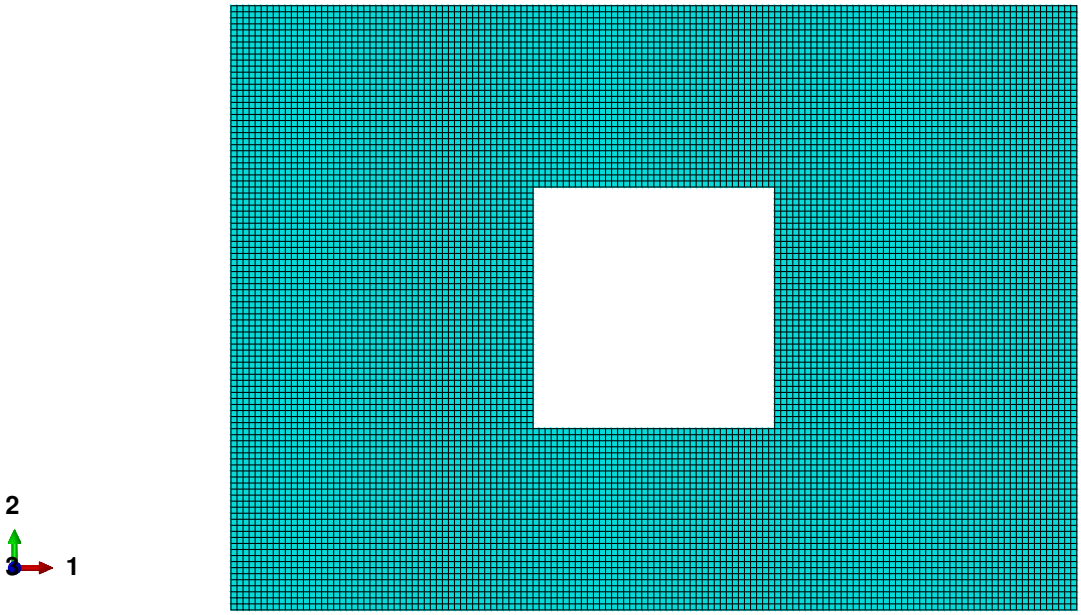

Figure 4.2: A meshed FE-model with corresponding global coordinate system

The load case was modelled by applying a load to the surface, and boundary conditions to the edges. In this case a surface pressure of 4 kN/m^2 was applied in the negative 3-direction. The boundary conditions were designed as a pinned support for one of the edges along the plate width and a rolled support for the other. The boundary conditions corresponding to the different supports were established by prescribing the displacements u_1, u_2 and u_3 as well as the rotations ur_1, ur_2 and ur_3, related to the coordinate system shown in Figure 4.2. For the pinned support the displacements and rotations were prescribed as follows:

$$\begin{gathered} u_1 = 0 \qquad u_2 = 0 \qquad u_3 = 0 \\ ur_1 = 0 \qquad ur_3 = 0 \end{gathered} \tag{4.1}$$

For the rolled support the following displacements were prescribed:

$$u_2 = 0 \qquad u_3 = 0 \tag{4.2}$$

The mesh was created so that section forces and deflections can be evaluated in each individual element. To create a structured and symmetric mesh, the plate is partitioned into several parts before meshing. Through partitioning and using square elements a mesh consisting of evenly lined up square elements can be applied to the model creating an orderly mesh.

Examples of results from models generated in Abaqus are shown in Figure 4.3 and Figure 4.4. In the first picture bending moment is illustrated. In Abaqus the bending moments are denoted SM1 and SM2, this corresponds to M_{yx} and M_{xy} in the notation described further in Chapter 5. SM1 is the moment that generates normal stress parallel to coordinate axis 1 and SM2 generates normal stress parallel to axis 2. The shear force denoted as SF4 and SF5 correspond to V_{yz} and V_{xz}. SF4 acts on the section facing in the direction of coordinate axis 1 and SF5 acts on the section facing in the direction of coordinate axis 2.

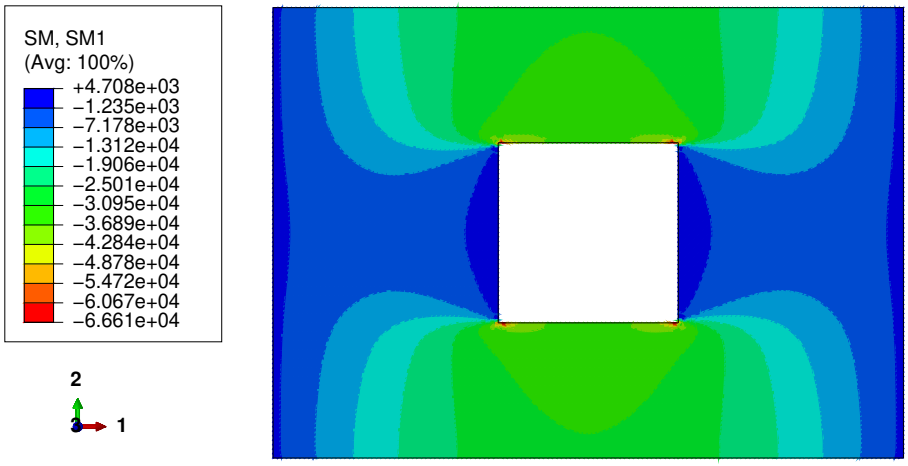

(a) Bending moment, SM1 distribution in the CLT plate.

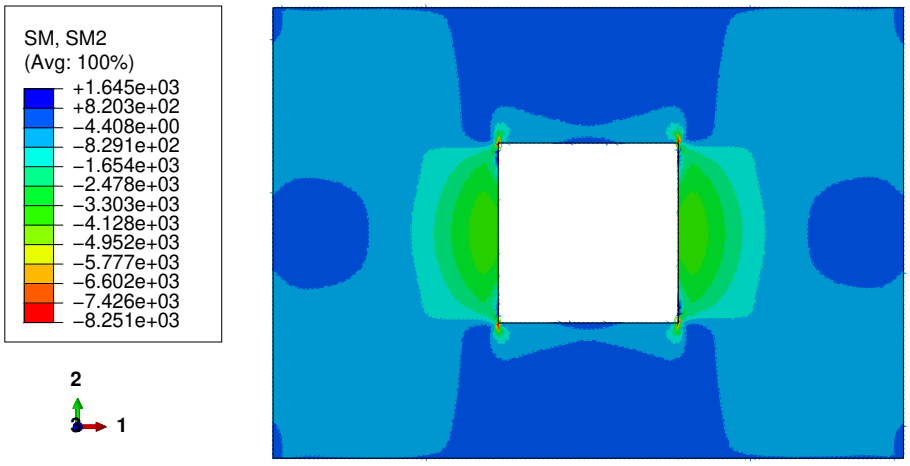

(b) Bending moment, SM2 distribution in the CLT plate.

Figure 4.3: Example of results obtained from Abaqus

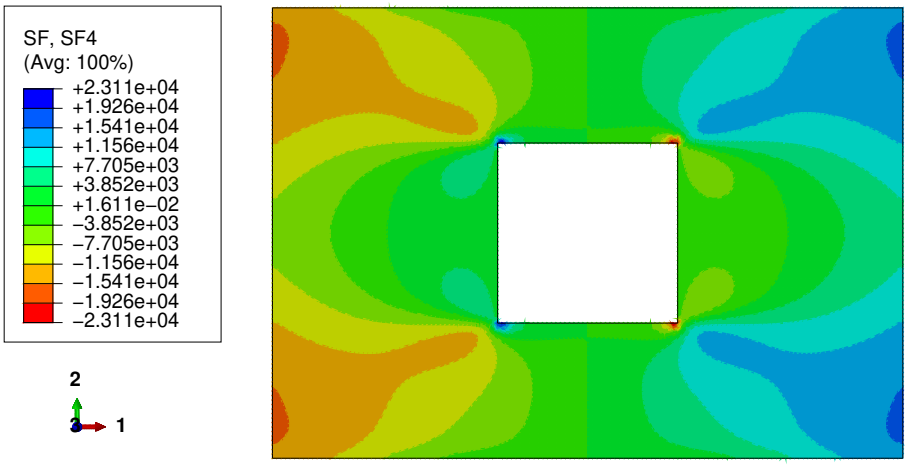

(a) Shear force, SF4 distribution in the CLT plate.

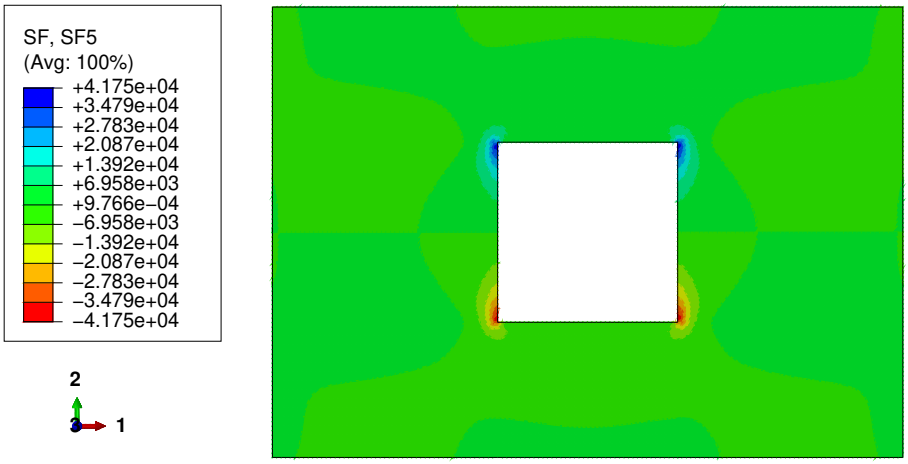

(b) Shear force, SF5 distribution in the CLT plate.

Figure 4.4: Example of results obtained from Abaqus

4.2 Evaluation of results

Results were obtained from every individual node in the model which means that thousands of individual data points were obtained from one simulation. As this process is repeated many times in a parameter study, the amount of data obtained from Abaqus becomes extensive.

In order to extract the sought results in terms of cross section forces and deflection in Abaqus, paths were set up in the model from which the results are collected and saved in text files. These paths were defined so that they coincide with the beams in the beam grillage model described in Section 3.4. Several paths were created, these include paths corresponding to the center lines of the beams, paths corresponding to the edges of the beams and transverse paths across the widths of the beams. The purpose of the transverse paths included was to evaluate the distribution across the beam widths at a number of sections.

Along the paths, data can be obtained, saved and then exported into text files which can be read by other programs. In this manner the results from Abaqus can be compared with the ones obtained from the beam model in a fairly seamless way.

An illustration of the paths created in Abaqus to collect the relevant data are shown in Figure 4.5a. The correspondence between the paths created in Abaqus and the beams in the studied beam model can be seen by comparing the paths in Figure 4.5a with the beam model illustrated in Figure 4.5b.

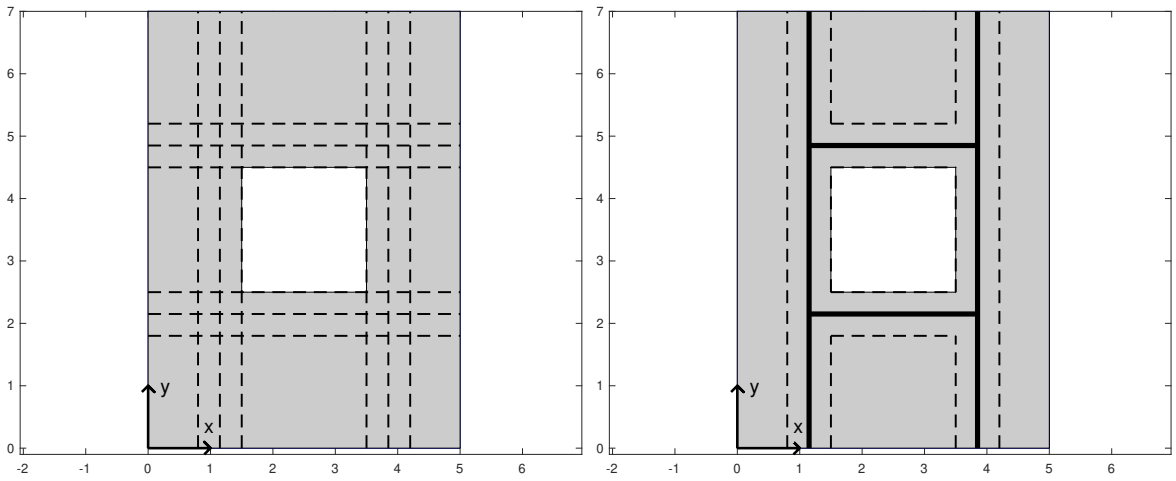

(a) Paths created in Abaqus corresponding to the beams in the grillage model.

(b) Grillage beams representing the CLT plate.

Figure 4.5: Illustration of the correspondence between the paths created in Abaqus and the beams included in the grillage model.

5 Comparison between grillage model and finite element model

It is relevant to evaluate the results from different models in order to identify similarities and differences. In this chapter, the different beam theories described in Chapter 3 are used for the grillage model and the results compared. When comparing beam theories deflection is an interesting quantity to compare. The stiffness is calculated differently depending on the beam theory used which is reflected in the deflection. It is also relevant to compare the difference in stiffness between a cross section generated in a finite element model and analytical beam models. Lastly a comparison between the grillage model and the finite element model is relevant in order to identify key differences. The models are compared in terms of bending moment, shear force and deflection.

It is also of interest to examine different compositions of layer thickness in CLT plates. This chapter introduces three compositions which are examined to identify key differences when applying the different beam theories to the cross sections.

5.1 Element layups

In this section the three different compositions of CLT are described. All three have a total thickness of 200 mm. The compositions differ in how the total thickness is distributed among the five layers.

The first composition is called *Composition - Equal distribution* and is used as the reference composition consisting of five 40 mm thick layers.

An investigation of the impact of using thicker outer layers in the strong direction of the CLT plate is done with the second composition evaluated. This second composition is called *Composition - Longitudinal distribution* and consists of outer layers with a thickness of 70 mm each and intermediate layers of thickness 20 mm each. This type of CLT plate, with significantly thicker outer layers is evaluated since it is commonly used in the industry as it is an cost efficient way to increase the stiffness in the strong direction of the CLT plate using small amount of material.

Also, a third composition is investigated where the transversal layers (directed in the weak direction of the CLT plate) is made thicker than the other layers. This to try get a more equal stiffness relation between the longitudinal and transversal direction of the CLT plate. This third composition is called *Composition - Transversal distribution* and contains significantly thicker transversal layers compared to the longitudinal ones. The composition consists of transversal intermediate layers with a thickness of 70 mm each and outer as well as intermediate longitudinal layers of thickness 20 mm each, all together creating a CLT plate of thickness 200 mm. The composition from top-to-bottom is described as $20-70-20-70-20$ mm with the outer layers oriented in the longitudinal direction of the CLT plate. In Figure 5.1 the three different investigated compositions are illustrated with the distributions drawn in scale.

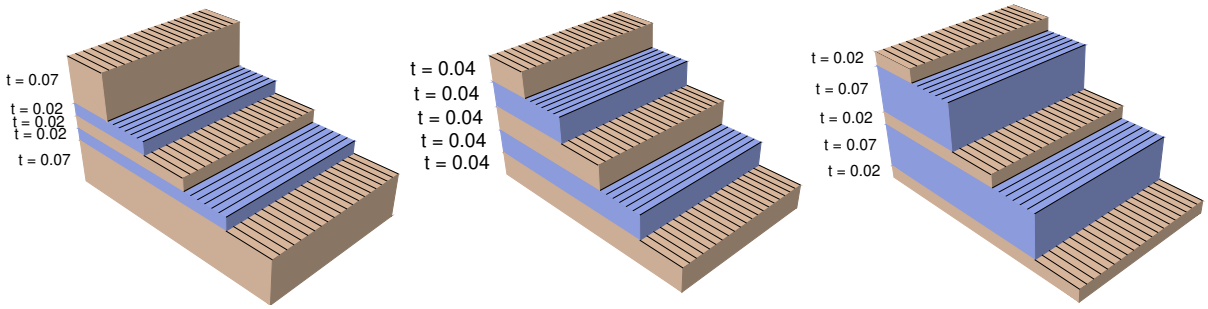

(a) Composition - Longitudinal distribution (70-20-20-20-70)

(b) Composition - Equal distribution (40-40-40-40-40)

(c) Composition - Transversal distribution (20-70-20-70-20)

Figure 5.1: Illustration of the different compositions used in this work

5.1.1 Material parameters

The material parameters used represent the characteristic values of structural timber of strength class C24. The notations reflect the direction in reference to the fibre direction of wood. Hence, E_0 describes the elastic modulus parallel to fibre direction. In the used notation G_{090} applies to longitudinal shear and G_{9090} to rolling shear. The values are presented in Table 5.1.

Table 5.1: Material parameters

Parameter	Value
E_0 [MPa]	11 000
E_{90} [MPa]	370
G_{090} [MPa]	690
G_{9090} [MPa]	69
ν_{090} [-]	0
ν_{900} [-]	0
ν_{9090} [-]	0

.

5.1.2 Cross section parameters

The following sections deal with bending moment and shear force. The bending moment and shear force are denoted using notations similar to the notation used in plate theory. However, the notation used in this work differs slightly from conventional plate theory, which can also vary between different authors and sources. In this work, M_{xy} denotes the bending moment per unit length around the y-axis that cause normal stresses in the x-direction, this bending moment is thereby valid for beams which cross section facing in the x-direction. The notation for cross section properties are derived from the notation for the section forces. Hence, I_{xy} refers to the moment of inertia for cross sections facing in the x-direction regarding moment around the y-axis. In this chapter the x-axis is parallel to the supported edges of the CLT plate, meaning that the x-axis is parallel to the short side and the y-axis to the long side of the CLT plate.

Three different beam theories are used to analyse the beams in the grillage model: two-dimensional Bernoulli-Euler, two-dimensional Timoshenko and three-dimensional Bernoulli-Euler. When using Bernoulli-Euler beam theory the Gamma method is used to calculate the effective moment of inertia. The moment of inertia derived using the Gamma method is denoted as effective moment of inertia, such as $I_{xy,eff}$.

For Timoshenko beam theory and capacity calculations, the net moment of inertia $I_{xy,net}$ is used. The net moment of inertia is calculated by ignoring the layers whose fiber direction is parallel to the evaluated cross section plane and only considering the layers whose fiber direction is directed perpendicular to the plane coinciding with the cross section surface, referring to Chapter 3. This is a conservative approach but since the transversal layers contributes to such a small amount of the total strength the simplification is reasonable. The cross section parameters are presented in Table 5.2 on the next page. The effective moment of inertia calculated with the Gamma method is dependent on the beam length. For beams 3 and 4 the beam length depends on the opening geometry. Hence the effective moment of inertia, $I_{xy,eff}$, changes with opening geometry. In Table 5.2 values for a centrally positioned 2×2 m^2 opening are presented.

Table 5.2: Cross section parameters

Parameter	Longitudinal composition (70-20-20-20-70)	Equal composition (40-40-40-40-40)	Transversal composition (20-70-20-70-20)
$h_{element}$ [m]	0.2	0.2	0.2
$w_{element}$ [m]	5	5	5
A [m^2]	1	1	1
$I_{yx,eff}$ [m^4/m]	624×10^{-6}	503×10^{-6}	312×10^{-6}
$I_{xy,eff}$ [m^4/m]	17.1×10^{-6}	131×10^{-6}	325×10^{-6}
$I_{yx,net}$ [m^4/m]	649×10^{-6}	528×10^{-6}	326×10^{-6}
$I_{xy,net}$ [m^4/m]	17.3×10^{-6}	139×10^{-6}	341×10^{-6}
$I_{yz,net}$ [m^4]	4573×10^{-6}	3430×10^{-6}	1715×10^{-6}
$I_{xz,net}$ [m^4]	1143×10^{-6}	2287×10^{-6}	4002×10^{-6}
$I_{xx,tor}$ [m^4]	1225×10^{-6}	1225×10^{-6}	1225×10^{-6}
$I_{yy,tor}$ [m^4]	1225×10^{-6}	1225×10^{-6}	1225×10^{-6}
κ_y [-]	0.258	0.243	0.308
κ_x [-]	0.334	0.208	0.306
$G_{y,eff}$ [MPa]	146	107	78.6
$G_{x,eff}$ [MPa]	64.5	65.9	154
$S_{yr,net}$ [m^3/m]	400×10^{-6}	1600×10^{-6}	3150×10^{-6}
$S_{yl,net}$ [m^3/m]	400×10^{-6}	1600×10^{-6}	3150×10^{-6}
$S_{xr,net}$ [m^3/m]	4550×10^{-6}	3200×10^{-6}	1800×10^{-6}
$S_{xl,net}$ [m^3/m]	4600×10^{-6}	3400×10^{-6}	1850×10^{-6}

5.2 Comparison between beam theories

In this comparison, a plate measuring 5×7 m^2 with a centrically placed opening measuring 2.0×2.0 m^2 is analysed using the grillage method. The surface load is set to 4 kN/m^2.

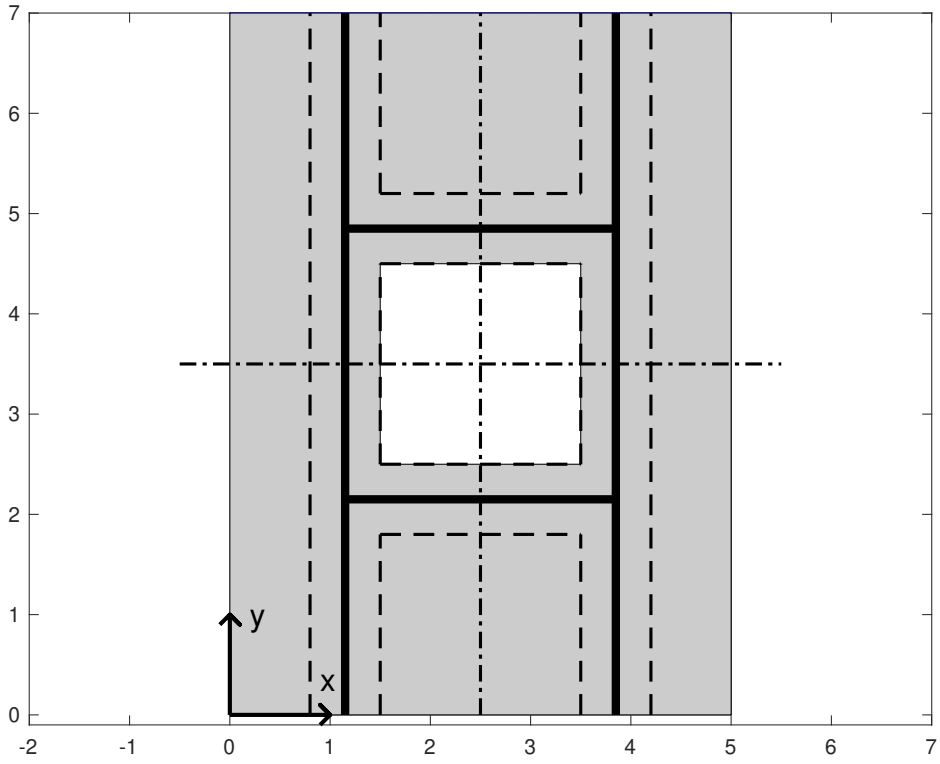

Figure 5.2: The plate used in the comparison between beam theories

Three different approaches were investigated; Bernoulli-Euler beam theory adopting the Gamma method, the Timoshenko beam theory and also a three-dimensional Bernoulli-Euler beam theory including the Gamma method. Three different quantities are evaluated and compared between the approaches; shear force, bending moment and deflection. The comparative study is performed and presented for all three investigated compositions presented in Section 5.1. The results of the comparative study is presented in the sections below.

Shear Force

The shear force distribution depends on the loading and the geometry of the beams in the grillage model. Since these two factors are the same regardless of CLT composition in the beams results for the different compositions are identical. There is therefore no need to present shear force distribution for the different compositions. The graphs below plot shear force along the beams' local x-axis, the axial direction, denoted as $\bar{x}$. The values on the x-axis is stated in relation to the beam length, L, of the evaluated beam.

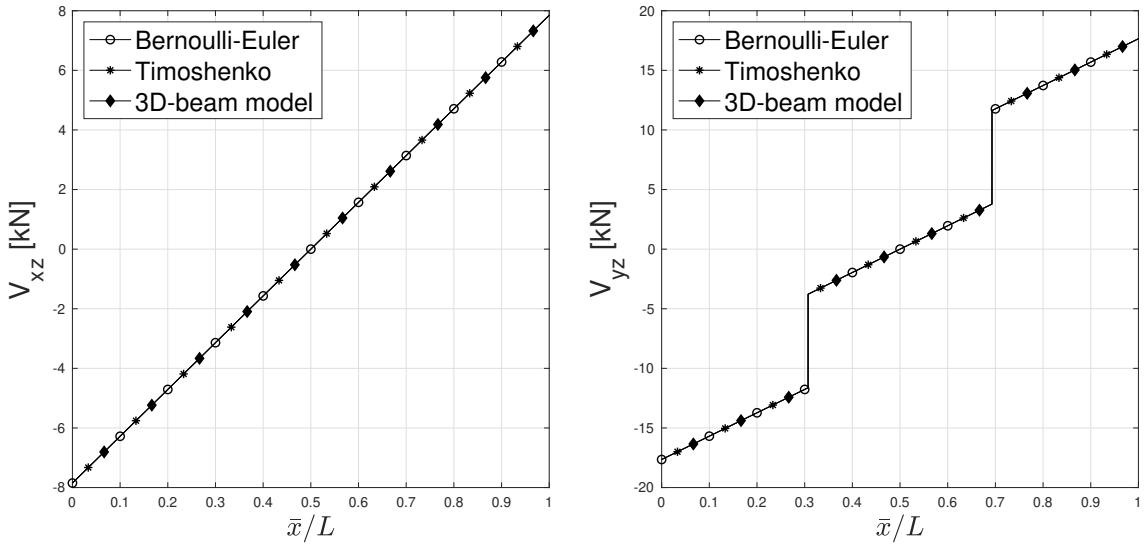

(a) Beams 3 and 4

(b) Beams 5 and 6

Figure 5.3: Comparison of shear force distribution between models using different beam theories

The shear force distributions presented in Figure 5.3a and Figure 5.3 are characteristic for the loading conditions of the beams in the grillage model. A straight line for a simply supported beam with distributed loads and three straight lines connected by vertical lines for a simply supported beam with distributed load and two point loads. The results do not depend on which beam theory is used to model the grillage model. The load case is in other words statically determined.

Bending Moment

The bending moment distribution for the shorter transversal beams, 3 and 4, and for the longer longitudinal beams, 5 and 6, are shown in Figure 5.4 and Figure 5.5. The geometry is symmetric so beams 3 and 4 are identical, the same is true for beams 5 and 6. For beams 5 and 6 there is no difference in bending moment distribution between the different CLT compositions because these beams are simply supported in all cases. When the three-dimensional beam model is used with restrained connections, the bending moment distribution in beams 3 and 4 depend on the CLT composition of the beams. The reason is that these beams are attached to beams 5 and 6. The CLT composition affects the stiffness relation between the longitudinal and transversal direction of the CLT plate, which in turn showed an influence of the end bending moment of beams 3 and 4, which can be seen in Figure 5.4. For these reasons bending moment distribution in beams 5 and 6 are presented only for one CLT composition, the composition with equal distribution, but for beams 3 and 4 the results are presented for each CLT composition separately where the difference in results between the compositions is noticeable.

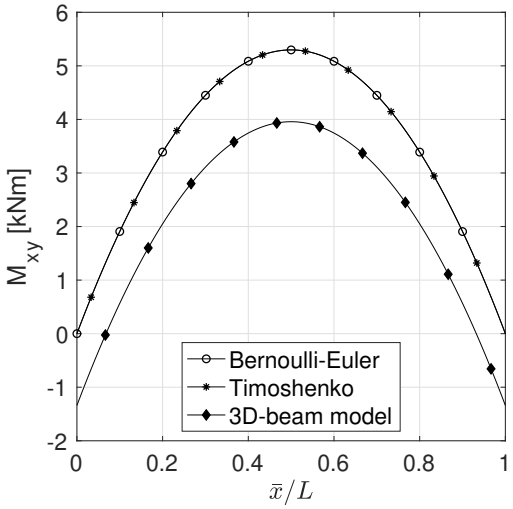

(a) Composition - Longitudinal distribution

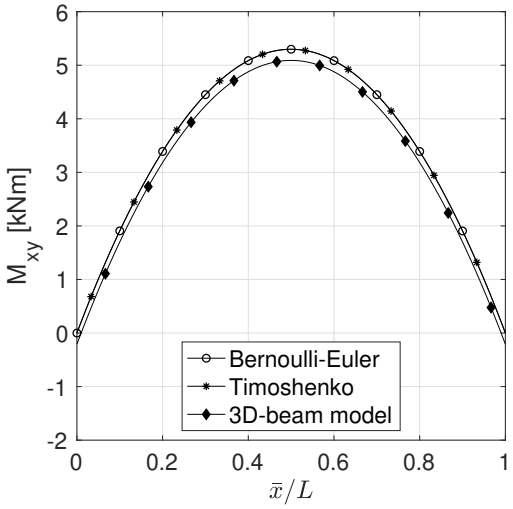

(b) Composition - Equal distribution

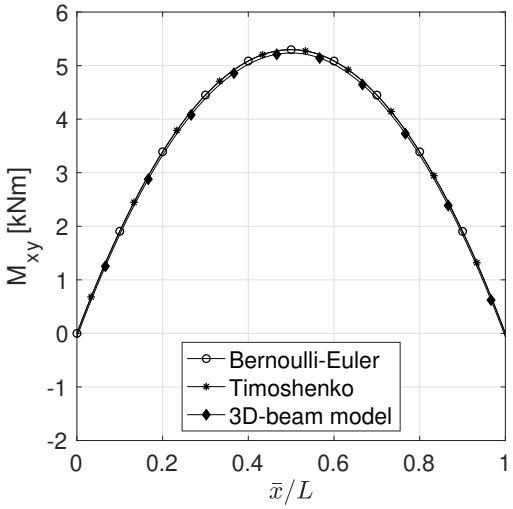

(c) Composition - Transversal distribution

Figure 5.4: Bending moment distribution in beams 3 and 4 for different CLT compositions and beam models

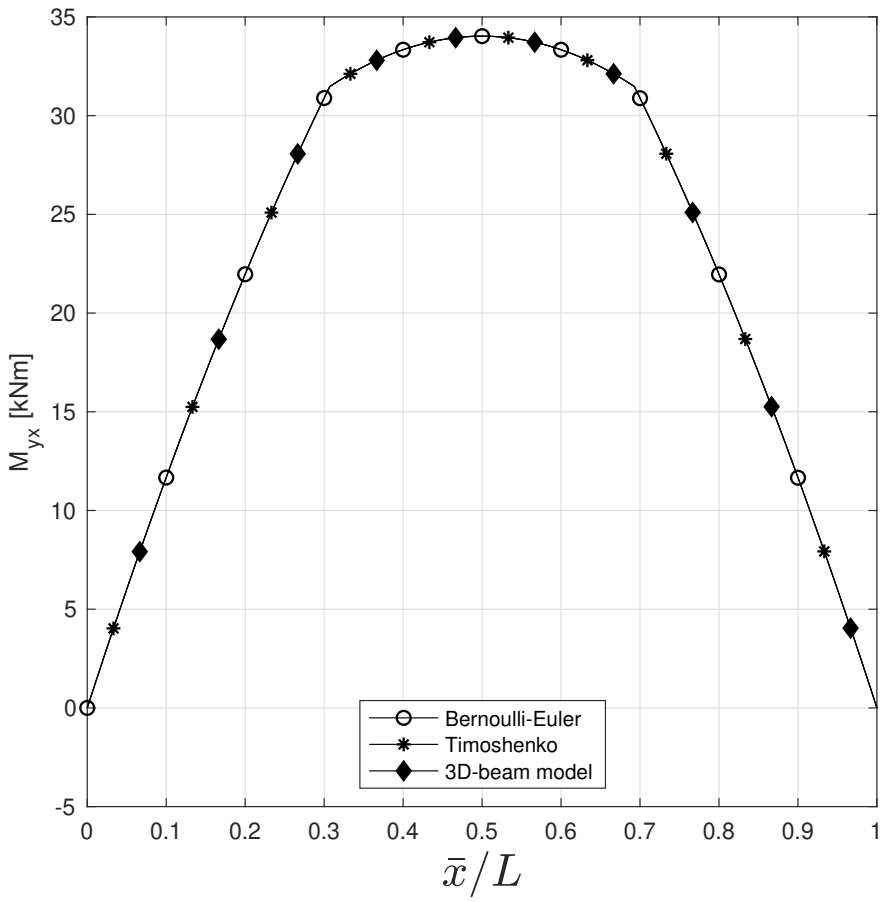

Figure 5.5: Bending moment distribution in beams 5 and 6 for different beam models, equal distribution.

Figure 5.4 shows that there is no difference in bending moment distribution for beams 3 and 4, when modelling these beams as simply supported beams using two-dimensional Bernoulli-Euler or Timoshenko beam theory. In these cases the CLT composition of the beam also does not affect the bending moment distribution.

When modelling the grillage model with three-dimensional beams with restrained connections, the bending moment distribution in beams 3 and 4 are affected by the CLT lay-up. In the three-dimensional model the connections between the transversal beams, 3 and 4, and the longitudinal beams, 5 and 6, are not hinged. This means that a reaction bending moment can develop in the connections. For the longitudinal distribution there is a noticeable reaction bending moment. The corresponding reaction bending moment in the model with equal distribution is smaller and in the transversal distribution the reaction bending moment is barely noticeable.

Figure 5.5 shows that there is no difference in bending moment distribution in beams 5 and 6 between the different models, it is also not affected by the CLT composition of the beams.

Deflection

When the grillage model is modelled using Bernoulli-Euler beam theory and three-dimensional beams the effective moment of inertia is calculated using the Gamma method. When using Timoshenko beam theory the net moment of inertia is used but shear deformations are accounted for using the effective shear stiffness. The different approaches result in different values for stiffness. The stiffness also depends on the composition of the CLT cross section. For these reasons the deflections for the beams presented in Figure 5.6 include six graphs, two graphs for each CLT composition.

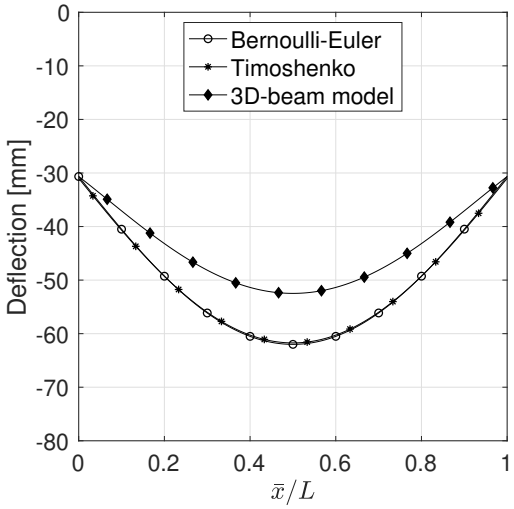

(a) Composition - Longitudinal distribution

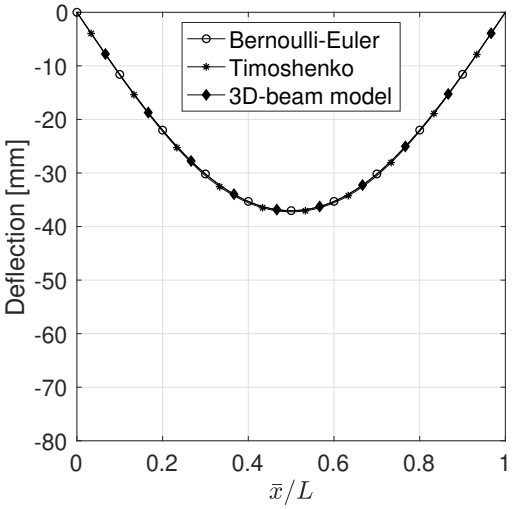

(b) Composition - Longitudinal distribution

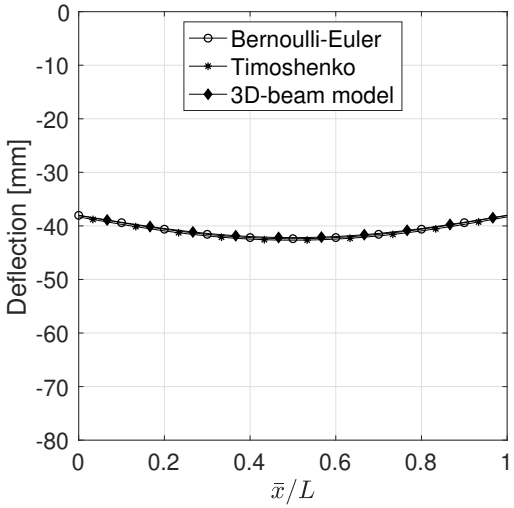

(c) Composition - Equal distribution

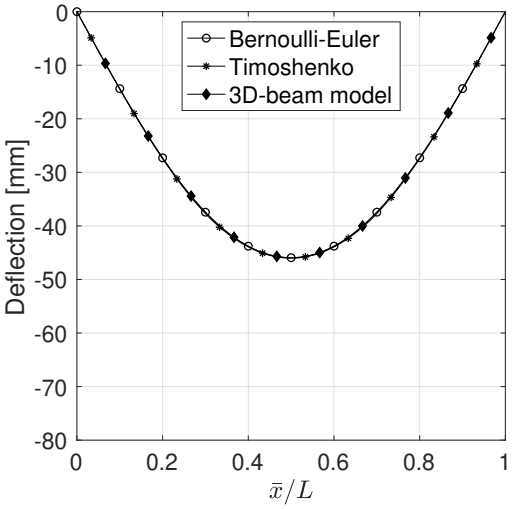

(d) Composition - Equal distribution

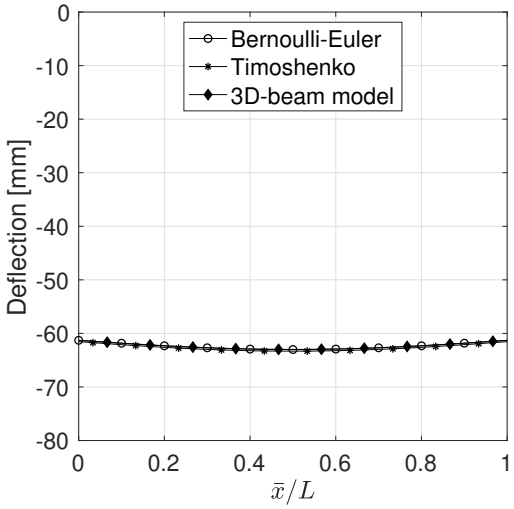

(e) Composition - Transversal distribution

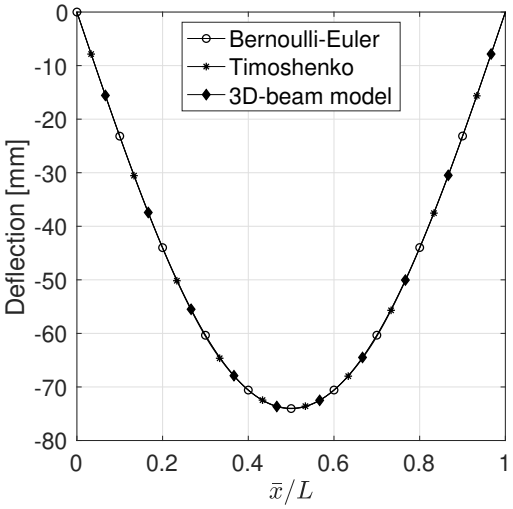

(f) Composition - Transversal distribution

Figure 5.6: Deflection for different CLT compositions, curves for beams 3 and 4 on the left and beams 5 and 6 on the right.

Figure 5.6 shows that the difference in deflection between models using the Bernoulli-Euler and Timoshenko beam theory amounts to a couple of millimeters at most. The noticeable difference in bending moment distribution shown in Figure 5.4a is reflected in Figure 5.6a where a noticeable difference of approximately 10 millimeters is present between the three-dimensional beam model and the other two models.

The CLT cross section with the longitudinal distribution results in a smaller deflection in the longitudinal beams, 5 and 6. Contrariwise, the deflection in the transversal beams, 3 and 4, is higher than for the other compositions. For the composition with the transversal distribution the relation is the opposite, largest deflection in the longitudinal beams and the smallest deflection in the transversal beams compared to the other compositions. However, the result is that the total deflection of the grillage model is roughly the same when the model using the longitudinal distribution is compared to the model using the transversal composition. The model using the equal CLT cross section composition has a smaller total deflection than the other two models.

5.3 Comparison of deflection

This section aims to compare the stiffness of a cross section generated using the finite element method program Abaqus with that calculated using the Gamma method or Timoshenko beam theory. The maximum deflection is compared as it is important to ensure that the different means of calculating stiffness give similar results in order to carry out a parameter study. For this purpose, a simply supported 1 m wide beam is modelled. In Abaqus the beam is modelled using a three-dimensional shell element and the composite layup tool. It is the same method as described in Chapter 4. In Matlab the beam is modelled using the Gamma method and the Timoshenko beam theory.

The test is divided into two separate investigations. The first part of the test consists of applying a uniformly distributed load on the beam with a magnitude of 4 kN/m. In the finite element model the load is modelled as a uniformly distributed surface load with a magnitude of 4 kN/m^2. The second part of the test consists of applying a point load in the middle of the span. The magnitude of the point load is set to 1 kN. In the finite element model a point load is placed centrically so that it is in the middle of the span and in the center of the beam width. The effect that the length of the beam has on the comparison is also investigated. The maximum deflection is recorded for a 1 m long beam up to a 10 m long beam with the other parameters kept constant. All three CLT cross section compositions are investigated.

The results are presented as maximum deflection plotted against beam length for all models. Maximum deflection from the models modelled in Matlab are also plotted in relation to the maximum deflection of the finite element model. The reason for the relative comparison is to investigate how much the stiffness of a cross section calculated using the Gamma method and Timoshenko beam theory differs from that of a cross section generated in Abaqus.

The length is increased from 1 m to 10 m in steps of 0.05 m. The step size was chosen based on the element size adopted in the finite element model, so that the element size throughout the test can remain constant while changing the beam length. The total amount of steps in this study is thereby equal to 90.

5.3.1 Uniformly distributed surface load

The variation of maximum deflection when changing the length of a simply supported 1 m wide CLT beam loaded with a constant surface load is evaluated. The investigation is made for the three different previously presented compositions of CLT beams separately. Note that the graphs below are constructed by the same number of data points, namely 90 data points each, one data point generated from each iteration. However, in the figures below only every twentieth data point or every thirtieth data point is marked with a symbol based on whether the figure contains two or three graphs. This is done solely to facilitate the reading of the graphs.

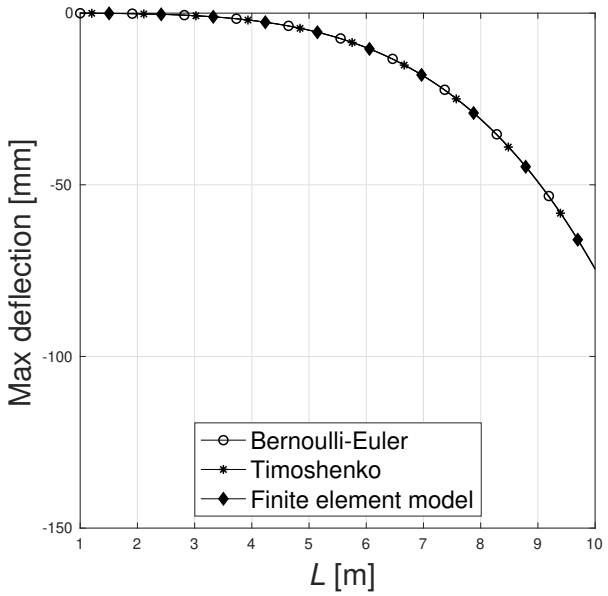

(a) Absolute values

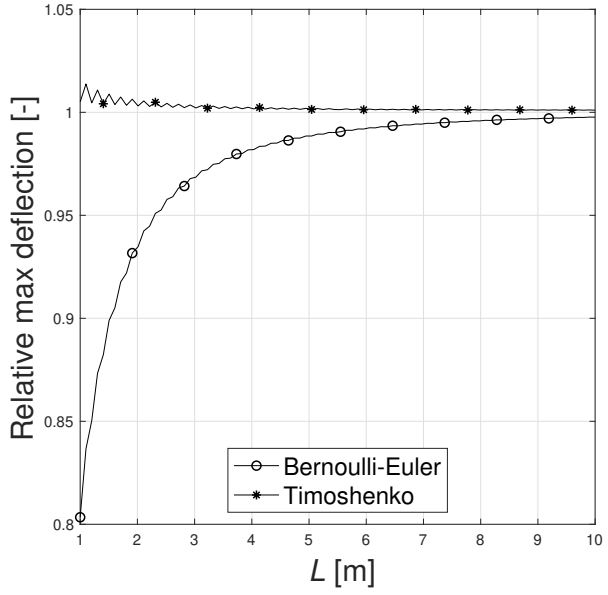

(b) Relative values in relation to the finite element model

Figure 5.7: Maximum deflection at different beam lengths, longitudinal distribution.

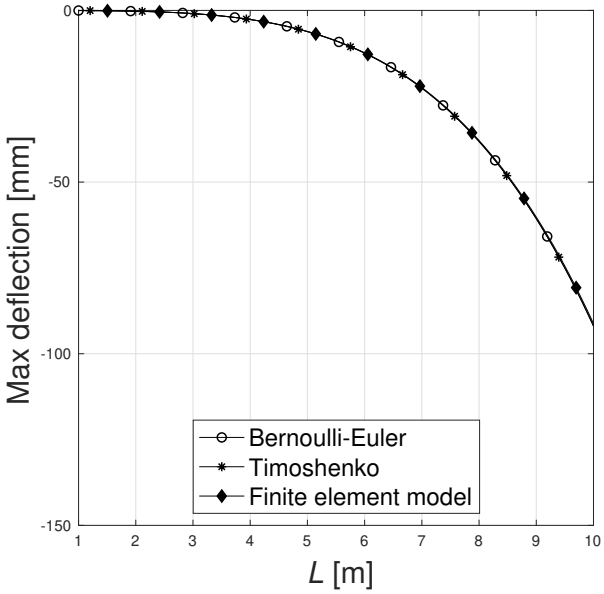

(a) Absolute values

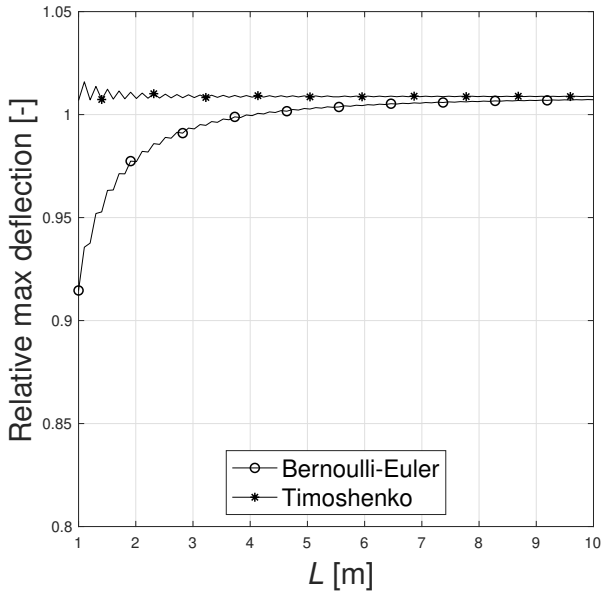

(b) Relative values in relation to the finite element model

Figure 5.8: Maximum deflection at different beam lengths, equal distribution.

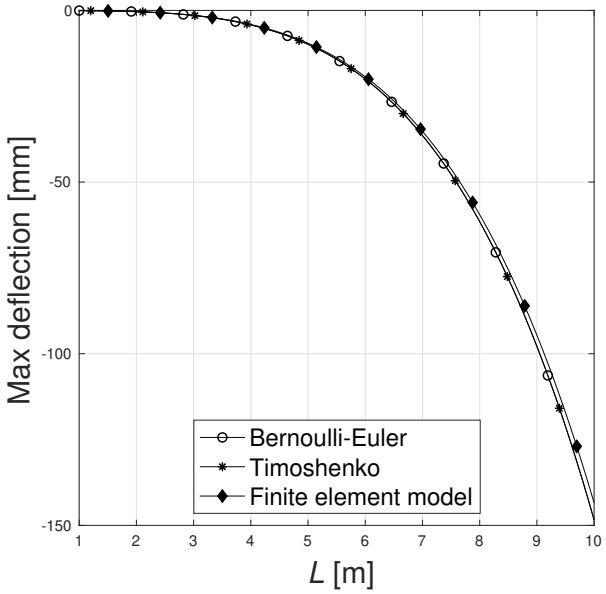

(a) Absolute values

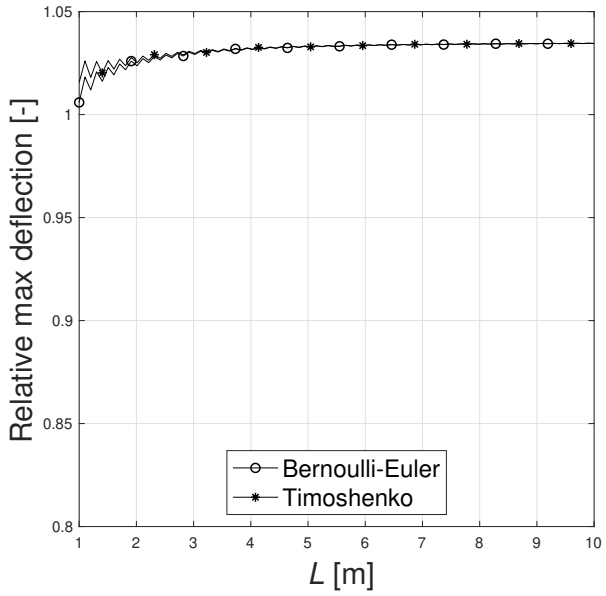

(b) Relative values in relation to the finite element model

Figure 5.9: Maximum deflection at different beam lengths, transversal distribution.

5.3.2 Point load

The variation of maximum deflection when changing the length of a simply supported 1 m wide CLT beam loaded with a constant centrically placed point load is also evaluated. The investigation is made for the three different previously presented compositions of CLT beams separately. The same principle of presentation of the graphs as described for the uniformly distributed load is applied also in this study.

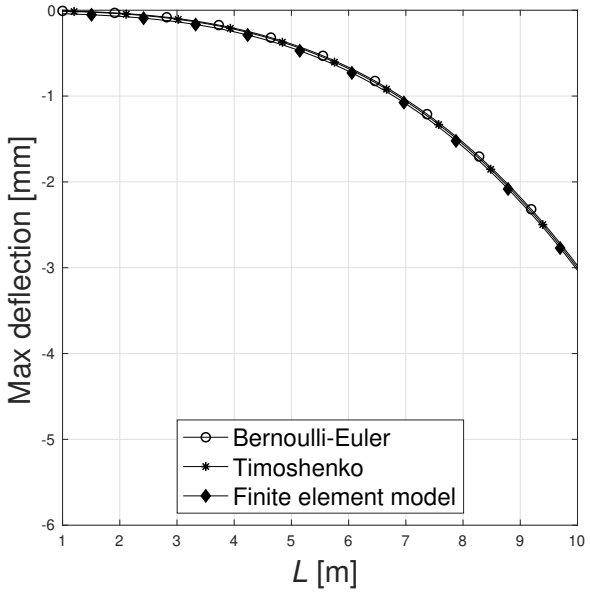

(a) Absolute values

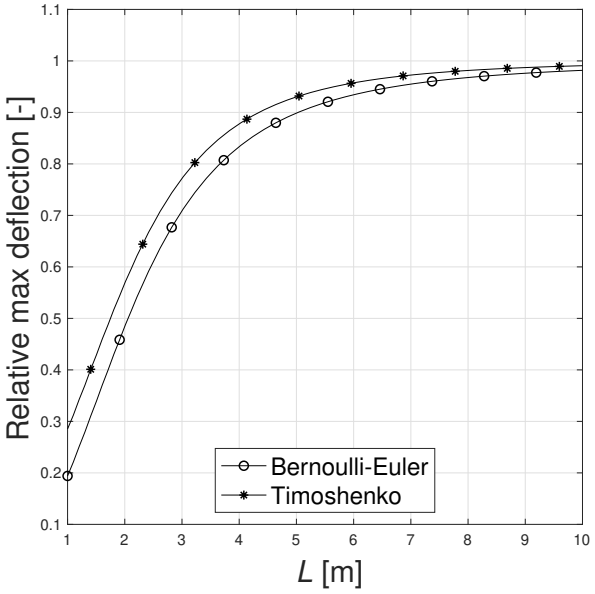

(b) Relative values in relation to the finite element model

Figure 5.10: Maximum deflection at different beam lengths, longitudinal distribution.

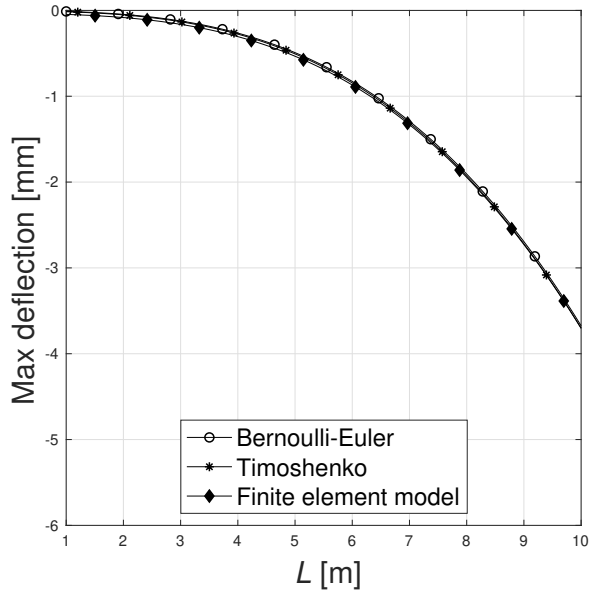

(a) Absolute values

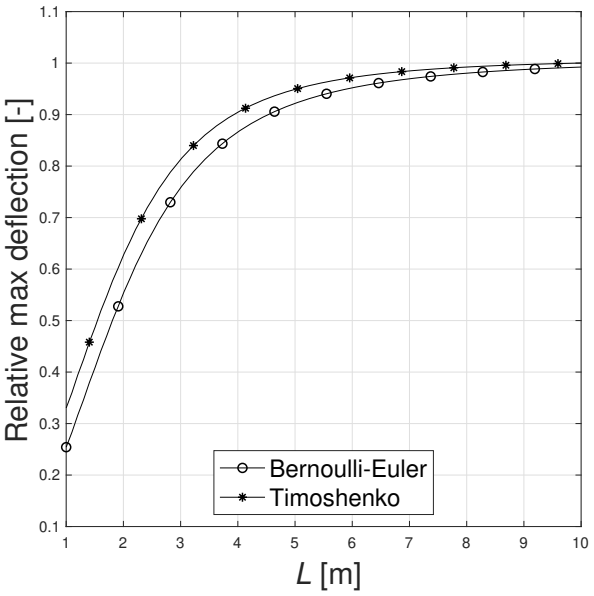

(b) Relative values in relation to the finite element model

Figure 5.11: Maximum deflection at different beam lengths, equal distribution.

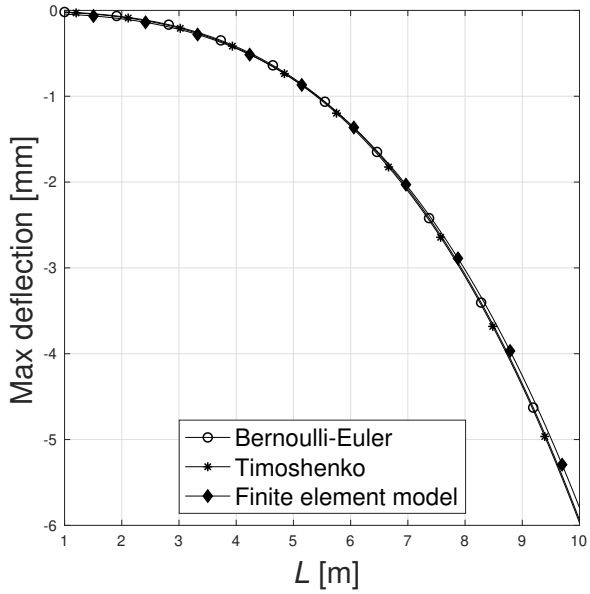

(a) Absolute values

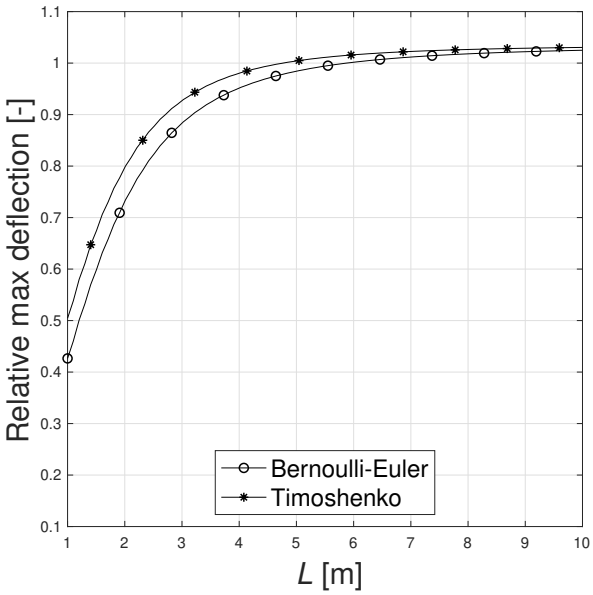

(b) Relative values in relation to the finite element model

Figure 5.12: Maximum deflection at different beam lengths, transversal distribution.

The difference in absolute deflection between the Matlab models and the finite element model is small for all cases. In relative terms some patterns become apparent. In the case of distributed load, the results from the model based on Timoshenko beam theory displays small differences compared to results from the finite element model. Results from the Bernoulli-Euler beam theory displays larger differences in comparison to results from the finite element model for shorter beam lengths. The differences are largest for the longitudinal composition and smallest for the transversal composition. On the other hand is the total deflection largest for the transversal and smallest for the longitudinal composition, an opposite relation.

In the case with a point load the absolute differences are also small. However, the relative differences compared to the finite element model for both Timoshenko and Bernoulli-Euler models are larger than for the distributed load and especially large for shorter beams. However, as the beam length increases the differences decrease. This is due to the fact that the finite element model allows for varying displacement in the beam's width direction. These deformations would become smaller in comparison to the bending of the beam when the beam length is increased.

This section shows that there are differences in stiffness between analytical models based on Bernoulli-Euler and Timoshenko beam theory compared to numerical models based on the finite element model. The differences are larger for shorter beams and small deflection values. The differences expressed in absolute terms are deemed to be sufficiently small in order to continue with a parameter study analysing the grillage method. Since the differences are small and the Gamma method is the most convenient method to use, further investigations in this thesis will use the Bernoulli-Euler beam theory with the Gamma method to represent the results from the grillage method.

5.4 Comparison between grillage model and finite element model

This section compares results from the finite element model to the grillage model in terms of bending moment distribution, shear force distribution and deflection. The effect of the different CLT compositions is not included in this section as this is investigated in the next section. In this section, the equal distribution CLT composition is used.

A finite element model of a CLT plate element is modelled in Abaqus. The plate measures 5×7 m^2 with an opening placed centrically measuring 2.0×2.0 m^2 and a surface load of 4 kN/m^2 acting on it. This is the same plate geometry and loading conditions that was used to analyse the different beam theories, presented in Section 5.2. The Gamma method is chosen to be used when comparing the grillage model with the finite element model because it is the most convenient method to use, and because it was shown in the previous sections that the differences in results between the beam theories are small. A series of comparisons are made in this step in order to identify key differences and relationships between the grillage model and the finite element model.

Different paths are set up in the finite element model from which data is extracted. The main paths coincide with the center lines and edges of the beams in the grillage model. Consequently, the location of the paths correspond to the geometry of the beams in the grillage model. Transverse paths across the beam widths are also set up in order to investigate the distribution of values across the beam width.

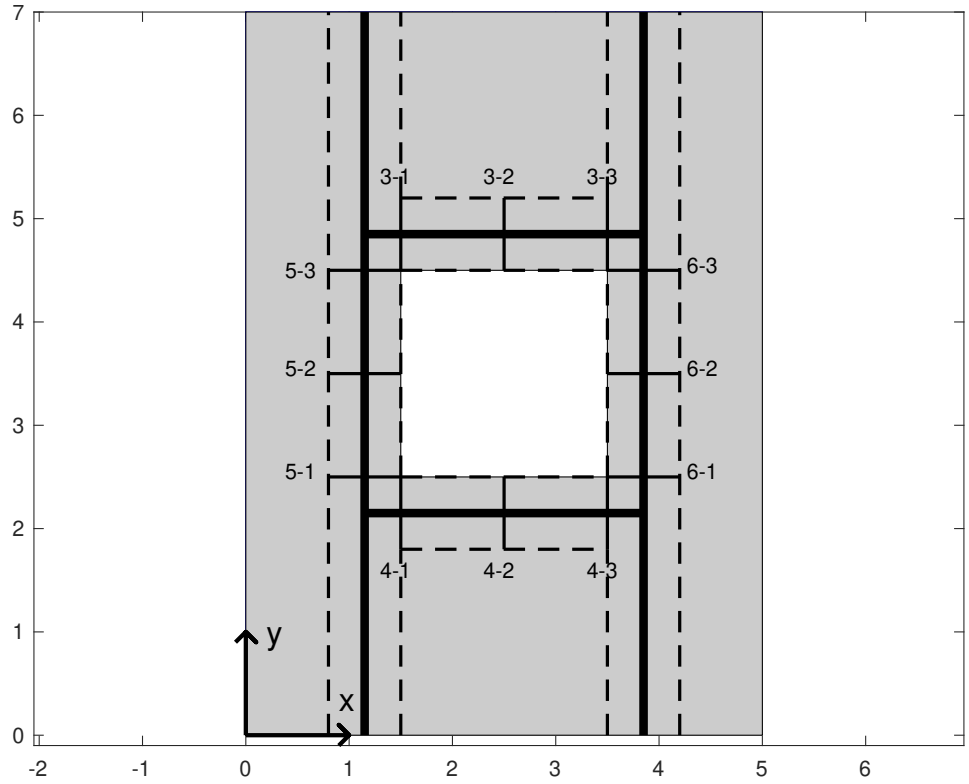

Figure 5.13: Plate element with the transversal paths in the finite element model introduced

In the model the beam width is set to $b = L/10$, namely one tenth of the span or length of the plate meaning that the main paths set up in the finite element model align with the opening's edges and 0.35 m as well as 0.7 m from the edges of the opening. In Figure 5.13, the area inside the dashed lines represent the beams, the dashed lines thereby corresponds to the edges of the beams. The thick lines correspond to the center lines of the beams and the numbered lines perpendicular to the beams' direction represents the additional paths that are used to evaluate the distributions along the beam width. Since the geometry and placing of the opening is symmetrical, results from beams 3 and 4 are identical, the same applies for beams 5 and 6. Hence only results from beam 3 and 5 are presented in this section.

The results are expressed in kN/m to ease the comparison of results from the finite element model with the results from the grillage model. Hence the results from the grillage model have been divided by the beam width, in order to be compared with the results from the finite element model.

5.4.1 Shear force distribution along width of beam

In this section, the shear force distribution along the transverse paths across the beam widths is presented in graphs. The paths correspond to the numbered paths in Figure 5.13. The value of the shear force from the grillage model at the specific point along the beam length is shown as a circle.

Beam 3

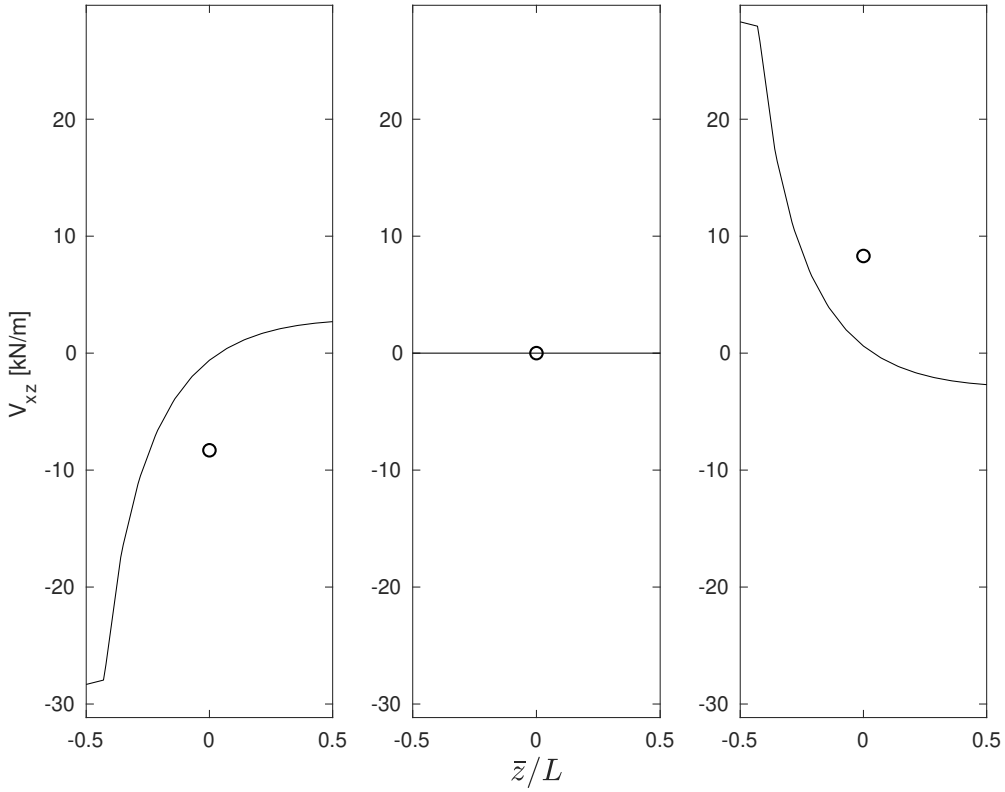

Figure 5.14: Shear force along width of beam 3, b, graphs show paths 3-1 (left), 3-2 (center) and 3-3 (right).

Figure 5.14 shows that according to the finite element model there is a concentration of shear force close to the corners of the opening. The extreme values at the corners of the opening indicate stress concentrations in the finite element model. Considering the high values at the corners it is relevant to investigate the shear force along the path that runs along the edge of the opening.

Beam 5

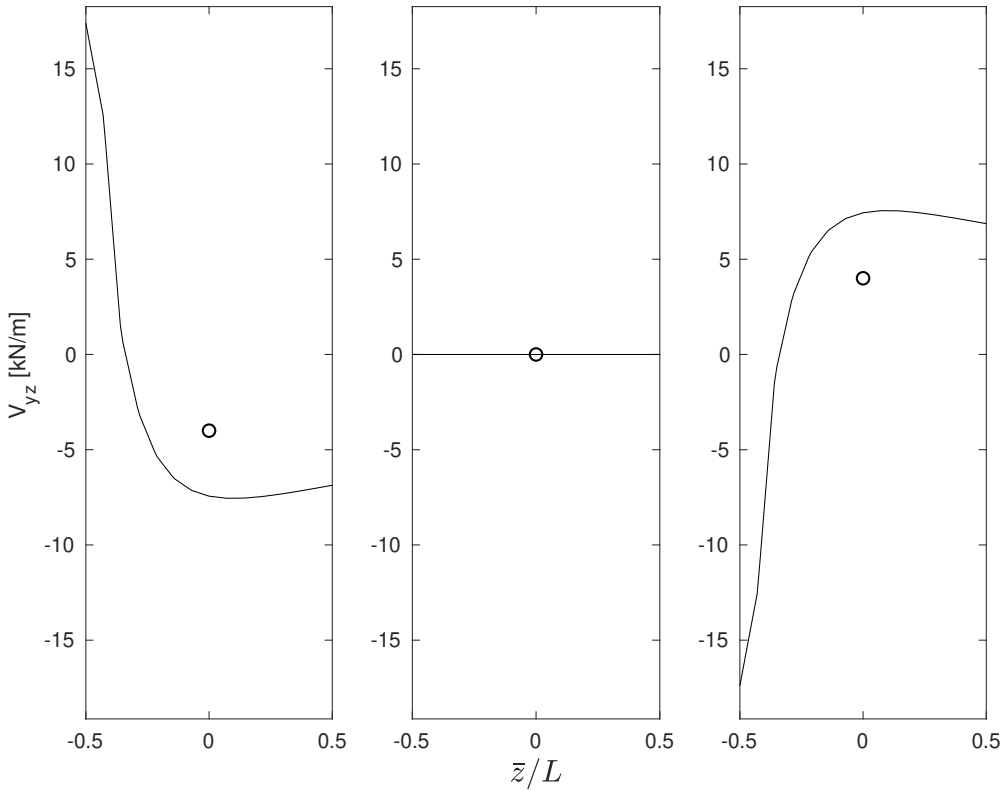

Figure 5.15: Shear force along width of beam 5, b, graphs show paths 5-1 (left), 5-2 (center) and 5-3 (right).

Figure 5.15 shows that the grillage model and the finite element model give similar values at half a beam widths distance from the edge of the opening. The values are similar in magnitude and have the same sign. However, as the distance to the opening decreases the value for the shear force changes sign and increases in magnitude. This also indicates the relevance to investigate the shear force along the path that runs along the edge of the opening.

5.4.2 Shear force distribution along length of beam

Beam 3

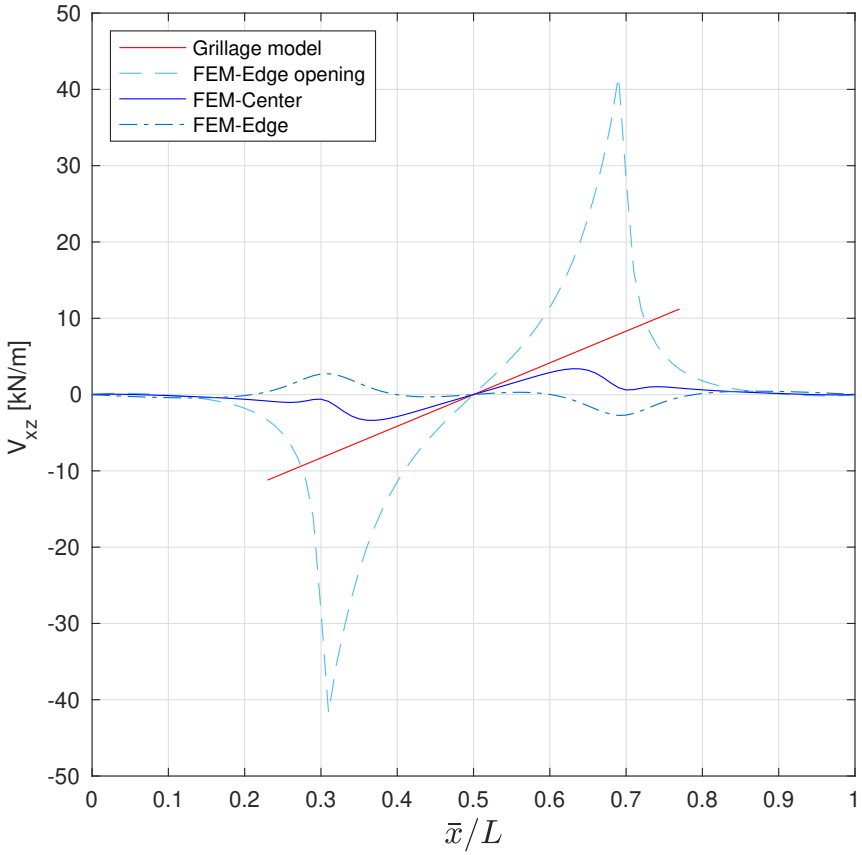

Figure 5.16: Shear force along length of beam 3

Figure 5.16 shows the shear force distribution along beam 3 in the grillage model and values for the corresponding paths in the finite element model. The curve representing the shear force in beam 3 is characteristic of the shear force distribution in a simply supported beam with a distributed load. The curve from the center path, in the finite element model, somewhat resembles the curve from the grillage model. The region of the curve from the center path spanning the width of the opening, in the finite element model, has the shape of a straight line. This is similar to the curve from the grillage model. The grillage model gives higher values than the center path of finite element model. The path along the edge of the opening in the finite element model gives extremely high values close to the corners of the opening. It should be noted that the maximum value from the curve from the edge path in the finite element model is not located at the corner of the opening but a small distance from the corner. This explains why the maximum value in Figure 5.16 is higher than the max value in Figure 5.14. The maximum values along the edge greatly exceeds the maximum value of the grillage model.

Beam 5

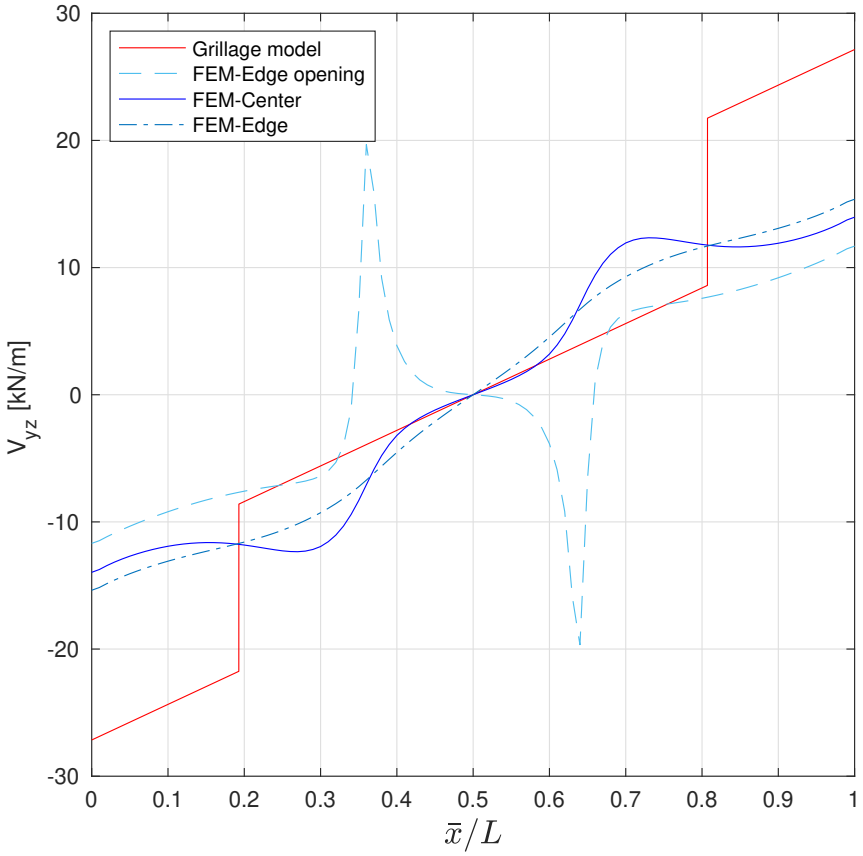

Figure 5.17: Shear force along length of beam 5

The curve given by the center path in the finite element model is similar to the curve given by the grillage model, but the vertical shifts are instead represented by continuous transitions. Both curves have the value zero at mid-length. The values from the path that runs along the edge of the opening in the finite element model are high close to the corners of the opening. Unlike in beam 3, the high values have different signs than the values from the grillage model or other paths in the finite element model.

As with beam 3, the maximum value from the curve from the edge path in the finite element model is not located at the corner of the opening but a small distance from the corner. This explains why the maximum value in Figure 5.17 is larger than the maximum value in Figure 5.15.

5.4.3 Bending moment distribution along width of beam

In this section, the bending moment distribution along the transverse paths across the beam widths is investigated. These paths corresponds to the numbered paths in figure 5.13. The value of the bending moment from the grillage model at the specific point along the beam length is shown as a circle.

Beam 3

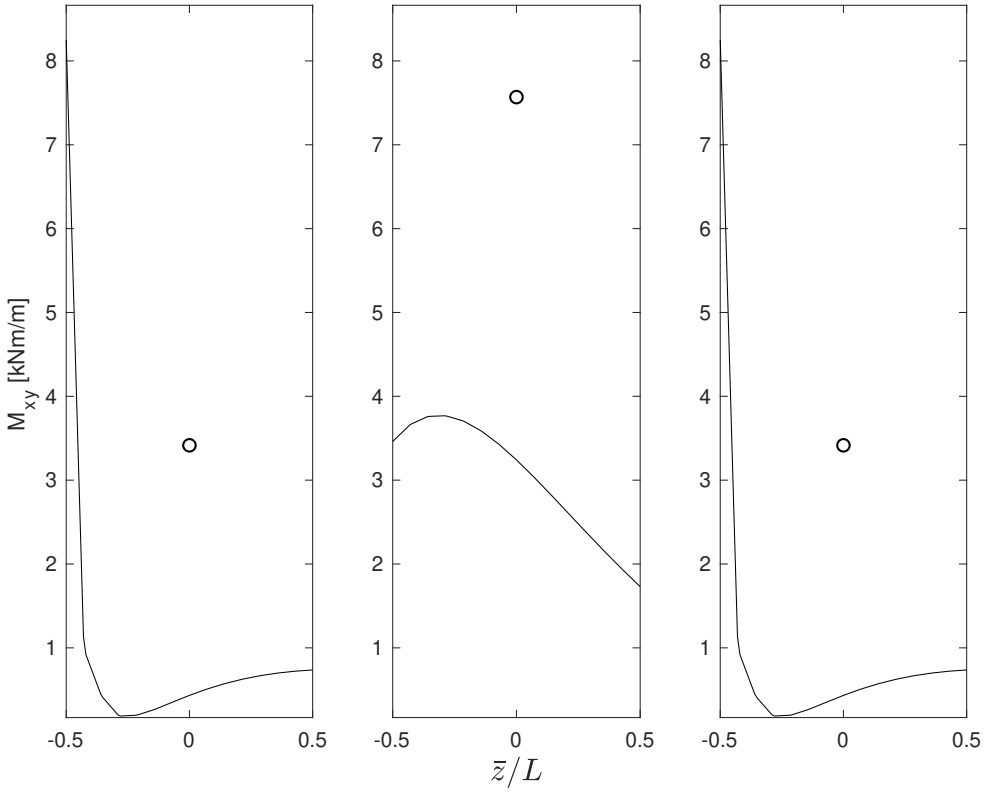

Figure 5.18: Moment along width of beam 3, b, graphs show paths 3-1 (left), 3-2 (center) and 3-3 (right).

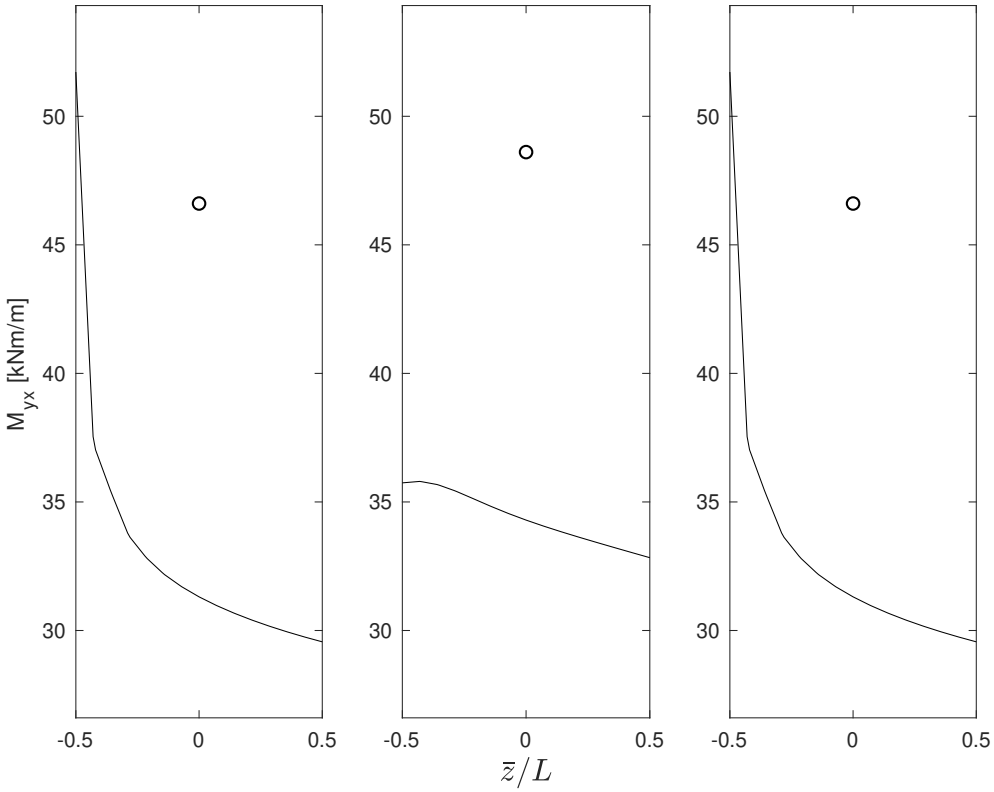

Figure 5.19: Moment along width of beam 5, b, graphs show paths 5-1 (left), 5-2 (center) and 5-3 (right).

Figure 5.18 and Figure 5.19 show that the bending moment increases as distance to the opening decreases, in the finite element model. Hence a higher value can be obtained if data is taken from a path closer to the hole. It also shows that the value of the bending moment is extremely high near the corners of the opening, higher than the value given by the grillage model. The high values close to the corners give an indication of stress concentrations in the finite element model. The extreme values at the points of stress concentration in the corners are not representative for the values obtained throughout the plate model. They should not be totally disregarded neither. Therefore, it is reasonable to also investigate the bending moment distribution along the edges of the opening.

5.4.4 Bending moment distribution along length of beam

Beam 3

The bending moment is plotted along the entire width of the plate element along three different paths, one path coinciding with the edge of the opening along beam 3, one coinciding with the center line of beam 3 and lastly one path coinciding with the inner edge of beam 3.

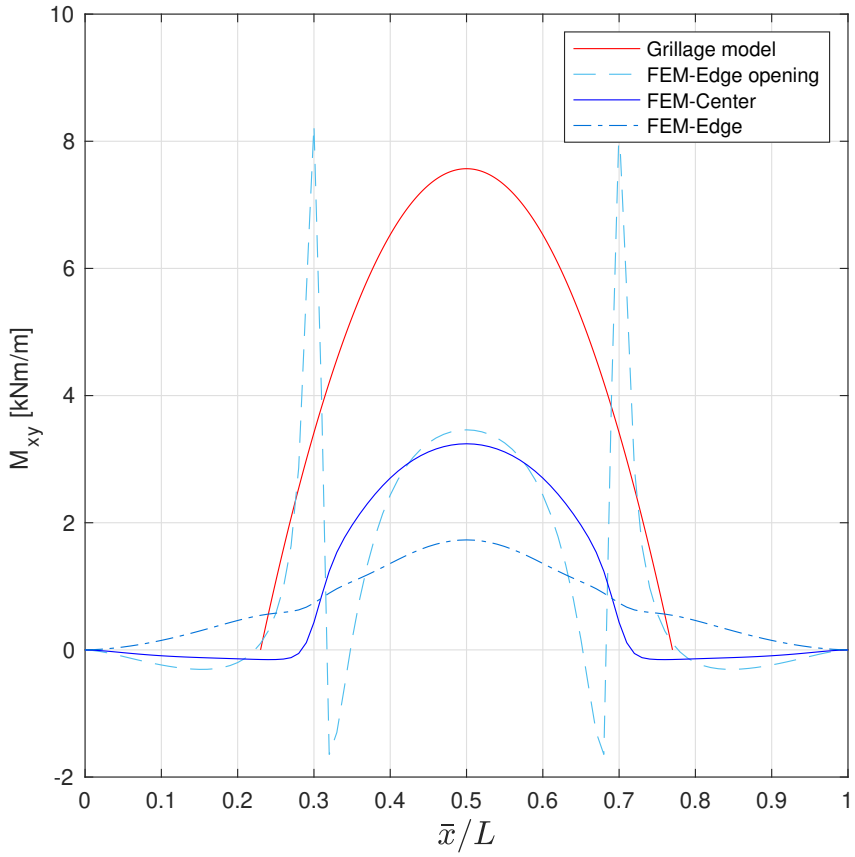

Figure 5.20: Bending moment distribution along length of beam 3

Figure 5.20 shows that the value of the bending moment calculated in the grillage model is higher than the value taken from the center path of the finite element model. The shapes of the curves for the center line of the beam are similar except that the curve from the grillage model spans the entire length of beam 3 which is longer than the width of the opening. Beam 3 has a longer span than the width of the hole because it connects to the center lines of beams 5 and 6. The values taken from the path that runs along the edge of the opening indicate stress concentrations close to the corners.

Beam 5

In the grillage model, beam 5 is a simply supported beam with a distributed load and two point loads. In the finite element model, the corresponding bending moments are plotted along three different paths along beam 5.

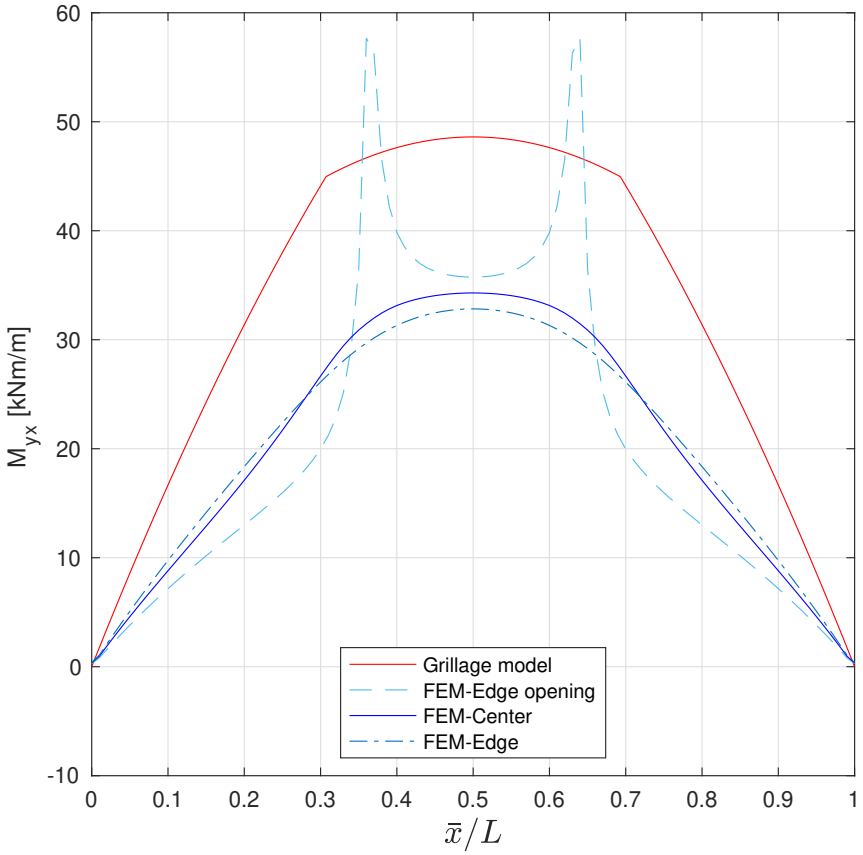

Figure 5.21: Bending moment distribution along length of beam 5

As with beam 3 the value of the bending moment calculated using the grillage model is higher than that of the center line in the finite element model. However, the difference is not as large as in beam 3. The effects of the point load in the grillage model are clearly seen in the bending moment diagram. The shape that they cause on the curve for the grillage model is similar to the shape of the bending moment diagram from the finite element model. Like beam 3, the maximum value close to the corners of the opening in the finite element model exceed the highest values from the grillage model.

5.4.5 Deflection along width of beam

In this section, the deflection along the transverse paths across the beam widths is presented. These paths corresponds to the numbered paths in figure 5.13. The value of the deflection from the grillage model at the specific point along the beam length is shown as a circle.

Beam 3

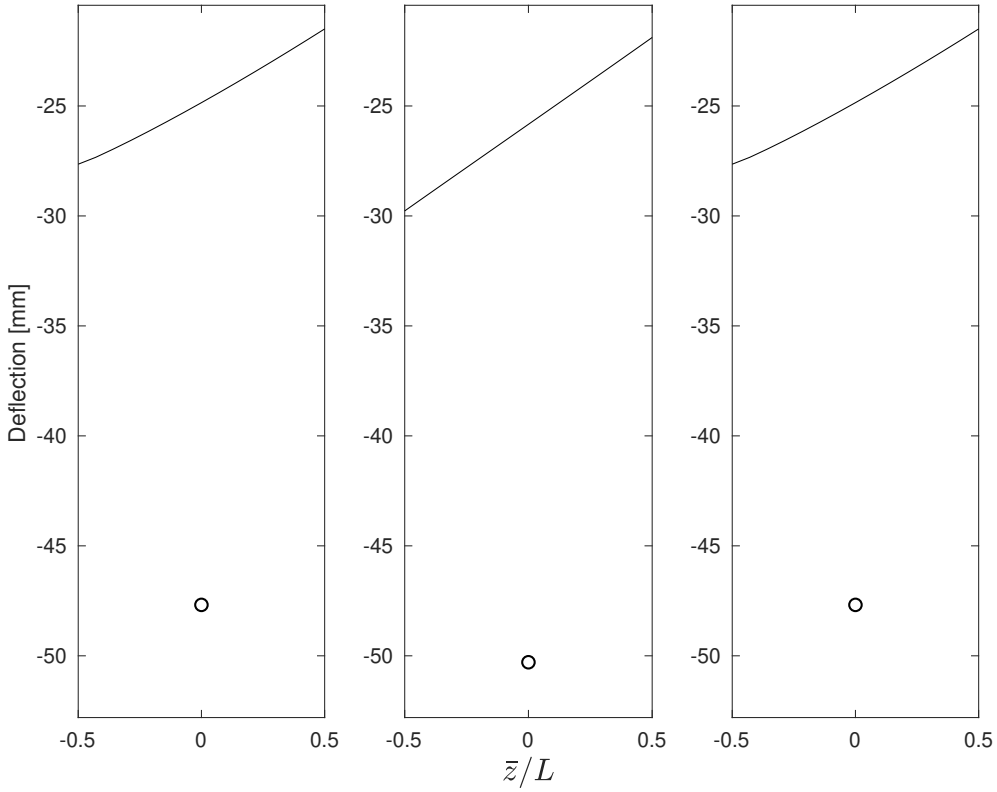

Figure 5.22: Deflection along width of beam 3, b, graphs show paths 3-1 (left), 3-2 (center) and 3-3 (right).

As with the bending moment it is clear that the deflection decreases as the distance from the opening increases. Because there is no equivalent of stress concentrations regarding deflection when using the finite element method, it is not relevant to investigate deflection in the same way as for bending moment and shear force. It is clear that the largest deflection occurs along the edges of the opening. Hence, the values for the deflection along the edges are relevant to design requirements regarding maximum deflection. It is thereby not necessary to show the value of deflection for the three separate paths that run along the beam length.

Beam 5

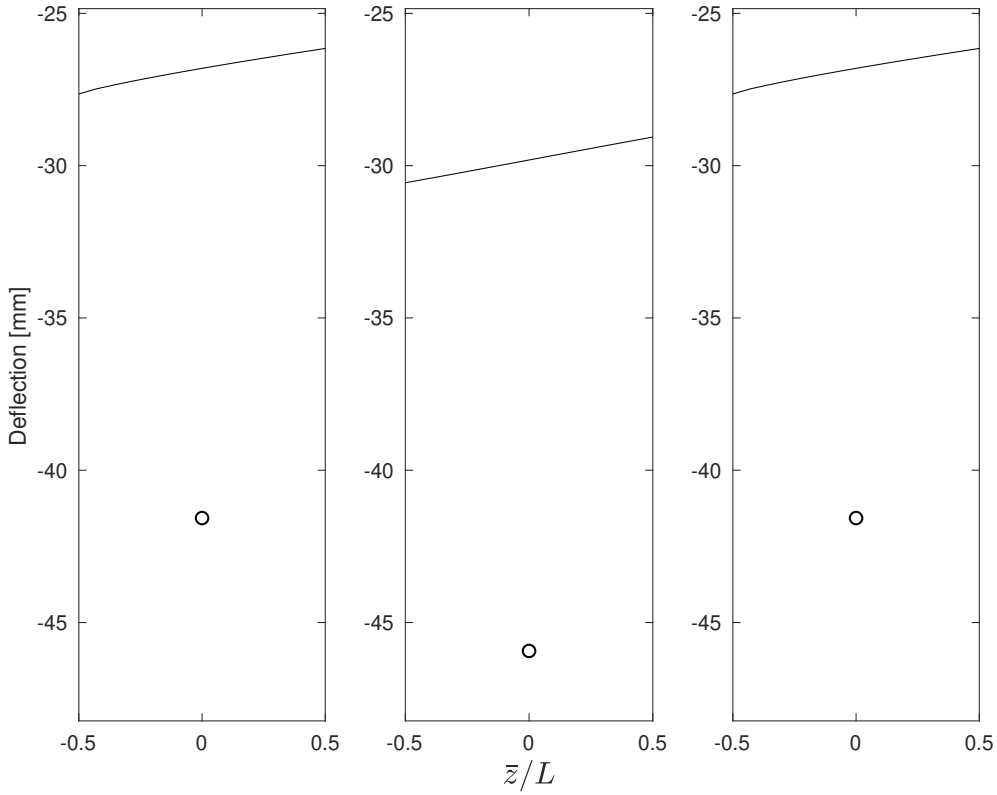

Figure 5.23: Deflection along width of beam 5, b, graphs show paths 5-1 (left), 5-2 (center) and 5-3 (right).

The deflection along the beam width of beam 5 shows the same pattern as in beam 3. For beam 3 the gradient of deflection towards the opening is steep in comparison to beam 5. However, the deflection given by the grillage model is still larger in both cases.

5.4.6 Deflection along length of beam

Beam 3

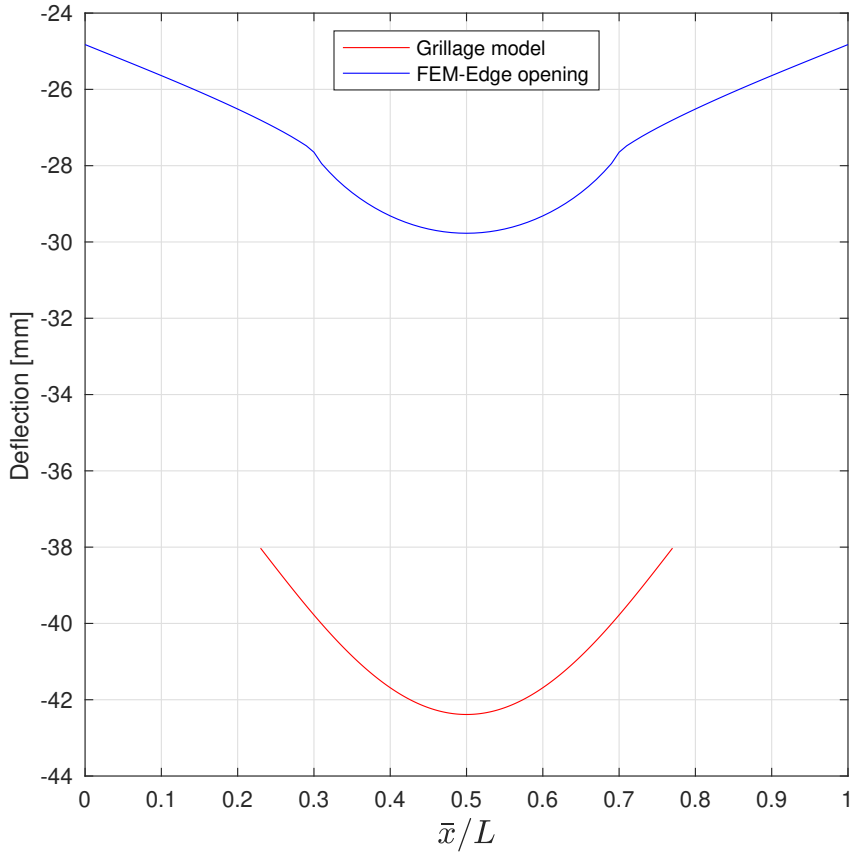

Figure 5.24: Deflection along beam 3

In Figure 5.24 neither deflection curves start at zero. The reason is that in both the grillage model and the finite element model the points at which the curves start are already deflected, in comparison to the unloaded case. In the grillage model beam 3 starts at a point on beam 5 which is deflected. In the finite element model the path along which data is collected also starts at a point which is deflected. The results show a large difference in deflection, due to differing starting values and also the shape of the curves.

Beam 5

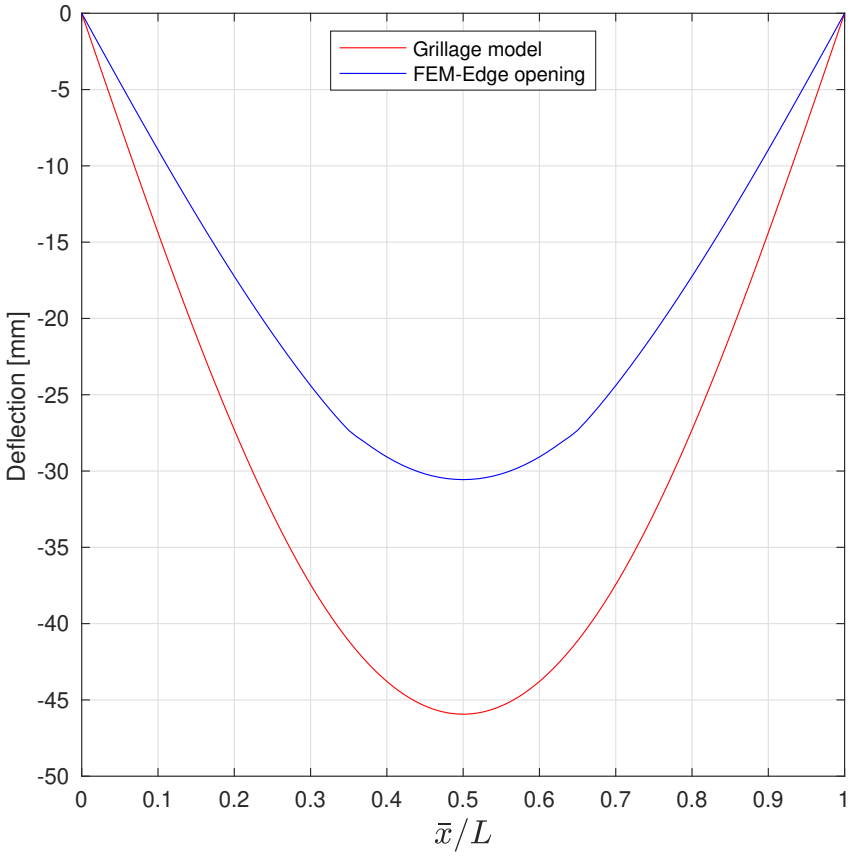

Figure 5.25: Deflection along beam 5

Similar to beam 3 the deflection of beam 5 is greater in the grillage model than the corresponding path in the finite element model.

6 Parameter study

In this chapter, results from the grillage model and the finite element model are compared and results from parameter studies relating to geometry parameters are presented. The investigated parameters include width, length and size of opening. Maximum values for shear force, bending moment and deflection are compared. In the finite element model, data is collected along the paths described in Chapter 4. The three cross section compositions described in Section 5.1 are analysed individually and then compared. A finite element model of a reference plate has also been created. The reference plate has no opening and is loaded with the same uniformly distributed load of 4 kN/m^2. Values are taken from two different paths in the reference plate, one path along each of the center lines of the reference plate (longitudinal and transversal direction). Both paths span across the whole length and width of the plate, respectively. In the reference plate the bending moment and shear force across the width of the plate have the value zero.

Section force capacities

The shear force and bending moment are presented in terms of degree of utilization in comparison to the respective capacities. The theory behind the calculation of the moment and shear force capacities are presented earlier in Section 3.6. The required input parameters to determine the capacities are presented in Table 6.1, where also the assumed magnitudes of the individual parameters are presented.

Table 6.1: Input parameters for calculation of load-bearing capacities

Parameter	Value	Explanation
k_{sys} [-]	1.0	System effect factor used to determine the moment capacity.
f_{mk} [MPa]	24	Characteristic bending strength.
$f_{vk,090}$ [MPa]	4	Characteristic longitudinal shear strength.
$f_{vk,9090}$ [MPa]	1.1	Characteristic rolling shear strength.

Using the above determined input parameters as well as parameters determined in Chapter 5, the magnitude of the following capacities for the CLT plate are established for the three evaluated compositions individually.

To determine the bending moment capacity equation (3.31) is used and to determine the longitudinal and rolling shear force capacity equation (3.33) and equation (3.34), respectively, are used. For the calculation of the included parameters in these equations a reference is made to Section 3.6.

Table 6.2: The plate strength determined for the three different compositions

Capacity	**Composition**		
	Longitudinal distribution (70-20-20-20-70)	Equal distribution (40-40-40-40-40)	Transversal distribution (20-70-20-70-20)
$M_{xy,r}$ [kNm/m]	13.9	55.5	102.2
$M_{yx,r}$ [kNm/m]	155.8	126.7	78.2
$V_{xz,r,long}$ [kN/m]	173.3	346.7	432.6
$V_{xz,r,roll}$ [kN/m]	47.7	95.3	119.0
$V_{yz,r,long}$ [kN/m]	564.6	621.2	704.9
$V_{yz,r,roll}$ [kN/m]	157.0	181.5	199.2

In the parameter study these capacities for the CLT plate are used to determine the degree of utilization when one parameter is varied. When the utilization in the following parameter study exceeds 1.0 the characteristic strength of the CLT is reached, leading to failure in the CLT element.

6.1 Width of opening

This section presents results from models with different opening widths, ranging from 0.001 m to 3.6 m. The length of the opening is always 1 m. The maximum width is determined by the constraints of the grillage model requiring that the opening cannot be placed closer than one beam width to the edge of the plate. The smallest and largest opening examined are shown in Figure 6.1.

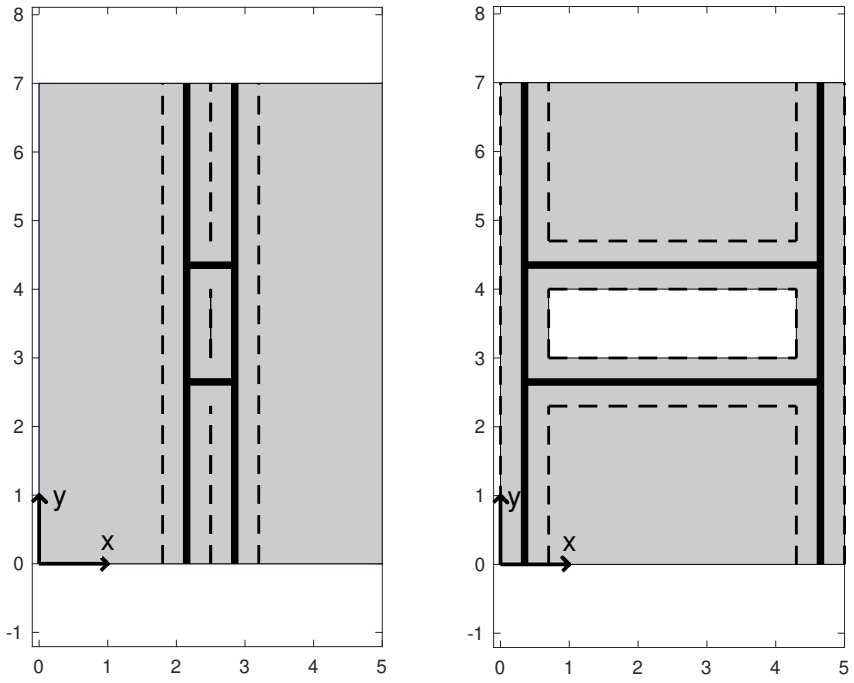

Figure 6.1: Minimum and maximum opening width for the geometry of this parameter study

Due to symmetry, results are reported for only one beam in each direction. As mentioned earlier, each parameter study investigates three different quantities; shear force, bending moment and deflection. The short transversal beams are numbered 3 and 4. The longitudinal beams are numbered 5 and 6. See Figure 3.7 for illustration.

6.1.1 Shear force

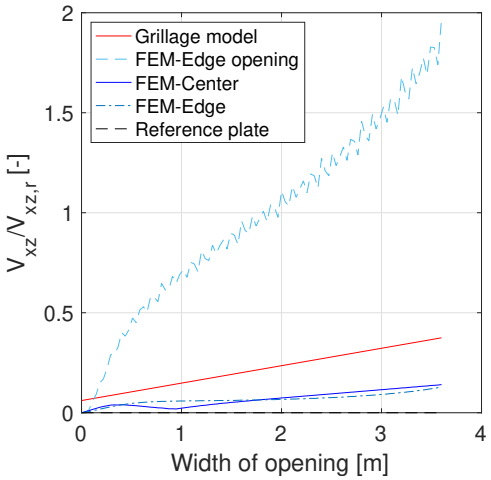

(a) Composition - Longitudinal distribution

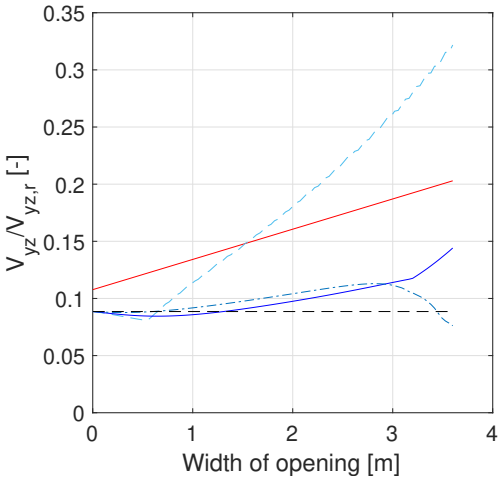

(b) Composition - Longitudinal distribution

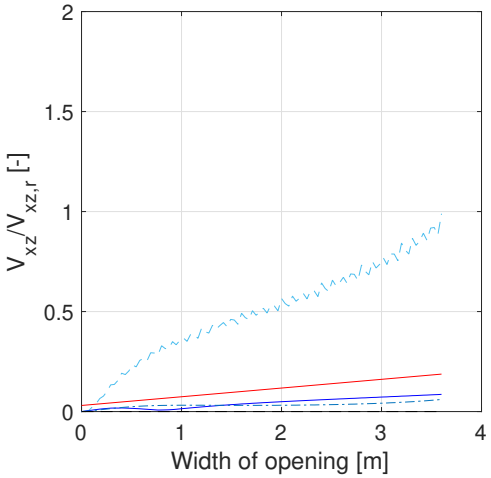

(c) Composition - Equal distribution

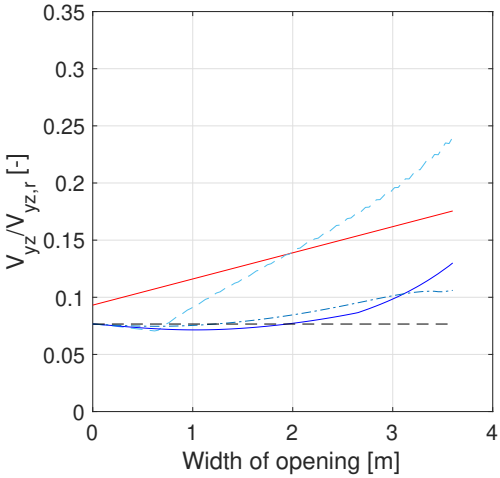

(d) Composition - Equal distribution

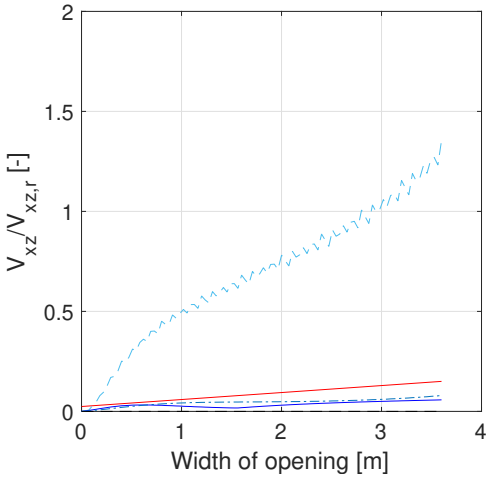

(e) Composition - Transversal distribution

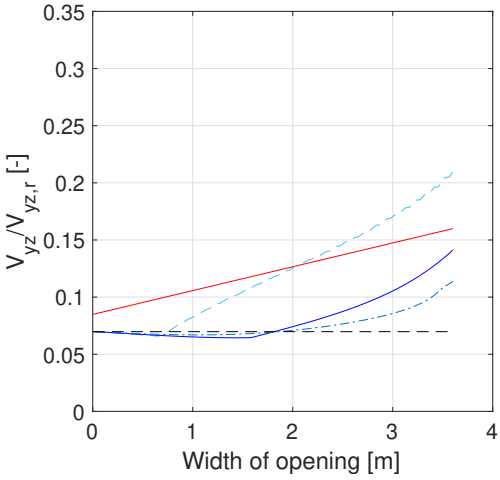

(f) Composition - Transversal distribution

Figure 6.2: Normalized maximum shear force vs. width of opening for the three considered compositions. Left column beam 3, right column beam 5.

Figure 6.2 shows that the three different cross section compositions show the same general pattern, increasing maximum shear force as the width of the opening increases. However, they differ in degree of utilization. For the grillage model the degree of utilization is highest in the longitudinal composition and lowest in the transversal composition. It is different in the finite element models where the longitudinal composition again has the highest degree of utilization but the equal composition has the lowest.

As the width of the opening increases, beam 3 in the grillage model becomes longer meaning that the total load increases because it is subjected to a line load according to the grillage model. In Figure 6.2 a), c) and e), this is expressed by that the maximum shear force in beam 3 (V_{xz}) increases linearly. In the finite element models, the maximum shear force, V_{xz} in the center path increases, then decreases, only to increase again. This pattern is most obvious for the longitudinal composition, see Figure 6.2a, where the increase and subsequent decrease occurs between opening widths of approximately $0 - 1$ meter. In Figure 6.2c and Figure 6.2e, the same pattern exist but less pronounced. For the transversal composition shown in Figure 6.2e, the increase and decrease occurs for an opening width of approximately $0 - 1.5$ meters. The maximum values of shear force V_{xz} for the path along the edge of the opening increases rapidly and the curve is not smooth.

The curves representing the maximum shear force in beam 5 (V_{yz}) in Figure 6.2 increases linearly according to the grillage model, just like the corresponding curves for beam 3. Again, it is explained by an increased load on beams 3 and 4, which in turns leads to a larger total load on beams 5 and 6, resulting in an increasing maximum shear force, V_{yz}. In the finite element model, the maximum shear force, V_{yz}, in the center path first decreases to values lower than the reference plate and then increases. The path that runs along the edge displays increasing maximum shear force but not as pronounced as in the paths that corresponds to beam 3 (V_{xz}).

The degree of utilization for shear forces V_{xz} and V_{yz} are generally relatively small. If the curve showing the maximum shear force in the edge of the opening in the finite element model is disregarded, a utilization of no more than approximately $30\% - 40\%$ of the capacity is reached. However, shear force might not be the limiting factor when bending moment and deflection is considered. The curve showing the maximum shear force at the edge of the opening in the finite element model differs from the other curves because this curve also contains results from stress concentrations close to corners of the opening in the model.

6.1.2 Bending moment

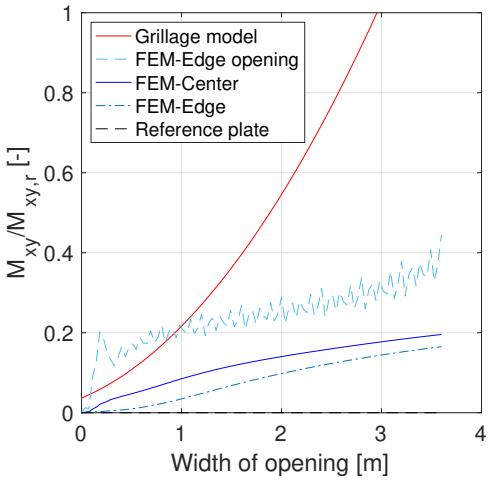

(a) Composition - Longitudinal distribution

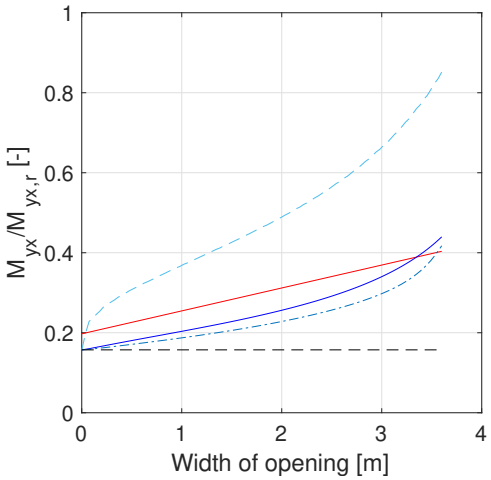

(b) Composition - Longitudinal distribution

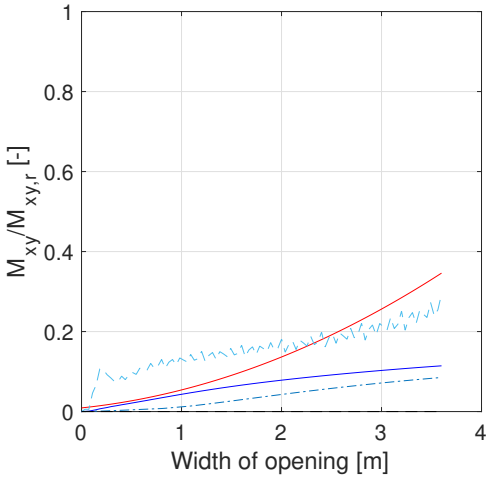

(c) Composition - Equal distribution

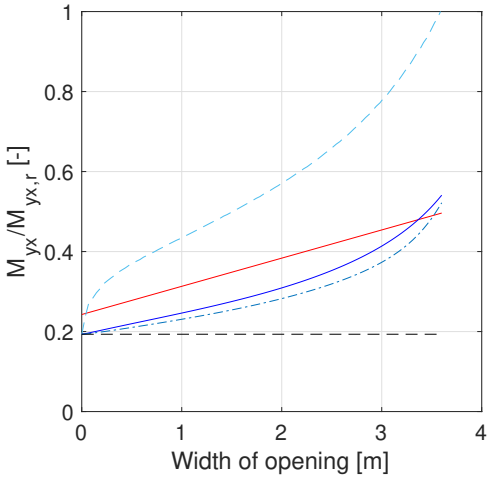

(d) Composition - Equal distribution

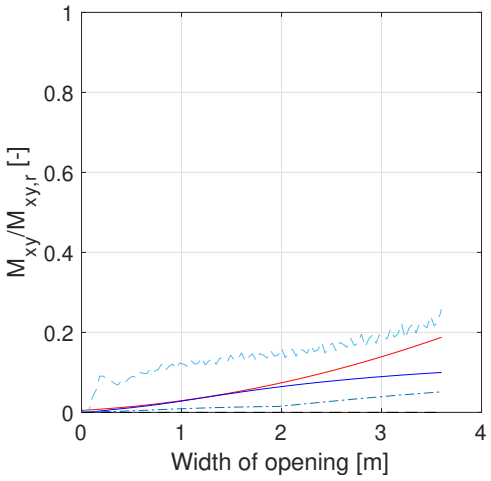

(e) Composition - Transversal distribution

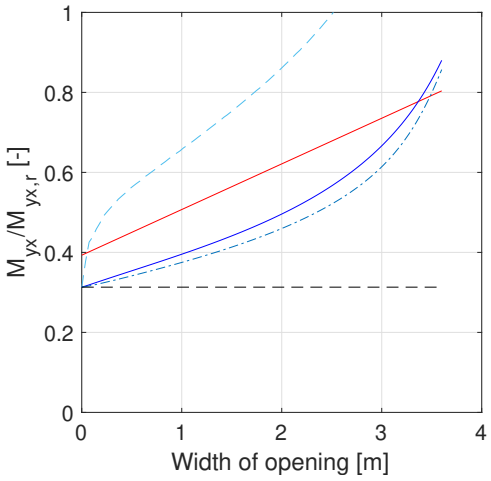

(f) Composition - Transversal distribution

Figure 6.3: Normalized maximum bending moment vs. width of opening for the three considered compositions. Left column beam 3, right column beam 5.

As the width of the opening increases the maximum bending moment in beam 3, (M_{xy}), increases rapidly according to the grillage model. That is expected due to the fact that the length of beam 3 in the grillage model increases. In the expression for maximum bending moment in a simply supported beam with a distributed load the length is squared. In the finite element model the maximum bending moment, M_{xy}, increases but the slope of the curve decreases as the width of the opening increases. The two diametrically different behaviours are explained by the differing load paths. In the finite element model, the load is carried around the opening meaning that the bending moment does not concentrate at the edge of the opening. In the grillage model, the load must be carried by beam 3 and distributed to beams 5 and 6.

The curves describing the maximum bending moment in beam 5, (M_{yx}) showed a smaller difference between the grillage model and the finite element model than for beam 3. In the grillage model, the maximum bending moment increases linearly whereas the corresponding values taken from the center path of the finite element model shows an accelerating increase. The maximum bending moment has a higher start value in the grillage model compared to the finite element model. The values from the grillage model intersects with those from the center path in the finite element model as the maximum bending moment in the finite element model increases rapidly for large opening widths. This occurs when the width of the opening reaches approximately 3.5 meters.

The results from the finite element model display an interesting pattern. When the width of the opening increases to widths above approximately half the plate width, the slope of the graphs showing the bending moment M_{xy} (transversal) decreases significantly. Concurrently the bending moment M_{yx} (longitudinal) begins to increase rapidly, see Figure 6.3. It indicates that when the opening reaches a certain width the stress distribution and thereby the bending moment in the plate is redistributed in such way that it does not affect beams 3 and 4 to the same extent. Instead the stresses are redistributed so that they circumvent the corresponding locations of beams 3 and 4. The wide opening also entails that the stresses and thereby also the bending moments are concentrated to a smaller part of the plate when transferred past the opening. This smaller part corresponds to the location of the longitudinal beams, beams 5 and 6, in the grillage model. Meaning that the bending moment gets concentrated in the position of beams 5 and 6, which explains the rapid increase in the finite element model results.

The different compositions show large differences in degree of utilization. For bending moment (M_{xy}) in beam 3, the longitudinal composition results in the highest degree of utilization whilst the transversal composition gives the lowest. This is seen clearly in Figure 6.4 which is a zoomed out version of Figure 6.3a. Here, the degree of utilization surpasses 120% of the capacity according to the grillage model although this is not in line with corresponding results from the finite element model.

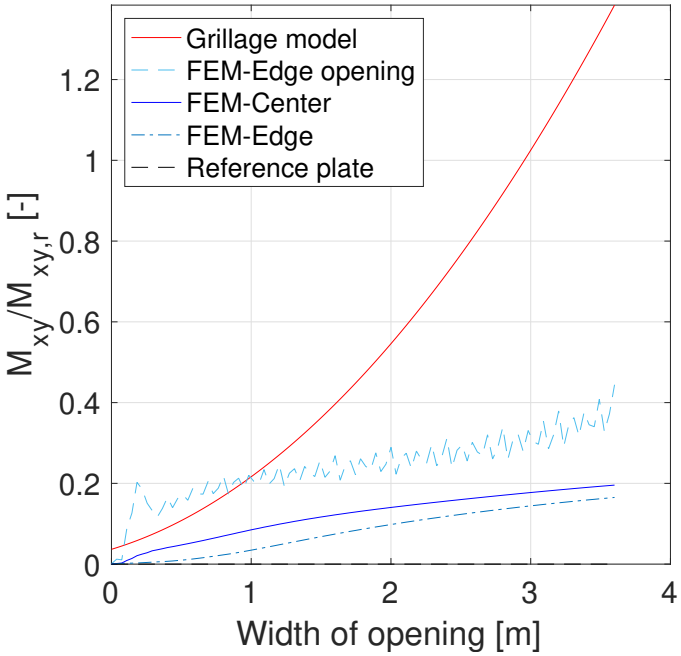

Figure 6.4: Graph showing maximum bending moment in beam 3 depending on opening width for the longitudinal cross section composition

6.1.3 Deflection

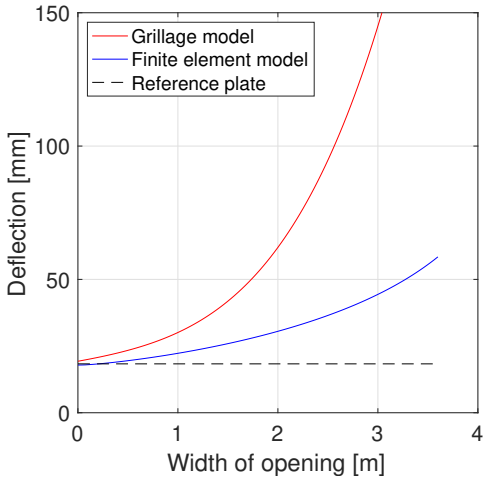

(a) Composition - Longitudinal distribution

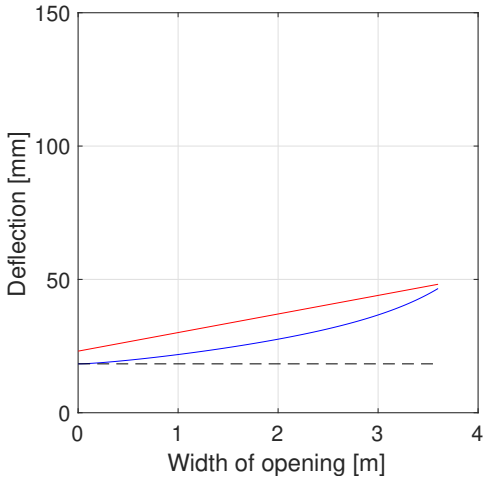

(b) Composition - Longitudinal distribution

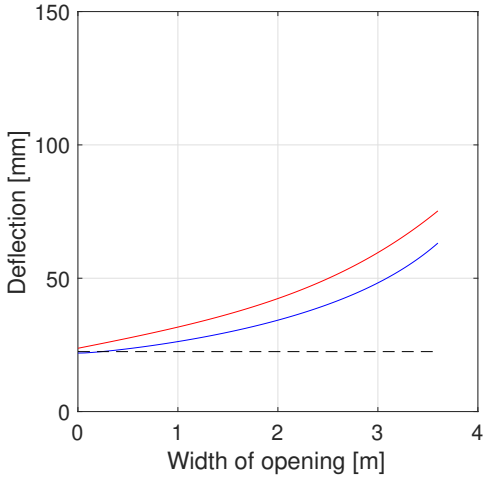

(c) Composition - Equal distribution

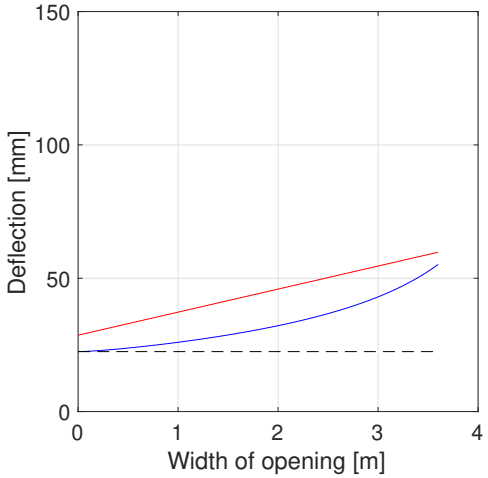

(d) Composition - Equal distribution

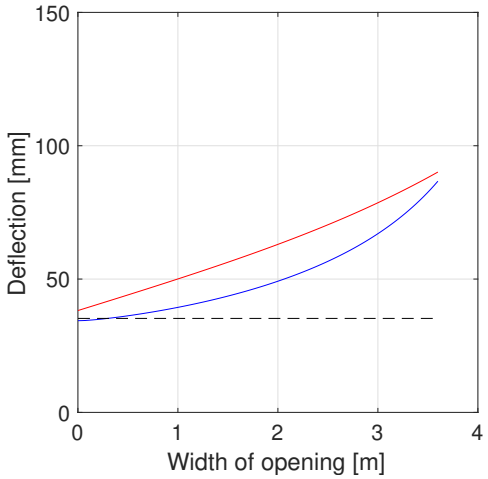

(e) Composition - Transversal distribution

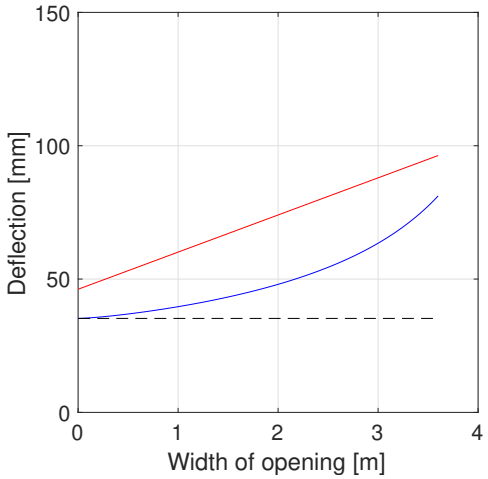

(f) Composition - Transversal distribution

Figure 6.5: Maximum deflection vs. width of opening for the three considered compositions. Left column beam 3, right column beam 5. and 6.

The deflection is consistently larger in the grillage model compared to the finite element model. The curves showing the deflection mirror the results from the maximum bending moment in Figure 6.3 in several ways. The curves showing maximum deflection in beam 3 according to the grillage model show significantly different behaviour between the cross section compositions. As the cross section composition change from a longitudinal distribution to a transversal, the deflection curve shifts from a rapidly increasing curve into a straighter curve indicating increased stiffness. This is not mirrored in the finite element model where the shape of the curves does not change, only the magnitude of the deflection. The difference between the results from the grillage model and the results from the finite element model increases with opening width, which is reminiscent of Figure 6.6 which is a zoomed out version of Figure 6.5a. The figure shows how the bending moment in beam 3 according to the grillage model is at a much higher level than in the finite element model as the width of the opening increases.

For beam 5, the maximum deflection also increases with increasing opening width. In the grillage model, the point loads on beams 5 increases with opening width which in turn increases bending moment and deflection. In the finite element model, the deflection also increases, here in an exponential manner. Overall the graphs representing beam 5 mirror those for bending moment shown in Section 6.1.2.

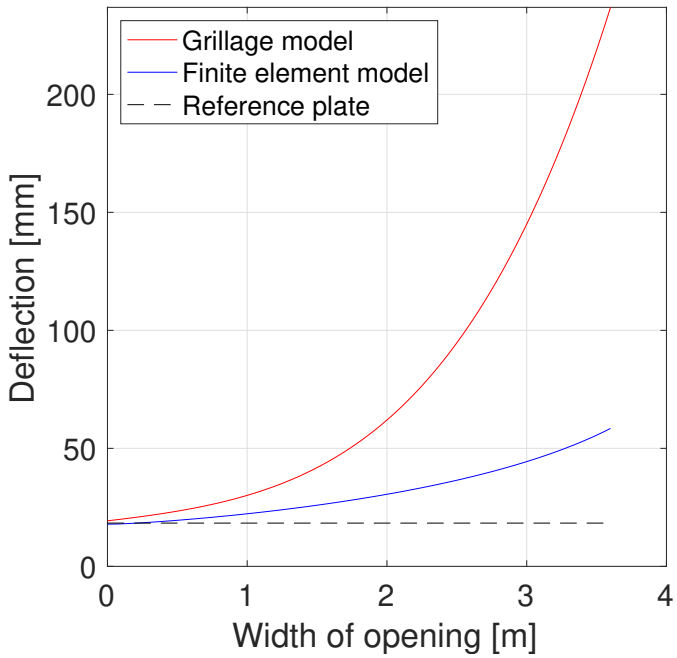

Figure 6.6: Graph showing maximum deflection in beam 3 depending on opening width for the longitudinal cross section composition

6.2 Length of opening

In this section, the effect of opening length on the maximum values for shear force, bending moment and deflection is investigated. Results are presented from models with different opening lengths, ranging from 0.001 m to 5.6 m. The maximum length is determined by the constraints of the grillage model requiring that the opening cannot be placed closer than one beam width to the edge of the plate. The width of the opening is kept constant at 1 m. The minimum and maximum opening lengths are illustrated in Figure 6.7.

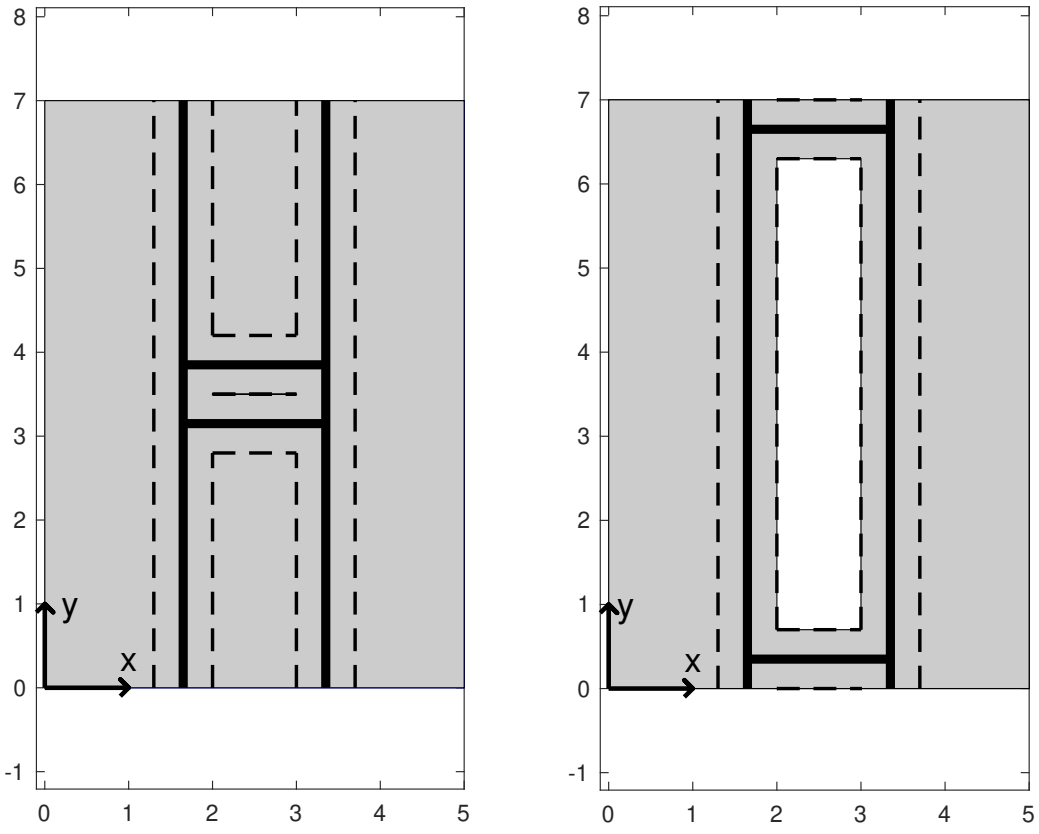

Figure 6.7: Minimum and maximum opening length for the geometry of this parameter study

6.2.1 Shear force

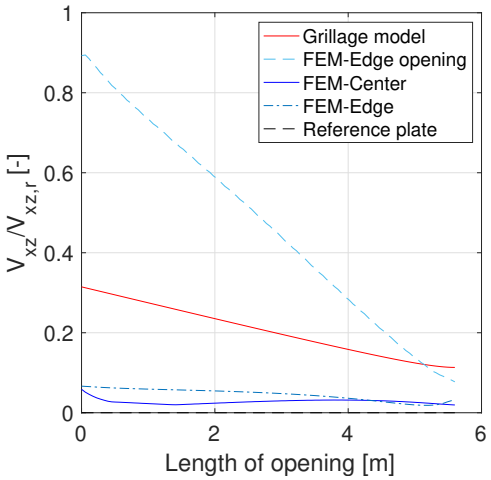

(a) Composition - Longitudinal distribution

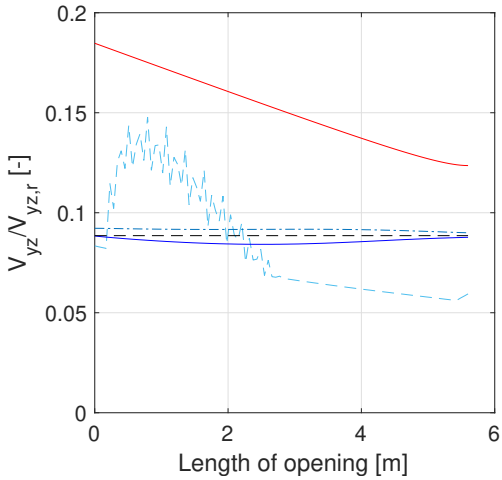

(b) Composition - Longitudinal distribution

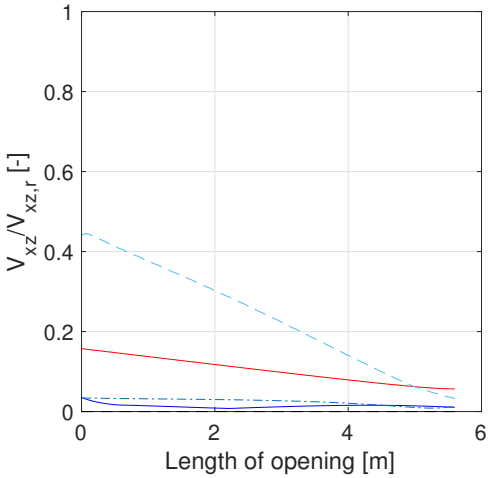

(c) Composition - Equal distribution

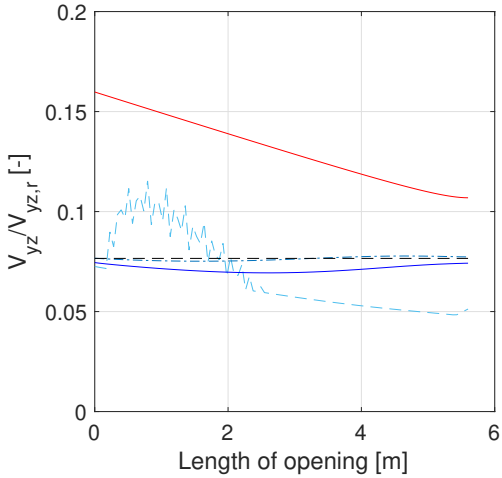

(d) Composition - Equal distribution

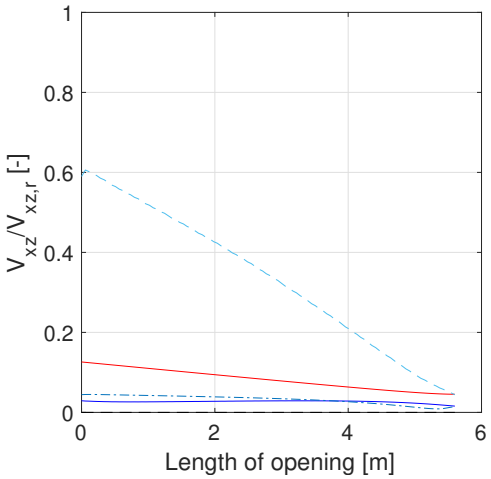

(e) Composition - Transversal distribution

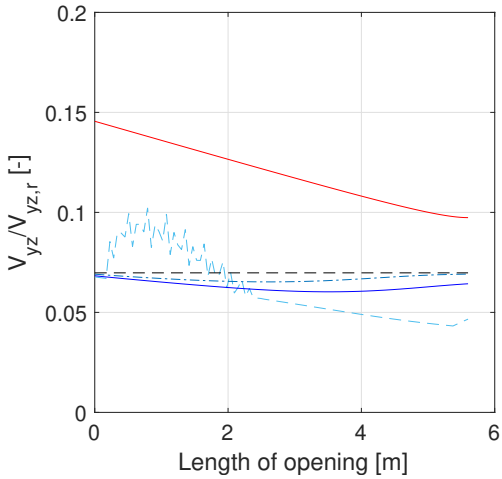

(f) Composition - Transversal distribution

Figure 6.8: Normalized maximum shear force vs. length of opening for the three considered compositions. Left column beam 3, right column beam 5.

For the finite element model the maximum shear force in comparison to the capacity decreases as the opening lengthens. In the grillage model, the maximum shear forces reduces linearly because the magnitude of the distributed load on beams 3 and 4 decreases as the beams move closer to the supported edges. For the graph in Figure 6.8a showing center path in the finite element model the maximum shear force, V_{xz}, decreases between a length of the opening of $0 - 1.5$ m and then increases from $1.5 - 4$ m, after that the curve stagnates. However, the maximum shear force, V_{xz}, along the path that runs along the opening edge decreases from a relatively high value down to a low value that is very similar to the one given by the grillage model.

In Figure 6.8b the curve showing the maximum value for the shear force in beam 5, V_{yz}, according to the grillage model, decreases as the length of the opening increases. As the length of the opening increases the point loads acting on beam 5 decrease in magnitude. This is the case because the line loads which act on beam 3 and 4 decrease in magnitude as the length of the opening increases.

In the finite element model, the value for the maximum shear force, V_{yz}, recorded from the center path, stays close to the value given by the reference plate. It decreases slightly from a value similar to that of the reference plate at first. The decrease stops at an opening width of approximately 3.0 m and then it increases again to reach a final value again similar to that for the reference plate. The same pattern is seen across all cross section compositions. This behaviour can be explained by the observation that when the opening is small in length, the plate in whole is similar to the reference plate with just a tiny opening in the middle, which results in similar maximum shear forces as for the reference plate. When the length of the opening increases the effect of the opening gets more distinct and the shear force in beam 5 and 6 decreases. The total load on the plate decreases when the area of the opening increases. When the length of the opening pass half the total length of the plate, the transversal connection between the two longitudinal parts do not transfer much load between the longitudinal parts. The load acting on the increasingly smaller parts of the plate diminishes and has lower impact on the results. Instead, the plate begin to act more like two separate parallel beams loaded with one surface load each and with just a small load acting on the connection between them.

The results from the paths that run along the edge of the opening in the finite element model show interesting results. For beam 3 the maximum shear force V_{xz} recorded along the corresponding edge path starts out considerably higher than values taken from the grillage model or other paths in the finite element model. As the opening length increases it decreases rapidly and approaches the values taken from the grillage model.

It should also be noted that when the length of the opening is examined the edge path corresponding to beam 3 produces a smooth curve whilst the edge path for beam 5 does not. Opposite of the results from the study of the width of the opening.

Observing the degree of utilization it is worth mentioning also here that the utilization of shear forces V_{xz} and V_{yz} are generally relatively small, excluding the curve representing the edge of the opening containing stress concentrations, referring to previous mentioned arguments in Section 6.1.1.

6.2.2 Bending moment

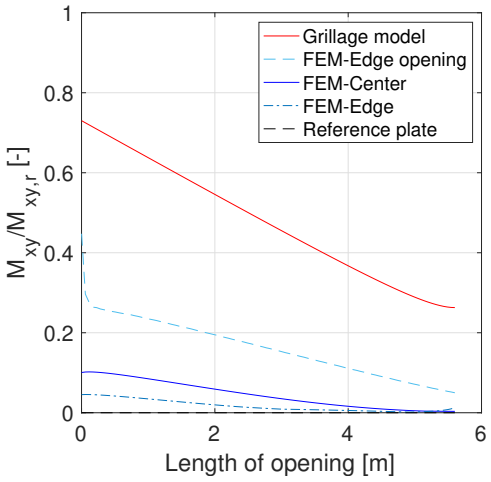

(a) Composition - Longitudinal distribution

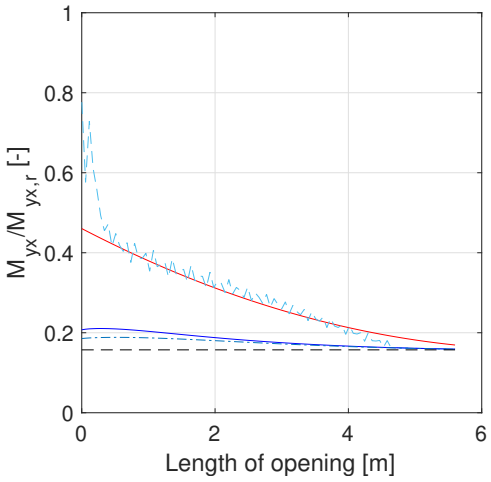

(b) Composition - Longitudinal distribution

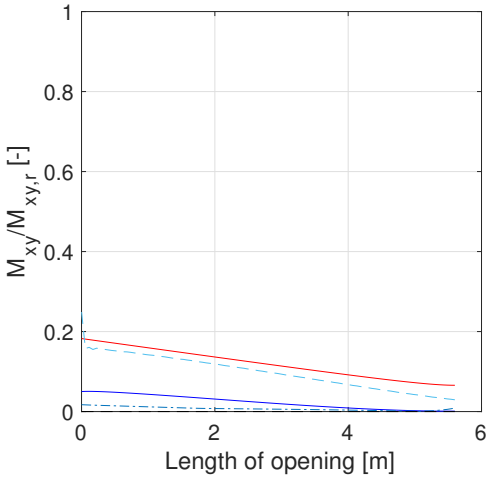

(c) Composition - Equal distribution

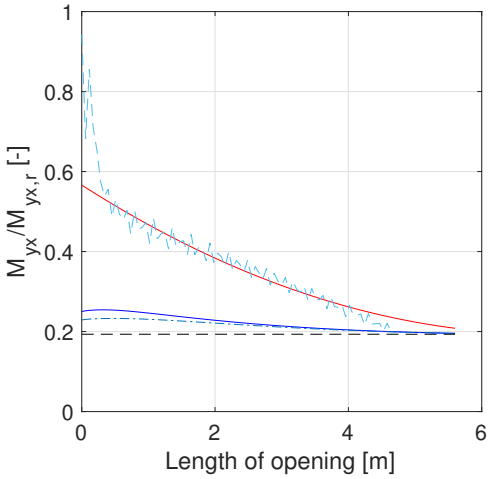

(d) Composition - Equal distribution

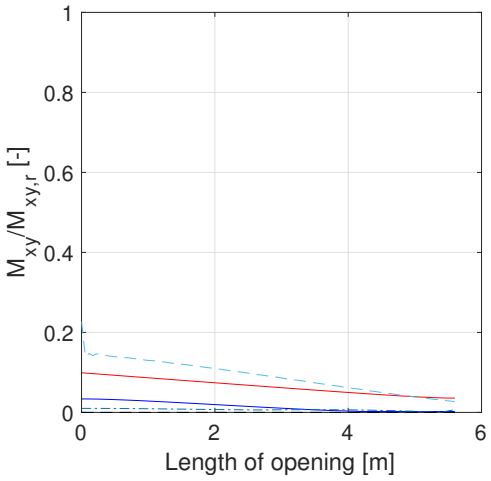

(e) Composition - Transversal distribution

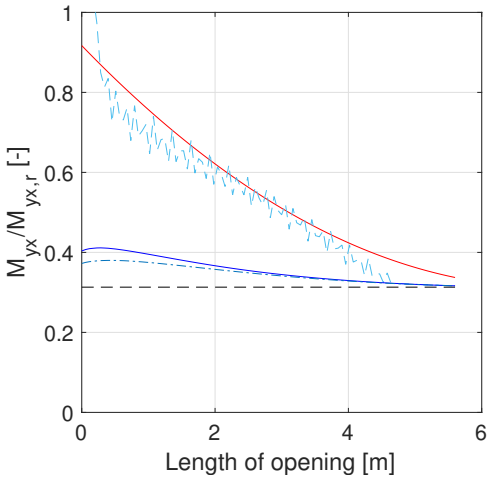

(f) Composition - Transversal distribution

Figure 6.9: Normalized maximum moment vs. length of opening for the three considered compositions. Left column beam 3, right column beam 5.

In both the finite element model and the grillage model maximum bending moment, M_{xy}, decreases as the length of the opening increases. In the grillage model the distributed load that acts on beam 3 decreases with opening length, which results in that the bending moment decreases.

In the finite element model the maximum bending moment, M_{xy}, along the center path approaches zero, which is also the value in the reference plate. It is similar to what was shown for the shear force, V_{xz}, described previously. The load that is carried transversely across the plate decreases as the length of the opening increases. However, unlike for what was shown for the shear force V_{xz} in Figure 6.8, the maximum bending moment M_{xy} according to the center path in the finite element model for small openings do not resemble the results obtained from the reference plate. Instead, the initial value for maximum bending moment begins at a relatively high value for the plate with a small opening, when compared to the non existent bending moment M_{xy} in the reference plate. This is explained by the fact that even though the opening is small in length, it is still 1 m wide. The stresses are redistributed around the opening. The redistribution of stresses in the plate close to the opening results in a bending moment, M_{xy}, in the region corresponding to beam 3 in the grillage model.

In Figure 6.9, the difference in maximum bending moment between results from the grillage model and the finite element model exhibits two patterns. For the bending moment M_{xy}, the difference is largest in the longitudinal distribution and lowest in the transversal distribution. For M_{yx}, it is the opposite.

In Figure 6.9b, the maximum bending moment M_{yx} in both the grillage model and the finite element model approaches the value given in the reference plate. As the length of the opening increases, the areas on either side of the opening start to resemble two separate simply supported plates. It is because of this the maximum bending moment in both the grillage model and the finite element model approaches the same value as in the reference plate.

As for the graphs illustrating the shear force V_{yz}, also the graph showing the bending moment M_{yx} along the edge of the opening in the finite element model has a staggered shape. Although, a kind of logarithmic shape can be distinguished from the shape of the curve.

Also in this study, it can be discerned that the spread in degree of utilization between the different compositions is marked. For bending moment M_{xy} a utilization of nearly 80% percent is reached for the longitudinal distribution according to the grillage method. This in comparison to less than 20% for the transversal distribution according to the same model is noteworthy.

6.2.3 Deflection

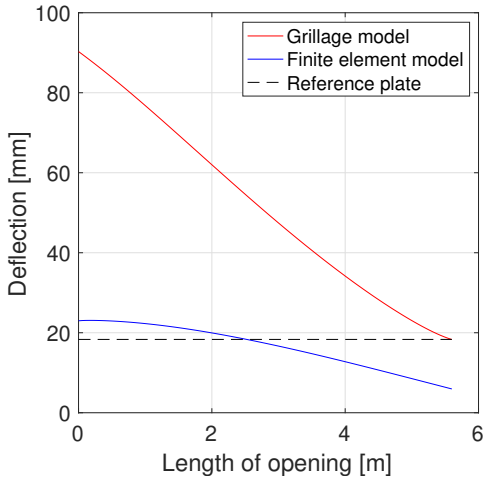

(a) Composition - Longitudinal distribution

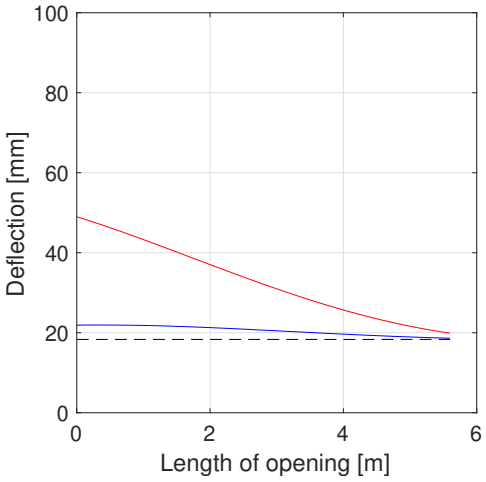

(b) Composition - Longitudinal distribution

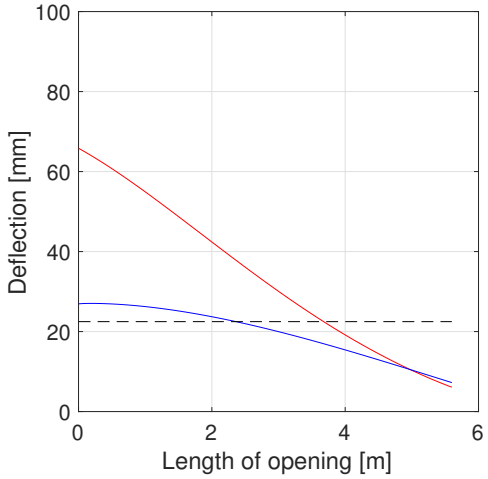

(c) Composition - Equal distribution

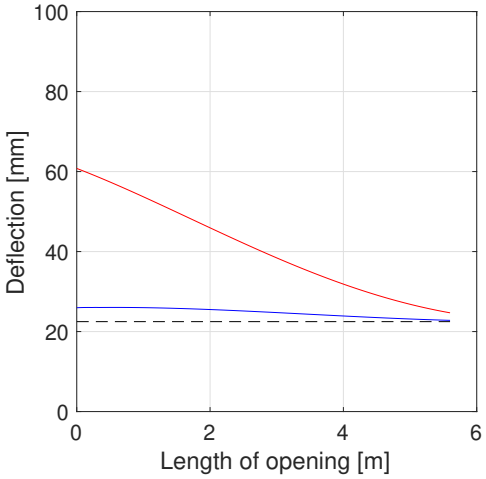

(d) Composition - Equal distribution

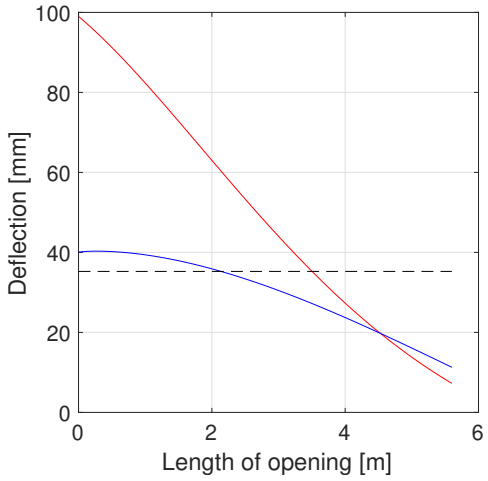

(e) Composition - Transversal distribution

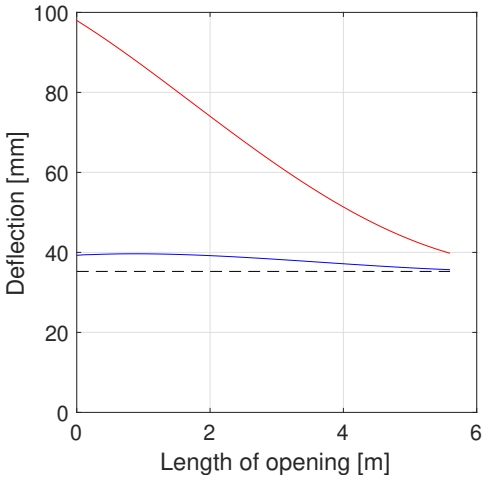

(f) Composition - Transversal distribution

Figure 6.10: Maximum deflection vs. length of opening for the three considered compositions. Left column beam 3, right column beam 5.

The results in the left column of Figure 6.10 is somewhat unclear in regards to the comparison between maximum deflection in the models with an opening and the reference plate. The reason that the maximum deflection along the transversal paths in the finite element model decreases, is because the region on the plate from which the deflection is measured changes as the opening length increases. As the opening length increases, the region measured moves closer to the supported edge which naturally gives a lower value of the deflection. In the grillage model the same is true as the value of the deflection at the supports of beam 3 decreases as the place of the support moves closer to the supports of beams 5 and 6. Another factor is that the magnitude of the distributed load on beam 3 decreases as the length of the opening increases. It is noticeable that the deflection in the grillage model starts at a higher value than in the finite element model but decreases more rapidly.

Also, for some of the cases there is a point where the two curves intersect each other within the investigated interval of the parameter study. This is the case for the deflection in the transversal beams, beams 3 and 4, with the equal and transversal distributions respectively. For the equal distribution this occur when the opening length reaches a value approximately 5 meters. For the transversal distribution the corresponding value is somewhat less, about 4.5 meters.

The results shown in the right column of Figure 6.10 are more clear for interpretation. The results from the grillage model show a higher deflection than those from the finite element model. The difference is greatest for the transversal distribution and lowest for the longitudinal. Both results from the grillage model and the finite element model move closer to those from the reference plate as the opening length increases. That is, as mentioned previously because that the geometry resembles two simply supported plates resting alongside each other as the opening length increases.

6.3 Size of opening

In this section, the effects of the opening size in the plate on the maximum values for shear force, bending moment and deflection are presented. For this purpose, the finite element model is set up with a minimum opening measuring 0.001×0.001 m^2. The size of the opening is increased to a maximum size of 3.6×3.6 m^2. The increase in opening size is also modelled according to the grillage method and the results compared.

The opening is kept in a square form and thereby not increasing the length of the opening to the maximum allowable length according to the grillage method, as was done previously when changing solely the length of the opening. The relation between the length and width of the opening remains constant so that the size of the opening is the only changing parameter.

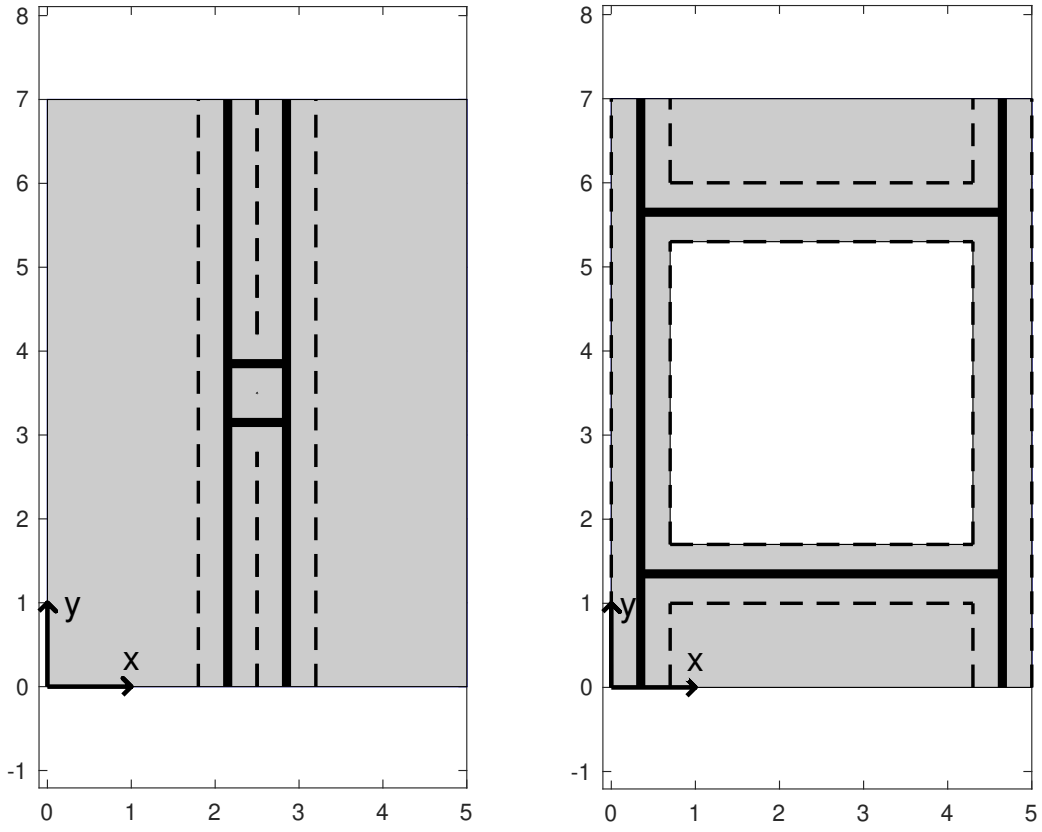

Figure 6.11: Minimum and maximum opening size for the geometry of this parameter study

6.3.1 Shear force

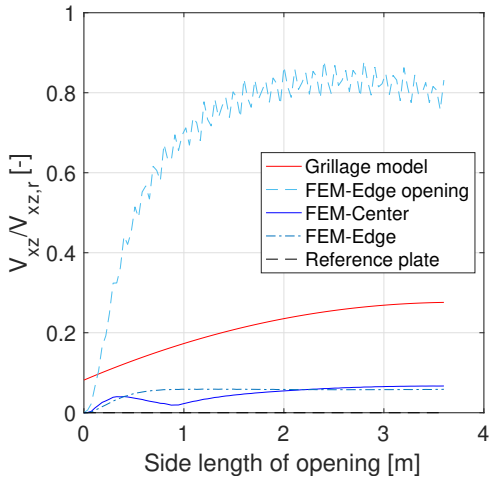

(a) Composition - Longitudinal distribution

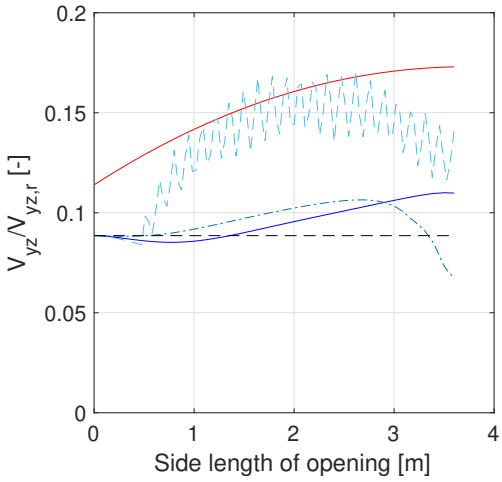

(b) Composition - Longitudinal distribution

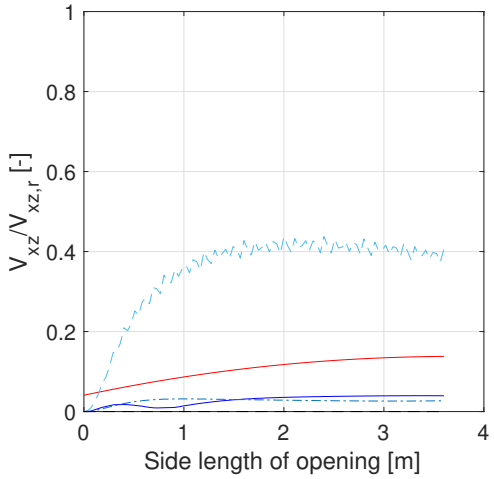

(c) Composition - Equal distribution

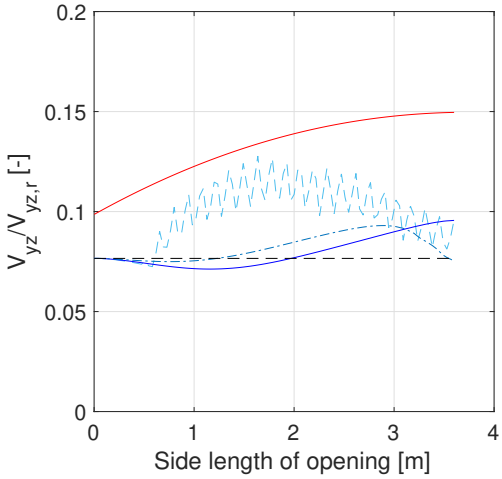

(d) Composition - Equal distribution

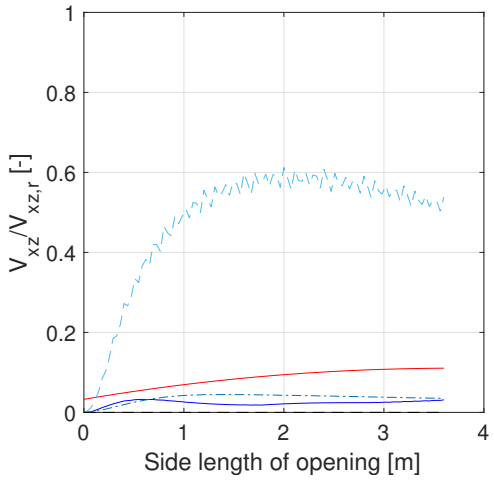

(e) Composition - Transversal distribution

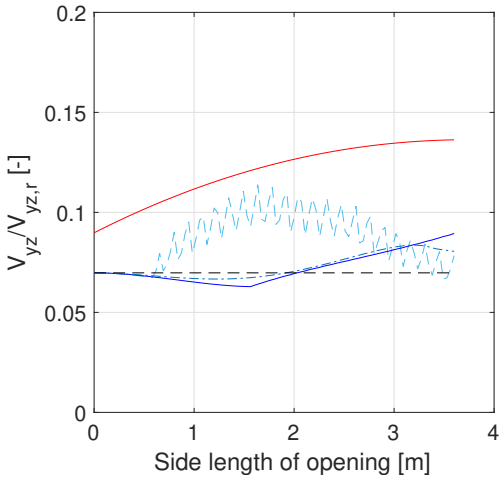

(f) Composition - Transversal distribution

Figure 6.12: Normalized maximum shear force vs. size of opening for the three considered compositions. Left column beam 3, right column beam 5.

As the size of the square opening increases, the length and width of the opening increase, the total load on the plate decreases because the loaded area decreases. In general, the results from Figure 6.12 can be interpreted by keeping the three aforementioned parameters in mind; length of opening, width of opening and the total load applied on the plate.

From previous sections, it is known that for the results from the grillage model the maximum shear force increases with increasing width, and decreases with increasing length. This hold true for both beams 3 and 5. The results in Figure 6.12 show that the maximum shear force in beams 3 and 5 increases but the gradient decreases with increasing size of opening. The two parameters, width and length, are having opposite effects resulting in the stagnating curves.

Regarding the degree of utilization, it is worth mentioning that the utilization of shear forces V_{xz} and V_{yz} are generally relatively small in comparison to the maximum capacity. If the curve showing the maximum shear force in the edge of the opening in the finite element model is disregarded, a utilization of no more than approximately 30% of the capacity is reached. The curve showing the maximum shear force in the edge of the opening in the finite element model is different from the other curves. That because this curve also contains results from stress concentrations close to the corners of the opening in the model.

It should be noticed that beams 3 and 5 both have similar degrees of utilization of approximately $15\% - 30\%$ of the capacity. This is advantageous when designing CLT plates as a similar utilization longitudinally and transversely means an increased total utilization of the material.

It is noticeable that when changing the size of the opening, namely both the length and width of the opening at the same time, none of the six curves representing results from the paths that run along the edge of the opening in the finite element model are smooth. In previous sections where length or width was changed exclusively either beam 3 or beam 5 exhibited the discontinuous curves but not both at the same time. It shows that the curves generated by changing the size of the opening is a mix between the results obtained from changing the length and the width of the opening exclusively, as done in previous sections.

6.3.2 Bending moment

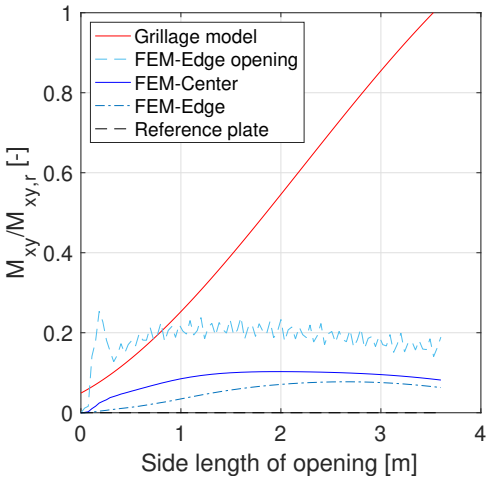

(a) Composition - Longitudinal distribution

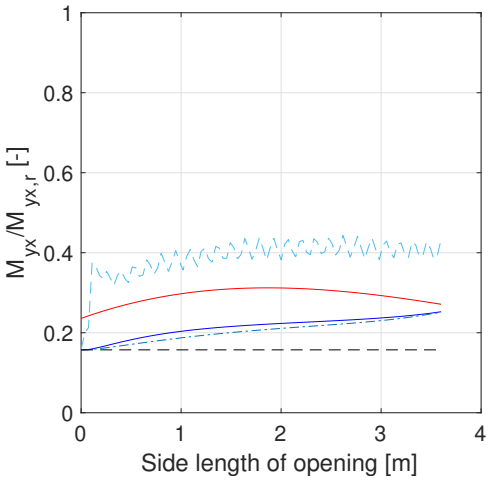

(b) Composition - Longitudinal distribution

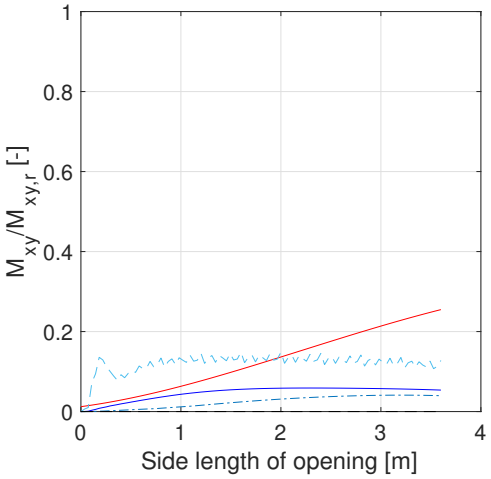

(c) Composition - Equal distribution

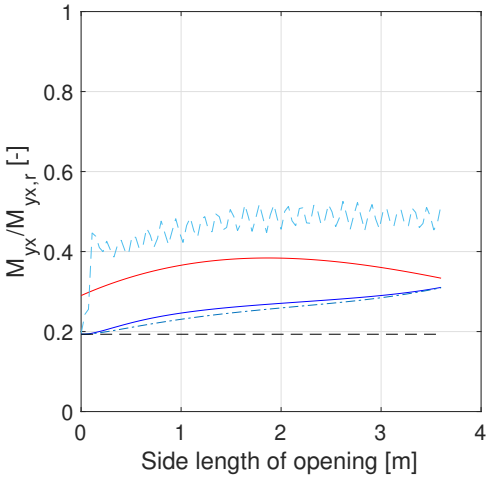

(d) Composition - Equal distribution

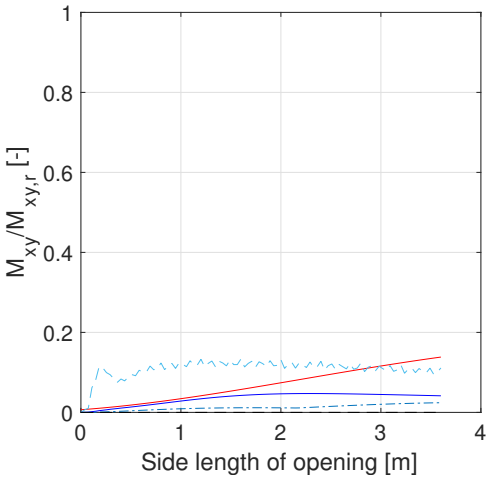

(e) Composition - Transversal distribution

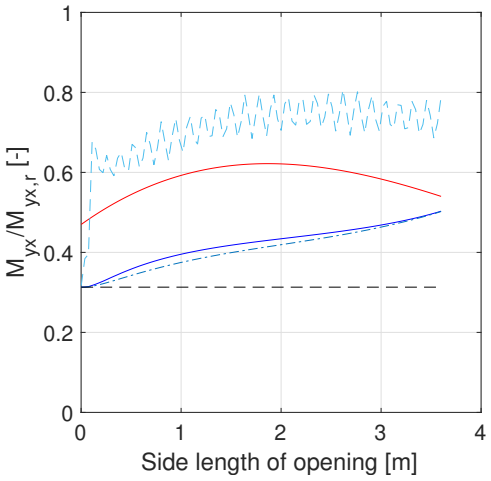

(f) Composition - Transversal distribution

Figure 6.13: Normalized maximum moment vs. size of opening for the three considered compositions. Left column beam 3, right column beam 5.

In Figure 6.13, the curves presenting maximum bending moment M_{xy} for beam 3 according to the grillage model show a similar pattern to previous chapters where the longitudinal distribution exhibits relatively high degree of utilization compared to the other compositions.

Results corresponding to beam 3 from the grillage model, taken from the finite element models center paths, show that the maximum bending moment first increases and then decreases. This again is a result of opposite effects from the increase of length and width. In terms of degree of utilization the transversal composition show the lowest degree of utilization and the longitudinal composition the highest.

The maximum bending moment in beam 5 according to the grillage model increases and then decreases. This is as well a result of opposite effects. The maximum bending moment increases as the length of beams 3 and 4 increases as more load is then transferred onto beams 5 and 6. However, as the length of the opening increases, the places where beams 3 and 4 rests on beams 5 and 6 move closer to the supported edges which leads to decreasing maximum bending moment. The form of the curve indicates that the effect of increasing opening width in relation to the effects of increasing opening length is largest in the beginning when evaluating smaller openings as the bending moment here increases. Later, when larger openings are evaluated the effects of increasing opening length takes over more and more in relation to the effects of increasing opening width, this is demonstrated by the decreasing gradient of the bending moment curve for the larger openings.

In the finite element model, the corresponding values for beam 5 do not reach a point where the maximum bending moment decreases. It is noticeable that the difference between the values from the grillage model and those from the center path in the finite element model decrease as the size of the opening increases. At the maximum size the difference is small between the models.

The large spread in degree of utilization for the bending moment when changing the size of the opening is noteworthy. For beam 3 the utilization varies between the different compositions from a maximum of approximately 15% for the transversal distribution to a maximum of 100% for the longitudinal distribution, both results according to the grillage model, referring to Figure 6.13a as well as Figure 6.13e. For beam 5 the variation is less, here the opposite relation is valid with a maximum utilization of 30% of the capacity for the longitudinal distribution and nearly 65% for the transversal distribution, according to the grillage model. The difference is illustrated by comparing Figure 6.13b and Figure 6.13f respectively.

6.3.3 Deflection

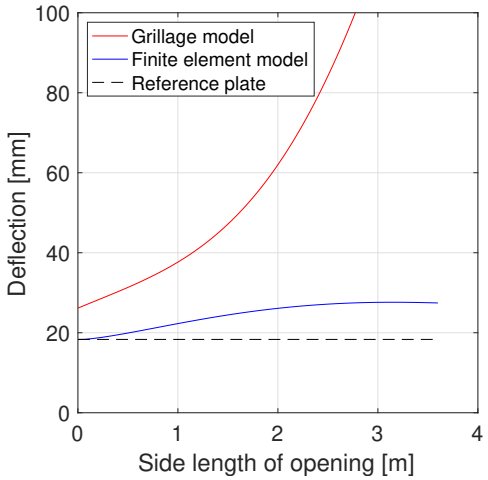

(a) Composition - Longitudinal distribution

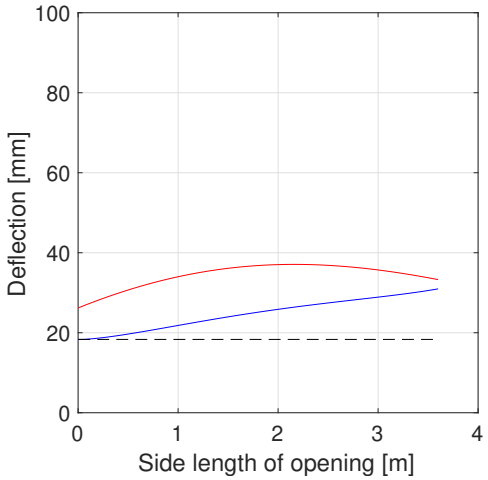

(b) Composition - Longitudinal distribution

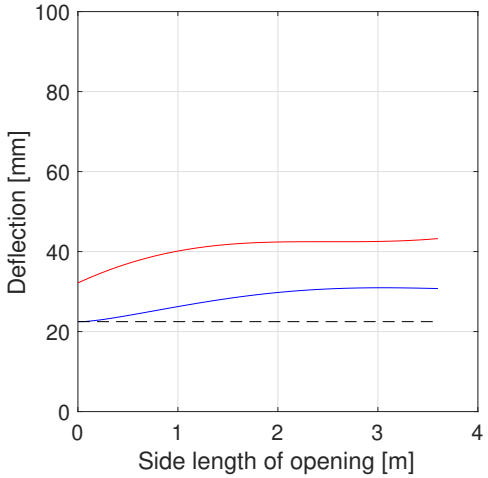

(c) Composition - Equal distribution

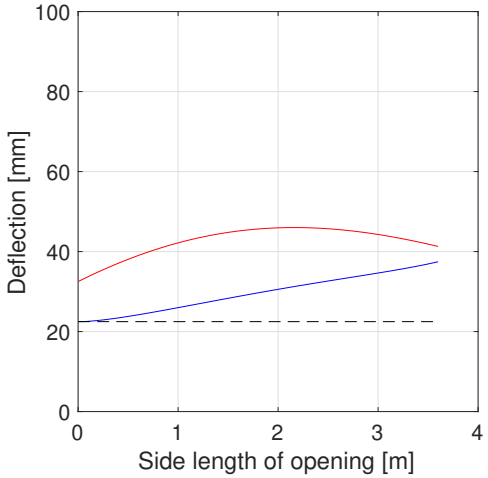

(d) Composition - Equal distribution

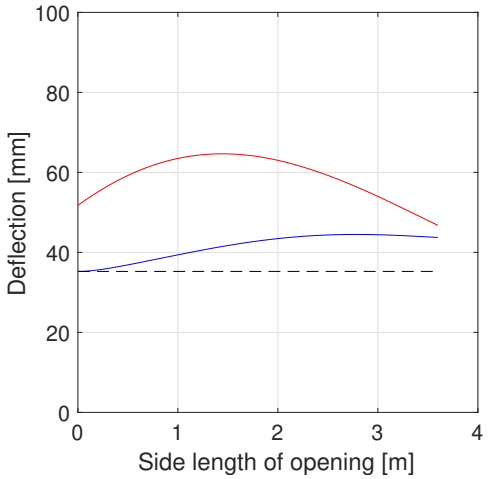

(e) Composition - Transversal distribution

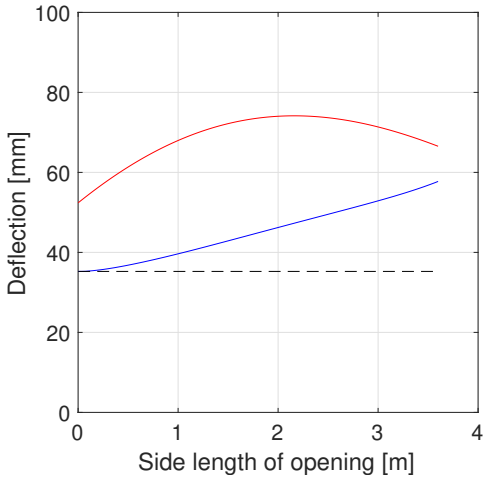

(f) Composition - Transversal distribution

Figure 6.14: Maximum deflection vs. size of opening for the three considered compositions. Left column beam 3, right column beam 5.

Overall, the results showing the maximum deflection according to the grillage model and the finite element model mirror those of the maximum bending moments. The shapes of the maximum deflection curves show greater variety than those of the maximum bending moment. Especially for the regions corresponding to beam 3 where the results from the different distributions according to the grillage model differ significantly in shape.

The results from the finite element model are less diverse. They are similar, showing small variation between the different cross section compositions.

Evaluating the results of deflection development when increasing the size of the opening, one major observation is made. When comparing the longitudinal distribution with the equal distribution it is seen that the difference in deflection in beam 3 according to the grillage model is remarkable. The deflection in beam 3 reaches a magnitude of more than 160 mm for the longitudinal distribution while the maximum deflection with the equal distribution do not exceed 50 mm according to the grillage model, referring to Figure 6.14c and the zoomed out version of Figure 6.14a represented in Figure 6.15. However, comparing the deflection in beam 5 between these two compositions according to the grillage model the difference is smaller. For the longitudinal distribution, the deflection stays below 40 mm and for the equal distribution the deflection reaches towards 50 mm, see Figure 6.14b and 6.14d respectively. This large difference between the two compositions regarding deflection in beam 3 but almost no difference regarding deflection in beam 5 is rather noteworthy.

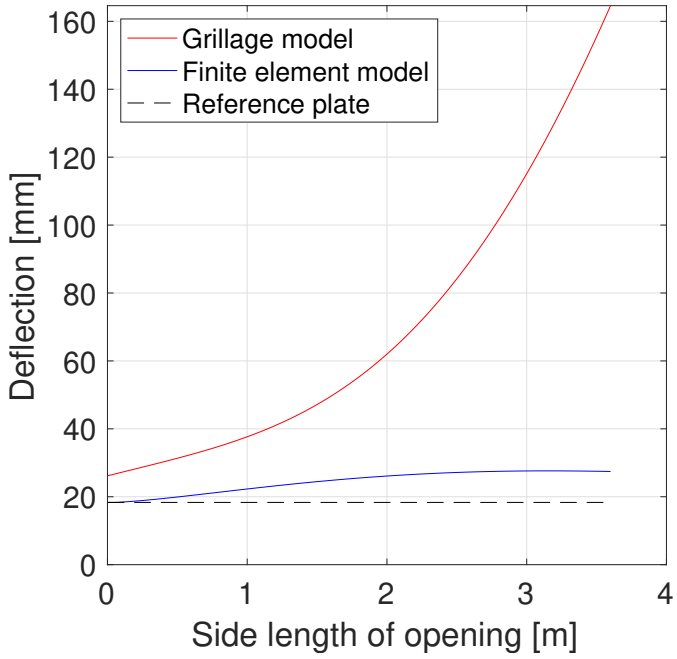

Figure 6.15: Graph showing maximum deflection in beam 3 depending on opening size for the longitudinal cross section composition

7 Discussion

Different approaches to evaluate the grillage model

In Section 5.2, a comparative study was made between different methods to calculate the section forces and deflection in the grillage model. The study was made regarding three different CLT beams with three different cross section compositions.

The study showed that the moment distribution along the transversal beams, beams 3 and 4 in the grillage model, differed between the different approaches used. Largest discrepancy were shown for the composition with the longitudinal distribution (70-20-20-20-70). It was observed that the bending moment diagram representing the three-dimensional Bernoulli-Euler model was parallel displaced downwards compared to the curves from the other two approaches. It was concluded that this difference depended on a reaction bending moment generated in the connection between the transversal beams, 3 and 4, and the longitudinal beams, 5 and 6 in the grillage model. The three-dimensional model takes this moment in the connection into account, but neither of the two-dimensional approaches that were studied.

The observation lead to the question why this negative bending moment in the connection was considerably larger for the composition with the longitudinal distribution compared to the other compositions.

The answer to this question may include multiple answers, but one thing noticed was that the longitudinal composition (70-20-20-20-70) showed the largest moment in the connection while the transversal composition (20-70-20-70-20) showed the lowest. This means that the composition with the largest stiffness in the transverse direction of the plate generated the smallest moment in the connection and the composition with the smallest stiffness in the transverse direction of the plate generated the largest moment in the connection. This indicates that the stiffness in the transverse direction of the CLT plate, which also corresponds to the stiffness in the transversal beams of the grillage model do affect this moment in the connection between the beams in the grillage model.

Consequently, for a CLT plate relatively stiff in the transverse direction compared to the longitudinal direction, the two-dimensional Bernoulli-Euler and Timoshenko beam theory as well as the three-dimensional Bernoulli-Euler approach gives similar results and therefore can be used for evaluation either one. However, for the case of CLT plates relatively slender in the transverse direction, the three-dimensional approach will end up in different results as the connection moment is significantly large.

Therefore, when using the two-dimensional approaches regardless whether it is the Bernoulli-Euler or the Timoshenko beam theory that is applied, an assumption is automatically made that the bending moment in the connection between the beams in the grillage model is equal to zero. This consequently also entail that the CLT plate is infinitely stiff in the transverse direction considering this phenomena. In the case of a transversely slender CLT plate the choice of approach must be taken with these assumptions and their possible application in mind.

Assumption of beam width in the grillage model

In the grillage model the choice was made to set the beam width equal to one tenth of the span length (b=$L/10$). This choice was originally made by the creators of this grillage model without a clear explanation for the choice.

It is reasonable to believe that the beam width in the grillage model affects the results. The results from the grillage model supersedes the results from the center path of the finite element model. Decreasing the beam width could possibly lead to results more similar to the finite element model. However, as this grillage model is intended to work as a design tool, a reduction of the beam width in the model to achieve more consistent results need further investigations.

In the parameter study the results where expressed in terms of unit per meter. In effect, results from the grillage model were divided by the beam width in order to be compared to the results from the finite element model. Changing the beam width would change these values without actually changing anything substantial in the grillage model. However, changing the beam width would also affect certain important parameters in the grillage model. An example of this is that the length of the transversal beams would change since they span between the center lines of the longitudinal beams. Decreasing the beam width would cause the center lines of the longitudinal beams to move closer to the edge of the openings, consequently shortening the transversal beams. So beam width affects both the interpretation of the results and the actual results making it difficult to evaluate the substantial overall effects.

Stress concentrations

When comparing the grillage method and the finite element method, referring to Section 5.4 the grillage method and finite element method showed similar results. When evaluating the shear force distribution, bending moment distribution and deflection both along the length and width of the beams between the grillage model and the finite element model the results were in the same order of magnitude. The results from the grillage model gave higher values than the finite element model results from the paths corresponding to the center paths of the beams. A large difference in results from the grillage model and the finite element model is that the finite element model includes stress concentrations close to the corners of the opening. Close to the corners the magnitude of shear force and bending moment increases rapidly, surpassing the magnitude of the results obtained from the grillage model.

Since the grillage model is otherwise a conservative approach, the fact that higher stresses are obtained from the finite element model questions whether the grillage method is safe to implement. However, the stress concentrations are only present in a small region of the plate. Designing the plate based on the values close to the corners of the opening would lead to oversized elements. Based on these facts, and that the stress concentrations are only present in a small region of the plate, it may be valid to neglect the values a the corners of the opening when designing this type of CLT elements.

Smooth curves

In the parameter studies, presented in Chapter 6, some curves in the presented graphs were not smooth. This was the case for some of the curves describing shear force and bending moment along the edge of the opening. In the parameter study, changing the width of the opening caused the curves describing shear force and bending moment across the width of the plate element to not be smooth. When changing the length it was the curves describing shear force and bending moment across the length of the plate that exemplified this behaviour. When changing the size of the opening, both the length and width simultaneously, both the sets of curves describing distributions across the width and length of the plate were not smooth.

There was a clear connection between the investigated parameter and which sets of curves ending up not smooth. The number of steps implemented to change the investigated parameter across, was chosen without consideration to the element sizes in the finite element model. Changing the dimensions of the opening resulted in geometries where an even mesh was impossible to fit to the geometry. Due to this, together with the partitions made in the model, some elements in the model got sizes smaller than the regular size of the other elements in the mesh. As the finite element program weights values within an elements a decreased size of certain elements in the mesh affects results. This is most likely the reason why some curves in the parameter studies showed a non-smooth behaviour.

This issue with non-smooth curves could possibly be fixed by adjusting the number of steps so that the increase in size of the investigated opening dimension in each step is equal to an even number of elements. This would ensure that the element size can remain constant throughout the parameter study, and thereby avoiding problems of weighting the values in the model. Doing this will most likely result in smooth curves also for the curves describing the development along the edge of the opening.

Grillage model discrepancies

The general grillage method overestimates shear force, bending moment and deflection when compared to results from a finite element model, especially when evaluating the sections forces in the transversal beams. There are several factors that lead to this overestimation. A part of the load on the beams in the grillage model is counted twice. The load acting on beam 3 originates from the area encompassed by the center lines of beams 3, 5 and 6. Half of the load from this area is counted towards beam 3. However, the load acting on beam 5 and 6 is counted as a surface load acting on the surfaces of these beams. The result is that the surface load acting on inner beam width of beams 5 and 6 is counted both towards these beams and towards beam 3.

Another condition that leads to exaggerated results in the grillage model is the way the length of beam 3 is set. It is set to the distance between the center lines of beams 5 and 6. Hence the length of beam 3 is always one beam width longer than the width of the actual opening. Since the bending moment depends heavily on the length of the beam span this leads to high maximum values, especially for wide openings.

Another factor is that in a grillage model loads can only be led to the supports through the beams and the beams can only lead the loads in their axial direction. As an example, load acting on the surface midway between the supported edge and beam 3 is taken up by beam 3, then lead to beams 5 and 6 as point loads acting on these beams and then finally lead trough beams 5 and 6 to the supported edge. In a plate however stresses can take on an infinite amount of directions, not forced to strictly orthogonal directions. This explains why the bending moment corresponding to beam 3, recorded along the center line in the finite element model, does not increase exponentially as the opening widens. The stresses are directed around the opening, not to the opening and along the edges of the opening as in the grillage model.

The strictly orthogonal load paths are logical for a beam grillage model but does not at all reflect the load paths in a plate in reality. Another example is when the placement of the opening is changed and moved closer to one of the long edges. According to the beam model, there will still be no difference in the force distribution between beam 5 and 6. In a plate however, the asymmetric geometry will of course lead to an asymmetric flow of forces. Additionally, there is the example of when the opening is placed with a distance of exactly one beam width from the supported side of the plate. According to the grillage model the beam close to the edge will transfer the load to beams 5 and 6. In the corresponding plate model, the area is fully supported along one of its sides meaning that the beam model fails to represent the flow of forces.

The cross section composition also affects the way the stresses flow in the plate. If the plate is stiffer in one direction the larger stresses will evolve in line with this direction. The grillage model however can not take into account the cross section composition by changing the direction of the flow of stresses. This leads to the large discrepancy between the grillage model and the finite element model seen when evaluating bending moment in beam 3 for a wide opening and a longitudinal cross section composition.

The grillage model could be altered in order to give results that are more in line with the results from the finite element model. However, by changing the grillage model with the aim of achieving lower values for bending moment shear force and deflection it could lead to a model that does not consistently produce higher values than the center paths in the finite element model. The need for the grillage model to be a conservative model during all circumstances causes it to be inaccurate during specific circumstances.

The strength of the model lies in its simplicity. The load cases are so simple that the calculations can be done by hand rather swiftly. The simplicity of the model may also be its weakness. The force distribution in a plate does not align neatly in a perpendicular way. This is clearly shown when regarding the way load is transferred from beam 1 to beam 3 and then to beam 5 in order to finally be led to the supporting edge according to the investigated grillage model.

8 Summary of results and conclusions

The aim of this thesis is to evaluate different ways to implement the grillage model, and whether results from the grillage model are comparable to results from a finite element model.

In Section 5.2, the general grillage method is implemented using three different ways to model the beams. Bernoulli-Euler beam theory according to the Gamma method, Timoshenko beam theory and finally three-dimensional Bernoulli Euler beam theory according to the Gamma method. The results from this comparison show that there is no difference in shear force distribution between the three approaches and that the shear force distribution is not affected by the cross section composition.

Regarding bending moment distribution the different models give different results for the transversal beams but there is no difference for the longitudinal beams. The results for the transversal beams show that when the Gamma method and Timoshenko beam theory is used there is no difference in bending moment distribution. The results are also not affected by the cross section composition. However, the implementation of three-dimensional Bernoulli-Euler beams with stiff connections causes the bending moment distribution to differ depending on cross section composition. In this case, the transversal beams are not simply supported on the longitudinal beams so a negative bending moment appears in the connections. This negative bending moment is comparatively large for the longitudinal distribution cross section composition whilst barely noticeable in the other cross section compositions. This negative bending moment generates a parallel shift downwards of the bending moment diagram.

Deflection in the beams is affected to large extent by the cross section composition. For the transversal beams, the longitudinal cross section composition give the highest deflection values and the transversal composition the lowest. The comparison of deflection between the beam models is affected by the difference in bending moment for the longitudinal composition in the transversal beams. The negative bending moment at the supports decrease the maximum bending moment which translates to a lower total deflection when compared to the other beam models. Other than this the difference in deflection between the beam models is negligible for both transversal and longitudinal beams. In the longitudinal beams the longitudinal cross section composition gives the lowest deflection values and the transversal cross section composition the highest. Overall the equal distribution cross section composition gives the lowest total deflection for the grillage model.

In section 5.3 it is seen that for a simply supported beam there is a small difference in absolute deflection when it is calculated analytically according to the Gamma method or using Timoshenko beam theory. Deflection values resulting from a finite element model using two-dimensional shell elements modelled with the composite layup tool are also similar in absolute terms. However, for short beams and small deflections there is a significant difference when the results from the analytical methods are compared to results from the finite element model.

Section 5 shows that in the finite element model, the section forces and deflection increase close to the opening. Close to the corners of the openings, values for bending moment and shear force increase rapidly to high values suggesting stress concentrations.

Bending moment and shear force distribution curves taken from center paths in the finite element model, coinciding with the center lines of the beams in the grillage model, are similar in shape compared to the curves representing the results from the grillage model. The same curves, but from the paths coinciding with the opening edge in the finite element model, have different shapes than those from the grillage model due to the extreme values close to the corners of the opening.

The results from Chapter 6 show that the grillage model consistently produces higher maximum values for bending moment and shear force than the finite element model when values are taken from the center path. The maximum deflection is also larger when comparing values from the grillage model to those from the path coinciding with the edge of the opening in the finite element model.

One combination of cross section composition and opening geometry stands out from the results because it shows a large discrepancy between the grillage model and the finite element model. Namely, the utilization of bending moment capacity in the transversal beams for a wide opening and a longitudinal cross section composition. For the widest of the studied openings, the degree of utilization according to the grillage model is nearly seven times that of the center path in the finite element model. This is also reflected in the results showing deflection for the same situation.

When comparing the effects of opening geometry it is clear that wide openings cause a large increase in bending moment, shear force and deflection compared to a reference plate without openings. The difference increases with the width of the opening. An opening where the length grows exhibits the opposite behavior as the difference in shear force, bending moment and deflection decreases as the length of the opening increases. The difference between the grillage model and the finite element model is generally smaller when examining a long opening compared to a wide opening.

In conclusion, it has been shown that the grillage model is a conservative approach compared to finite element models when disregarding the stress concentrations close to the corners of the opening. The results from the grillage model show higher values than those from the results representing the finite element model regarding maximum shear force, bending moment and deflection.

In Section 5.3 it is shown that there is no large difference in results regarding bending moment, shear force and deflection for a beam when analytical models are compared to a finite element model. Hence, differences between the grillage model and the finite element model depend on properties concerning the grillage model and not the way the cross section properties are modelled. Results from the grillage model exhibit discrepancies compared to results obtained from a complete finite element model.

Further studies

In further studies it would be interesting to look at how the grillage model can be adjusted to produce results more in line with results from the finite element model. The length of the short transversal beams can be adjusted in order to decrease the value of the bending moment in these. The area of the surfaces from which load is calculated can be altered in order to increase or decrease load on the beams. The changes must be analysed to find when they can be applied without risking to underestimate the section forces and deflection.

The stress concentrations present at the edge of the corners in the finite element model can not be dismissed without further investigation. How these concentrations compare to stress concentrations in real CLT elements should be analysed. It may very well be that openings in CLT elements may cause fracture at the corners, despite the section forces in other parts being below capacity.

Additional grillage models can be developed in order to dimension openings connected to the edges of CLT plate elements. Such a grillage model is easy to imagine for openings along the supported sides. A beam needs only to be removed from the current grillage model to accommodate this situation. However, an opening along the long unsupported edges is more complicated to formulate and would require the use of cantilever beams in the model.

Of course, the effects of support conditions can also be investigated. A development of a grillage model which can also be applied on a plate which is supported on all four edges would broaden the research further.

Bibliography

Austrell, Per-Erik, Ola Dahlblom and Jonas Lindemann (2004). *CALFEM - A finite element toolbox*. The Division of Structural Mechanics, LTH.

Berg, Sven, Jonas Turesson, Mats Ekevad and Johannes Huber (Mar. 2019). "Finite element analysis of bending stiffness for cross-laminated timber with varying board width". In: *Wood Material Science & Engineering* 14, pp. 392–403. DOI: 10.1080/17480272.2019.1587506.

Bodig, Jozsef and Benjamin A. Jayne (1982). *Mechanics of Wood and Wood Composites*. Van Nostrand Reinhold Company Inc.

Borgström, Eric and Johan Fröbel (2017). *KL-trähandbok - Fakta och projektering av KL-träkonstruktioner*. Svenskt Trä.

– (2019). *The CLT Handbook, CLT structures - facts and planning*. URL: https://www.swedishwood.com/siteassets/6-om-oss/publikationer/pdfer/clt-handbook-2019-eng-m-svensk-standard-2019.pdf (visited on 17/04/2020).

Burström, Per Gunnar (2007). *Byggnadsmaterial - Uppbyggnad, tillverkning och egenskaper*. Studentlitteratur AB.

Dahl, Kristian Berbom (2009). "Mechanical properties of clear wood from Norway spruce". PhD thesis. Norwegian University of Science and Technology.

Dinwoodie, J.M. (1989). *Wood: Nature's cellular, polymeric fibre-composite*. The Institute of Metals.

Falk, Andreas, Philipp Dietsch and Joachim Schmid (2016). *Proceedings of the Joint Conference of COST Actions FP1402 & FP1404 "Cross Laminated Timber – A competitive wood product for visionary and fire safe buildings"*. KTH Royal Institute of Technology, Division of Building Materials.

GWMI (2019). *Analysis of global cross-laminated timber (CLT) production capacities in 2020*. URL: https://www.globalwoodmarketsinfo.com/analysis-of-global-cross-laminated-timber-clt-production-capacities-in-2020/. (visited on 16/06/2020).

Heyden, Susanne, Ola Dahlblom, Anders Olsson and Göran Sandberg (2017). *Introduktion till strukturmekaniken*. Studentlitteratur AB.

Isaksson, Tord, Annika Mårtensson and Sven Thelandersson (2016). *Byggkonstruktion*. Studentlitteratur AB.

Jeleč, Mario, Vladka Rajčić, Henrik Danielsson and Erik Serrano (2016). "Structural analysis of in-plane loaded CLT beam with holes: FE-analyses and parameter studies". In: *Proceedings - meeting 49 : 16-19 August 2016, Graz, Austria, INTER, International Network on Timber Engineering Research*. Ed. by Rainer Görlacher. Timber Scientific Publishing, Karlsruhe, pp. 153–167.

Jeleč, Mario, Damir Varevac and Vladka Rajčić (2018). "Cross-laminated timber (CLT) – a state of the art report". In: *GRAĐEVINAR* 70.2, pp. 75–95.

Johansson, Marie (2016). "Structural properties of sawn timber and engineered wood products". In: *Design of timber structures Structural aspects of timber construction*. Ed. by Eric Borgström. Stockholm: Swedish wood. Chap. 2, pp. 26–68.

Ottosen, Niels and Hans Petersson (1992). *Introduction to the finite element method*. Pearson Education Limited.

Robertson, Adam, Frank Lam and Raymond Cole (Dec. 2012). "A Comparative Cradle-to-Gate Life Cycle Assessment of Mid-Rise Office Building Construction Alternatives: Laminated Timber or Reinforced Concrete". In: *Buildings* 2, pp. 245–270. DOI: 10.3390/buildings2030245.

SwedishWood (2017a). *Cellstruktur*. URL: https://www.traguiden.se/om-tra/materialet-tra/traets-uppbyggnad/traets-uppbyggnad/cellstruktur/ (visited on 17/04/2020).

– (2017b). *Large load-bearing structures in wood*. URL: https://www.swedishwood.com/building-with-wood/construction/a_variety_of_wooden_structures/large_load-bearing_structures_in_wood/ (visited on 17/04/2020).

– (2017c). *Sågprocessen*. URL: https://www.traguiden.se/om-tra/materialet-tra/sagverksprocessen/sagprocessen/sagprocessen/ (visited on 17/04/2020).

Wallner-Novak, Markus, Manfred Augustin, Josef Koppelhuber and Kurt Pock (2017). *Cross-Laminated Timber Structural Design Volume 2*. proHolz Austria.

Appendix A

Three-dimensional beam modelling

A.1 Solution for determining the global stiffness matrix and load vector for the three-dimensional case

The element stiffness matrix is computed by using the following expression (Austrell et al., 2004):

$$\mathbf{K}^e = \mathbf{G}^T \bar{\mathbf{K}}^e \mathbf{G} \tag{A.1}$$

Where:

$$\bar{\mathbf{K}}^{\mathbf{e}} = \begin{bmatrix}
k_1 & 0 & 0 & 0 & 0 & 0 & -k_1 & 0 & 0 & 0 & 0 & 0 \\
0 & \frac{12EI_{\bar{z}}}{L^3} & 0 & 0 & 0 & \frac{6EI_{\bar{z}}}{L^2} & 0 & -\frac{12EI_{\bar{z}}}{L^3} & 0 & 0 & 0 & \frac{6EI_{\bar{z}}}{L^2} \\
0 & 0 & \frac{12EI_{\bar{y}}}{L^3} & 0 & -\frac{6EI_{\bar{y}}}{L^2} & 0 & 0 & 0 & -\frac{12EI_{\bar{y}}}{L^3} & 0 & -\frac{6EI_{\bar{y}}}{L^2} & 0 \\
0 & 0 & 0 & k_2 & 0 & 0 & 0 & 0 & 0 & -k_2 & 0 & 0 \\
0 & 0 & -\frac{6EI_{\bar{y}}}{L^2} & 0 & \frac{4EI_{\bar{y}}}{L} & 0 & 0 & 0 & \frac{6EI_{\bar{y}}}{L^2} & 0 & \frac{2EI_{\bar{y}}}{L} & 0 \\
0 & \frac{6EI_{\bar{z}}}{L^2} & 0 & 0 & 0 & \frac{4EI_{\bar{z}}}{L} & 0 & -\frac{6EI_{\bar{z}}}{L^2} & 0 & 0 & 0 & \frac{2EI_{\bar{z}}}{L} \\
-k_1 & 0 & 0 & 0 & 0 & 0 & k_1 & 0 & 0 & 0 & 0 & 0 \\
0 & -\frac{12EI_{\bar{z}}}{L^3} & 0 & 0 & 0 & -\frac{6EI_{\bar{z}}}{L^2} & 0 & \frac{12EI_{\bar{z}}}{L^3} & 0 & 0 & 0 & -\frac{6EI_{\bar{z}}}{L^2} \\
0 & 0 & -\frac{12EI_{\bar{y}}}{L^3} & 0 & \frac{6EI_{\bar{y}}}{L^2} & 0 & 0 & 0 & \frac{12EI_{\bar{y}}}{L^3} & 0 & \frac{6EI_{\bar{y}}}{L^2} & 0 \\
0 & 0 & 0 & -k_2 & 0 & 0 & 0 & 0 & 0 & k_2 & 0 & 0 \\
0 & 0 & -\frac{6EI_{\bar{y}}}{L^2} & 0 & \frac{2EI_{\bar{y}}}{L} & 0 & 0 & 0 & \frac{6EI_{\bar{y}}}{L^2} & 0 & \frac{4EI_{\bar{y}}}{L} & 0 \\
0 & \frac{6EI_{\bar{z}}}{L^2} & 0 & 0 & 0 & \frac{2EI_{\bar{z}}}{L} & 0 & -\frac{6EI_{\bar{z}}}{L^2} & 0 & 0 & 0 & \frac{4EI_{\bar{z}}}{L}
\end{bmatrix} \tag{A.2}$$

with k_1 denoting the axial stiffness and k_2 the torsional stiffness.
These are calculated through $k_1 = \dfrac{EA}{L}$ and $k_2 = \dfrac{GI_{tor}}{L}$.

The transformation matrix $\mathbf{G}$ is determined by:

$$\mathbf{G} = \begin{bmatrix} n_{x\bar{x}} & n_{y\bar{x}} & n_{z\bar{x}} & 0 & 0 & 0 & 0 & 0 & 0 & 0 & 0 & 0 \\ n_{x\bar{y}} & n_{y\bar{y}} & n_{z\bar{y}} & 0 & 0 & 0 & 0 & 0 & 0 & 0 & 0 & 0 \\ n_{x\bar{z}} & n_{y\bar{z}} & n_{z\bar{z}} & 0 & 0 & 0 & 0 & 0 & 0 & 0 & 0 & 0 \\ 0 & 0 & 0 & n_{x\bar{x}} & n_{y\bar{x}} & n_{z\bar{x}} & 0 & 0 & 0 & 0 & 0 & 0 \\ 0 & 0 & 0 & n_{x\bar{y}} & n_{y\bar{y}} & n_{z\bar{y}} & 0 & 0 & 0 & 0 & 0 & 0 \\ 0 & 0 & 0 & n_{x\bar{z}} & n_{y\bar{z}} & n_{z\bar{z}} & 0 & 0 & 0 & 0 & 0 & 0 \\ 0 & 0 & 0 & 0 & 0 & 0 & n_{x\bar{x}} & n_{y\bar{x}} & n_{z\bar{x}} & 0 & 0 & 0 \\ 0 & 0 & 0 & 0 & 0 & 0 & n_{x\bar{y}} & n_{y\bar{y}} & n_{z\bar{y}} & 0 & 0 & 0 \\ 0 & 0 & 0 & 0 & 0 & 0 & n_{x\bar{z}} & n_{y\bar{z}} & n_{z\bar{z}} & 0 & 0 & 0 \\ 0 & 0 & 0 & 0 & 0 & 0 & 0 & 0 & 0 & n_{x\bar{x}} & n_{y\bar{x}} & n_{z\bar{x}} \\ 0 & 0 & 0 & 0 & 0 & 0 & 0 & 0 & 0 & n_{x\bar{y}} & n_{y\bar{y}} & n_{z\bar{y}} \\ 0 & 0 & 0 & 0 & 0 & 0 & 0 & 0 & 0 & n_{x\bar{z}} & n_{y\bar{z}} & n_{z\bar{z}} \end{bmatrix} \tag{A.3}$$

where $n_{x\bar{x}}$ defines cosine of the angle between the x- and $\bar{x}$-axis. The same theory is applied for all the other included variables as well (Austrell et al., 2004).

The element load vector is computed by using the following expression (Austrell et al., 2004):

$$\mathbf{f}_l^e = \mathbf{G}^T \bar{\mathbf{f}}_l^e \tag{A.4}$$

The same transformation matrix $\mathbf{G}$ is used as above in order to determine the element stiffness matrix and:

$$\bar{\mathbf{f}}_{\mathbf{l}}^{\mathbf{e}} = \begin{bmatrix} \frac{q_{\bar{x}}L}{2} \\ \frac{q_{\bar{y}}L}{2} \\ \frac{q_{\bar{z}}L}{2} \\ \frac{q_{\bar{\omega}}L}{2} \\ \frac{-q_{\bar{z}}L^2}{12} \\ \frac{q_{\bar{y}}L^2}{12} \\ \frac{q_{\bar{x}}L}{2} \\ \frac{q_{\bar{y}}L}{2} \\ \frac{q_{\bar{z}}L}{2} \\ \frac{q_{\bar{\omega}}L}{2} \\ \frac{q_{\bar{z}}L^2}{12} \\ \frac{-q_{\bar{y}}L^2}{12} \end{bmatrix} \tag{A.5}$$

A.2 Evaluation of the section forces from the global stiffness matrix and load vector

To determine the section forces from the global stiffness matrix and load vector an evaluation is made based on the solutions of the basic equations:

$$\begin{aligned} EA\frac{d^2\bar{u}}{d\bar{x}^2} + q_{\bar{x}} = 0 \qquad & EI_{\bar{z}}\frac{d^4\bar{v}}{d\bar{x}^4} - q_{\bar{y}} = 0 \\ EI_{\bar{y}}\frac{d^4\bar{w}}{d\bar{x}^4} - q_{\bar{z}} = 0 \qquad & GI_{tor}\frac{d^2\bar{\varphi}}{d\bar{x}^2} + q_{\bar{\omega}} = 0 \end{aligned} \tag{A.6}$$

The displacements along the in the model included beams are obtained from these equations by calculating the sum of the homogeneous and the particular solutions for this system as follows (Austrell et al., 2004):

$$\mathbf{u} = \begin{bmatrix} \bar{u}(\bar{x}) \\ \bar{v}(\bar{x}) \\ \bar{w}(\bar{x}) \\ \bar{\varphi}(\bar{x}) \end{bmatrix} = \mathbf{u}_h + \mathbf{u}_p \tag{A.7}$$

Where:

$$\mathbf{u}_h = \bar{\mathbf{N}}\bar{\mathbf{C}}^{-1}\mathbf{G}\mathbf{a}^{\mathbf{e}} \tag{A.8}$$

and

$$\mathbf{u}_p = \begin{bmatrix} \bar{u}_p(\bar{x}) \\ \bar{v}_p(\bar{x}) \\ \bar{w}_p(\bar{x}) \\ \bar{\varphi}_p(\bar{x}) \end{bmatrix} = \begin{bmatrix} \frac{q_{\bar{x}}L\bar{x}}{2EA}\left(1 - \frac{\bar{x}}{L}\right) \\ \frac{q_{\bar{y}}L^2\bar{x}^2}{24EI_{\bar{z}}}\left(1 - \frac{\bar{x}}{L}\right)^2 \\ \frac{q_{\bar{z}}L^2\bar{x}^2}{24EI_{\bar{y}}}\left(1 - \frac{\bar{x}}{L}\right)^2 \\ \frac{q_{\bar{\omega}}L\bar{x}}{2GI_{tor}}\left(1 - \frac{\bar{x}}{L}\right) \end{bmatrix} \tag{A.9}$$

In equation A.8 denoting the homogeneous solution to the system the transformation matrix $\mathbf{G}$ as well as the nodal displacement vector $\mathbf{a^e}$ are given and described above. However, the matrices $\bar{\mathbf{N}}$ and $\bar{\mathbf{C}}$ are defined as follows (Austrell et al., 2004):

$$\bar{\mathbf{N}} = \begin{bmatrix} 1 & \bar{x} & 0 & 0 & 0 & 0 & 0 & 0 & 0 & 0 & 0 & 0 \\ 0 & 0 & 1 & \bar{x} & \bar{x}^2 & \bar{x}^3 & 0 & 0 & 0 & 0 & 0 & 0 \\ 0 & 0 & 0 & 0 & 0 & 0 & 1 & \bar{x} & \bar{x}^2 & \bar{x}^3 & 0 & 0 \\ 0 & 0 & 0 & 0 & 0 & 0 & 0 & 0 & 0 & 0 & 1 & \bar{x} \end{bmatrix} \tag{A.10}$$

$$\bar{\mathbf{C}} = \begin{bmatrix} 1 & 0 & 0 & 0 & 0 & 0 & 0 & 0 & 0 & 0 & 0 & 0 \\ 0 & 0 & 1 & 0 & 0 & 0 & 0 & 0 & 0 & 0 & 0 & 0 \\ 0 & 0 & 0 & 0 & 0 & 0 & 1 & 0 & 0 & 0 & 0 & 0 \\ 0 & 0 & 0 & 0 & 0 & 0 & 0 & 0 & 0 & 0 & 1 & 0 \\ 0 & 0 & 0 & 0 & 0 & 0 & 0 & 1 & 0 & 0 & 0 & 0 \\ 0 & 0 & 0 & 1 & 0 & 0 & 0 & 0 & 0 & 0 & 0 & 0 \\ 1 & L & 0 & 0 & 0 & 0 & 0 & 0 & 0 & 0 & 0 & 0 \\ 0 & 0 & 1 & L & L^2 & L^3 & 0 & 0 & 0 & 0 & 0 & 0 \\ 0 & 0 & 0 & 0 & 0 & 0 & 1 & L & L^2 & L^3 & 0 & 0 \\ 0 & 0 & 0 & 0 & 0 & 0 & 0 & 0 & 0 & 0 & 1 & L \\ 0 & 0 & 0 & 0 & 0 & 0 & 0 & 1 & 2L & 3L^2 & 0 & 0 \\ 0 & 0 & 0 & 1 & 2L & 3L^2 & 0 & 0 & 0 & 0 & 0 & 0 \end{bmatrix} \tag{A.11}$$

The section forces are then evaluated through (Austrell et al., 2004):

$$\begin{aligned} N &= EA\frac{d\bar{u}}{d\bar{x}} & V_{\bar{y}} &= -EI_{\bar{z}}\frac{d^3\bar{v}}{d\bar{x}^3} & V_{\bar{z}} &= -EI_{\bar{y}}\frac{d^3\bar{w}}{d\bar{x}^3} \\ T &= GI_{tor}\frac{d\bar{\varphi}}{d\bar{x}} & M_{\bar{y}} &= -EI_{\bar{y}}\frac{d^2\bar{w}}{d\bar{x}^2} & M_{\bar{z}} &= EI_{\bar{z}}\frac{d^2\bar{v}}{d\bar{x}^2} \end{aligned} \tag{A.12}$$